The design of a pressure vessel and testing procedures for the determination of the effect of high temperature pressurised helium on valve contact welding

Hein Schmidt
B.Eng. (Mechanical)

Mini-dissertation submitted to the Faculty of Engineering, School of Mechanical and Materials Engineering, Potchefstroom University for CHE, in partial fulfilment of the requirements for the degree of Master in Engineering.

Study Leader: Prof. J. Markgraaff
Potchefstroom

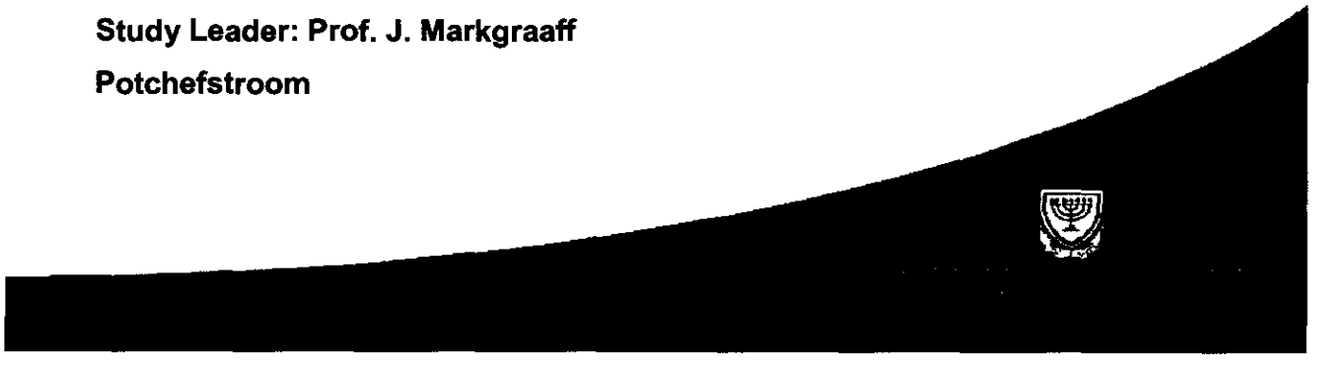

This dissertation is dedicated to:

Werner Janse van Rensburg (18 March 1978 – 04 April 2004) for showing me to never give up, no matter how bad things seem.

Pauline Nel for her unselfishness and continuous support.

Abstract

The PBMR (Pebble Bed Modular Reactor) is one of the current developments in the field of nuclear power generators. The control philosophy of the PBMR system relies heavily on the controlling of valves. The current control valves are subjected to a maximum temperature of 350°C with a pressure difference of 90 bar. Control optimisation can be obtained by including "hot valves" into the system. The biggest improvement is possible with a bypass-valve after the low-pressure turbine outlet. This valve will be subjected to a temperature of 720°C with a pressure difference of 52 bar. PBMR personnel raised the concern that the components of these valves (valve seat and sealing surfaces) in contact with the hot helium gas could tend to weld to each other when they are in contact. An investigation was done to establish whether these surfaces tend to weld together.

As no literature was found on testing for prevention of welding of materials under high temperature pressurised helium conditions (Chapter 2), a testing facility was designed to test the hot bypass-valve material (AISI H10) under operating conditions. This included the design of a pressure vessel according to ASME VIII Division I [30] (Chapter 3) to be able to simulate the helium operating conditions and a bolted connection (Chapter 4) to simulate the valve contact conditions.

A finite element analysis was done, using ALGOR FEMPRO software (Chapter 5), to verify the internal stresses of the pressure vessel based on the maximum allowable stresses for material UNS N06230 (Haynes® 230® Alloy), from Appendix 4 of ASME VIII Division 2 [37]. Firstly, a steady state heat transfer analysis was done to calculate the pressure vessel temperature distribution. During a static stress analysis, these results were used to assign the temperature dependent material properties to the various finite element elements. The helium pressure and external pressure were simulated as uniform surface pressures. Based on the Tresca effective stress results the maximum allowable 0.2% yield strength of Haynes 230 was exceeded. According to this analysis, the pressure vessel will yield when subjected to the specified operating conditions. The calculated stresses also exceeded the ASME VIII Division 2 - Appendix 4 maximum allowable material stresses.

It is recommended that the same analysis be done with another FEM analysis software package, to verify the calculated material stresses. This analysis should be incorporated into the follow-up study, where the water-cooling system must also be designed. Before the manufacturing of the pressure vessel can commence, a third party inspector must approve the design. Any design updates necessary from the inspector's report should also be included in the follow-up study.

Uittreksel

Die PBMR (Korrelbed Modulêre Reaktor) is een van die huidige ontwikkelings in die veld van kernkrag opwekkers. Die beheer filosofie van die PBMR stelsel is gegrond op die beheer van kleppe. Die huidige beheerkleppe is onderworpe aan 'n maksimum temperatuur van 350°C by 'n druk verskil van 90 bar. Beheer optimering is moontlik deur die insluiting van "warm kleppe" in die stelsel. Die grootste verbetering sal moontlik wees met 'n verbyvloei-klep na die uitlaat van die lae druk turbine. Die klep sal onderworpe wees aan 'n temperatuur van 720°C by 'n druk verskil van 52 bar. PBMR personeel is egter bekommerd dat die komponente van die kleppe (klepbedding en seëlvlakke) wat in aanraking met die warm helium gas is, kan neig om aan mekaar vas te sweis. 'n Ondersoek is gedoen om vas te stel of die seëlvlakke wel sal neig om aan mekaar vas te sweis.

Aangesien geen literatuur gevind is wat handel oor die toets van die voorkoming van sweising van materiale onder hoë temperatuur, hoë druk helium toestande nie (Hoofstuk 2), is 'n toets opstelling ontwerp om die "warm klep" materiale (AISI H10) te toets onder bedryfstoestande. Dit het die ontwerp van 'n drukvat volgens ASME VIII Divisie 1 [30] ingesluit, om die helium bedryfstoestande te kan simuleer en 'n bout konneksie (Hoofstuk 4) om die klep seël kondisies te simuleer.

'n Eindige element analise is gedoen met behulp van ALGOR FEMPRO sagteware (Hoofstuk 5), om die drukvat materiaal spannings te verifieer, gebaseer op die maksimum toelaatbare spannings vir UNS N06230 (Haynes® 230® Allooi), volgens Bylaag 4 van ASME VIII Divisie 2 [37]. 'n Gestadige hitte oordrag analise is gedoen om die temperatuur verspreiding in die drukvat te bepaal. Tydens 'n statiese spannings analise is die resultate gebruik om temperatuur afhanklike materiaal eienskappe toe te ken aan die eindige element elemente. Die helium druk en eksterne druk is gesimuleer as uniforme oppervlak drukke. Gebaseer op die Tresca effektiewe spannings resultate word die maksimum toelaatbare 0.2% swig spanning van Haynes 230 oorskry. Volgens die analise sal die drukvat swig indien dit blootgestel word aan die bedryfstoestande. Die berekende spannings oorskry ook die ASME VIII Divisie 2 - Bylaag 4 [37] maksimum toelaatbare materiaal spannings.

Dit word voorgestel dat dieselfde analise met 'n ander eindige element pakket gedoen word, om die berekende materiaal spannings te verifieer. Hierdie analise moet in die opvolg studie geïnkorporeer word waar die water verkoeling sisteem ook ontwerp moet word. 'n Derde party inspekteur moet die drukvat ontwerp goedkeur voordat vervaardiging daarvan kan plaasvind. Enige ontwerp opdaterings wat voortspruit uit inspekteur se kommentaar moet ook in die opvolg studie hanteer word.

Table of Contents

List of Figures

List of Tables

Chapter 1: Introduction

This chapter puts the study into perspective. The problem is broken down from the highest level (PBMR) to a level describing the material needs of the valve seats and sealing surfaces. The need for this study is also given.

1.1 Background

The PBMR (Pebble Bed Modular Reactor) is one of the current developments in the field of nuclear power generators (schematic representation in Figure 1-1). This system uses a direct cycle gas turbine based power conversion unit. To obtain the desired amount of energy output, a maximum operating temperature of 900°C must be reached in the reactor unit. The power conversion unit of the PBMR is based on a closed three-shaft Brayton cycle. Helium, as a chemically inert gas, is used as working fluid in the power conversion unit. The main reasons for using helium are the increase in obtainable power and cycle efficiency.

The PBMM (Pebble Bed Micro Model, schematic representation in Figure 1-2) is a model of such a Brayton cycle that mimics the design and control of the PBMR while operating with nitrogen instead of helium [19]. To control the PBMR process, the opening percentage of the process control valves is regulated. In the current layout of the system, butterfly and ball valves are used. Under normal operating conditions, these valves are subjected to temperatures of 110°C with a pressure difference of 90 bars, while the maximum valve operating temperature elevates to 350°C at the same pressure difference.

Thus, the control philosophy of the system relies heavily on controlling the valves. The current control philosophy can however be changed and optimized by the use of "hot valves". Hot valves will operate at temperatures varying between 700°C and 900°C. These valves will regulate the flow of hot gases between different system components.

The problem statement originates from the possible use of the valves at these high temperatures.

1.2 Problem statement

Through personal communication with engineers on the PBMR project, the need for using "hot valves" was discussed. This included a study undertaken by MHI (Mitsubishi Heavy

Industries) for the PBMR, where the possibility of using hot bypass-valves on the low- and high-pressure turbo units was investigated. This study indicated that using hot bypass-valves on the aforementioned turbo units created a very small window of improvement in the obtainable controllability of the system. It was also noticed that according to MHI the best location for a hot bypass-valve was at the power turbine unit (thus after the low-pressure turbine outlet). This bypass arrangement is shown in Figure 1-1. The outlet temperature and pressure of the low-pressure turbine are respectively T ≈ 720°C and P ≈ 52bar (V704 Demonstration Plant results for the low pressure turbine (MPS-SS0051), Personal communication - PBMR).

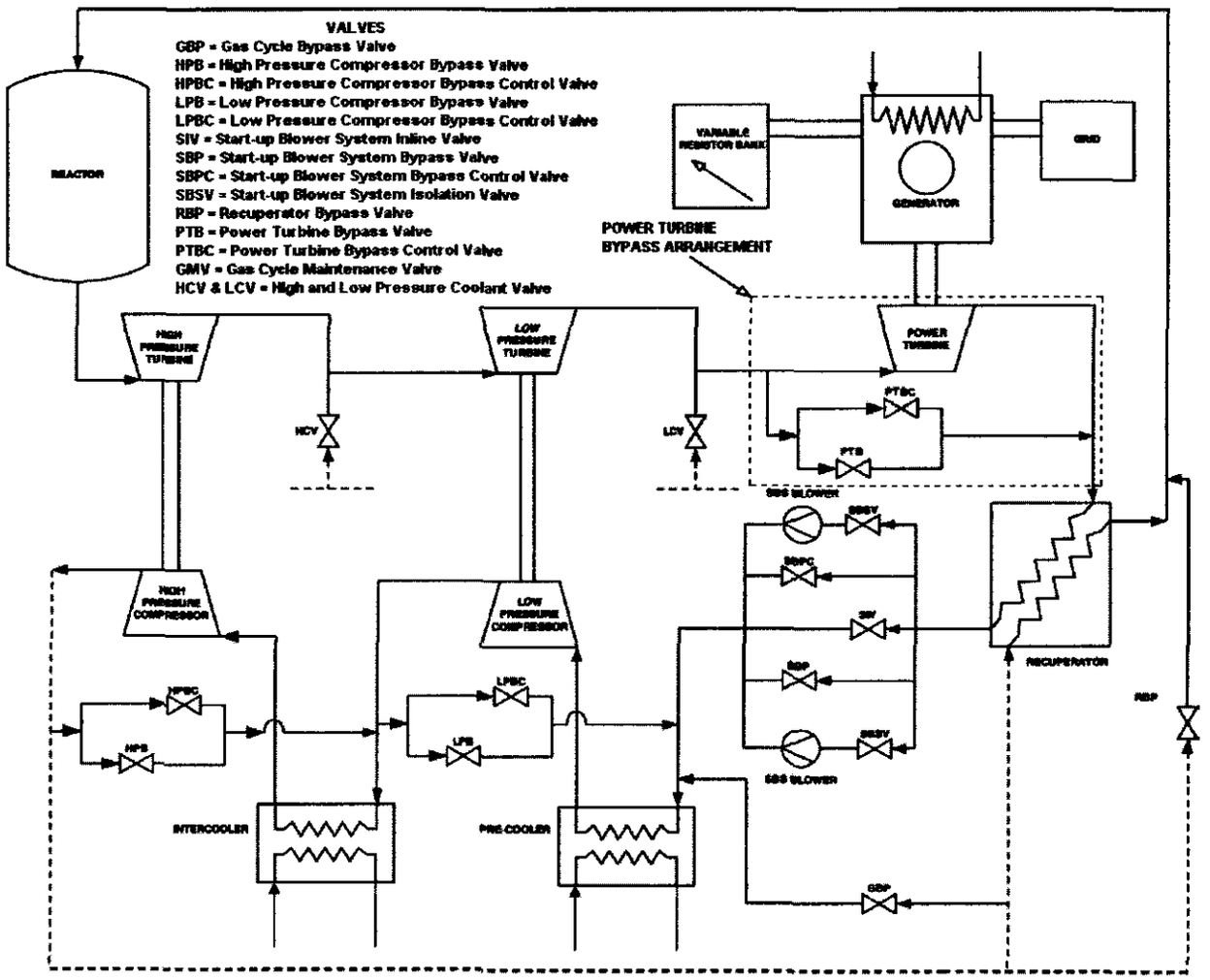

Figure 1-1: Schematic layout of PBMR (modified after A. Koster et al. [19])

These valves are not included in the current design of the PBMR system. PBMR personnel raised the concern that the components of these valves in contact with the hot helium gas (valve seat and sealing surfaces) may weld to each other when in contact. If the sealing

surfaces weld together, control over the process will be lost. Thus, research was required on valve materials for "hot valves". Tests should be conducted on the valve sealing surfaces to verify if contact welding is augmented by PBMR operating conditions.

The next step of the study was to do a survey on current available literature dealing with either the testing of valve materials or the testing of material coatings for prevention of valve contact welding. This survey included literature of material tests that were done under high temperature pressurised helium conditions.

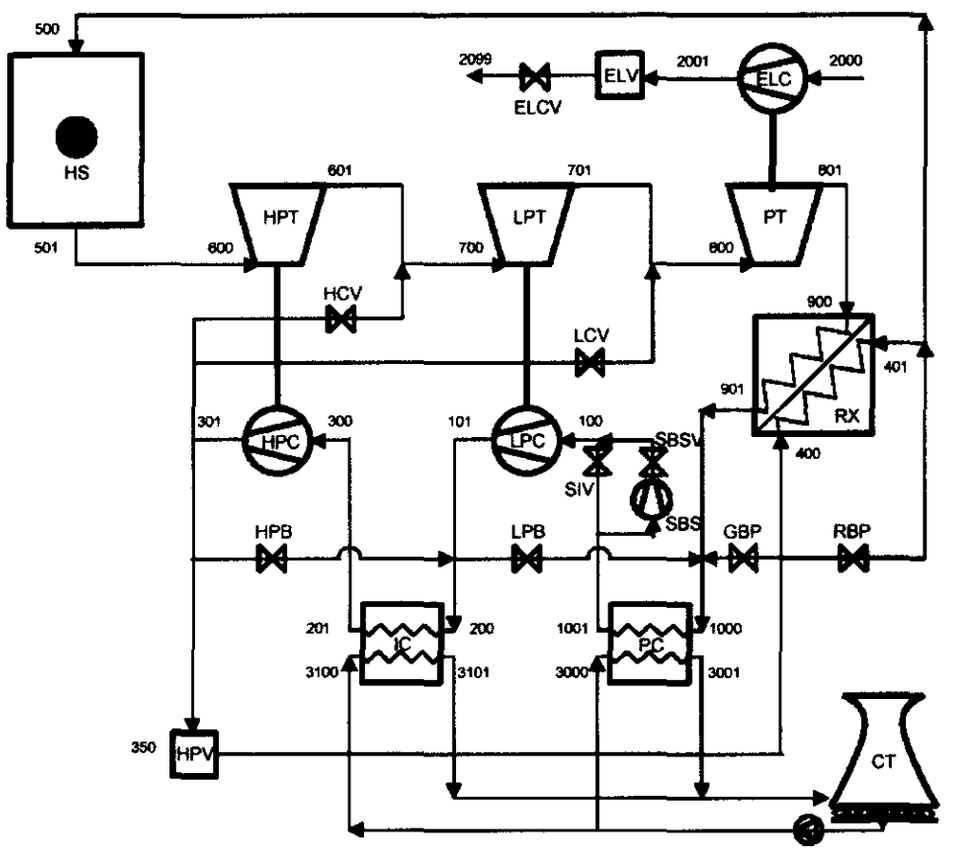

Figure 1-2: Schematic layout of PBMM [41]

The results from the literature survey would determine the objectives of the study. If suitable literature was found with solutions to the contact-welding problem, the solutions could be applied to the PBMR power turbine bypass-valves. If no suitable literature of valve contact welding elimination was found, an experimental design was required. The experimental design would govern the required experimental facility and equipment. Therefore, the literature survey and purpose of the study is given in Chapter 2.

Chapter 2: Literature study

In this chapter, literature relevant to the study is presented. This literature includes testing of valve materials and testing of coating materials.

2.1 Literature

Böhlo and Liebe [1] tested large diameter valves under helium conditions at 900°C (no reference to pressure was found). The valve seat materials considered were materials with a DIN specification code DIN 1.4876 (Incoloy 800) and DIN 2.4663 (Inconel 617). It was found that the decrease of contact between valve sealing surfaces is smaller for Inconel 617 than for Incoloy 800 (no reference made of force magnitudes). Further tests were necessary due to another fact, being the logarithmic increase of leakage when temperatures exceed 800°C. The high leakage rate was due to the dramatic decrease in creep strength of the materials at these temperatures [1].

Thermochemical heat treatment such as nitriding or carburizing together with a hard coating is known as a "duplex treatment" [4]. Hard coatings like titanium nitride (TiN), chromium containing amorphous hydrogenated carbon (known as Cr-DLC) and a-C:H (also known as DLC) were investigated as treatment for X20Cr13 ferritic stainless steel (DIN 1.4021, AISI 420), as used in ball valve component materials. The surface hardness of some coated surfaces was 2500 HK (Knoop Hardness) for a TiN coating and 3000 HK for the a-C:H coating.

Indentation tests and scratch tests were carried out on coated surfaces. The TiN-coated surfaces were found to have a hardness varying from 2500 HK at the surface of the coating to 1500 HK at a depth of 2.3 μm, thus giving a high interfacial adhesion of the coatings to the diffusion treated metal surface. The valve actuation torque was decreased with the use of coatings on the ball valve. The decrease in actuation torque ranged between 20% - 65% depending on the coating used and the pressure. The non-metal-containing a-C:H coated surfaces showed the best results due to their high wear resistance [4].

Chromium nitride (CrN) and TiN films on steel surfaces give rise to relatively high hardness and increased wear resistance [5]. Kawana et al. [5] developed ceramic coatings for valve seats by using cathodic arc ion plating. The dissolving rate of Cobalt (Co) into high-temperature high-pressure water (Light water reactor (LWR) coolant environment) decreased drastically by the use of the CrN coating. The CrN coatings also showed very good wear and

corrosion resistance under the aforementioned conditions. By coating the surfaces with 7μm CrN, the elution rate of Co was quartered. CrN and TiN coatings improved the galling and wear resistance of Stellite ® coatings in the LWR coolant environment.

Ceramic coatings are used on large-diameter valve seats for protection against scratches and radiation damage [6]. It also has the ability to prevent inter-diffusion between the metal gasket and seat surfaces of metal sealed gate valves. The same article [6] states that ceramic-coated seat surfaces should have a Vickers hardness of $H_{v0.3} > 10^3$ and maximum roughness $R_{max} <$ 0.3 μm. Plasma sprayed WC-Co seat surfaces show promise for use on large diameter (2.0 m diameter) metal-sealed gate valves under harsh conditions in the International Thermonuclear Experimental Reactor (ITER) environment. This reactor is of Japanese design.

The Mc Nally Institute has a web page [2] dealing with the selection of materials for hardfacing seals. The following materials are discussed: (a) reaction bonded silicon carbide, (b) self-sintered silicon carbide, (c) siliconized graphite, and (d) tungsten carbide. It is shown in [2] that carbon/graphite in conjunction with reaction-bonded silicon carbide has the best wear characteristics of all the possible face combinations. However, some chemicals (Sodium Hydroxide, Potassium Hydroxide, Nitric Acid, Green Sulphate Liquor, Calcium Hydroxide, and Hydrofluoric Acid) can attack this hardfacing material. Self-sintered silicon carbide has a higher chemical resistance, but can be too brittle for certain designs. Tungsten carbide is unsuitable for use in a nuclear application, because cobalt is used to bond Tungsten carbide. The reason for this is that cobalt converts to ^{60}Co and ^{58}Co due to irradiation in the nuclear reactor [5]. Two hard faces are used where the product tends to stick the surfaces together [2].

Matthews and Eskildsen [3] proposed the use of Diamond like carbon (DLC) as engineering coating. DLC has a vast range of applications and it decreases friction and lengthens tool life. They do not recommend the use of this coating above 300°C. However, DLC and standard IonSlip coatings provided the best performance in a study by Wiklund and Hutchings to lower the galling susceptibility of titanium and its alloys [16]. In this study [16], the maximum applied contact force of 200 N related to a Hertzian pressure of 5 GPa if the contact remained elastic. No mention of experimental temperature is given in the article. Thus, DLC seems to be a good coating candidate for high contact forces, but at moderate temperatures.

Austenitic stainless steel, Nitronic 60, showed high galling wear resistance, which can be attributed to its low stacking fault energy, high work-hardening rate, and the ability to form lubricating oxide layers on the wear surfaces [10]. The aforementioned attributes seem to be increased by the addition of small amounts of nitrogen. However, according to Schumacher [10], this is not entirely true. An increase in nitrogen content increased the strength and cold

work hardening factor, but there was no noteworthy change in the wear rate and only a slight negative effect on the galling resistance. Schumacher showed that the addition of Ni to the austenitic stainless steels has a detrimental effect on the wear and galling resistance of the austenitic stainless steel.

NITRONIC 60 can be used in contact with various grades of stainless steels (including the following AISI types 410, 416, 303, 304, 316, and 17-4PH) as well as itself, without concern for galling, even at contact stresses exceeding 344.74 MPa (50000 psi) (no reference of temperature) [7]. This contact stress greatly exceeds the normal contact stresses of a butterfly valve [7].

NOREM ® hardfacing alloy might be suitable as a substitute for the cobalt-base hardfacing alloys in butterfly valves [17]. NOREM ® can also be used for repairing gate valve discs, provided that the valve seats are made of Stellite ®.

The best iron-based hardfacing materials, to use on gate valves under pressurised water reactor (PWR) conditions, are valves coated with alloy EB 5183 and NOREM 04 [11]. With these hardfacing coatings no hot leakage was detected, due to stroke cycling of the valves.

Stellite ® was previously used for hardfacings of valve seats. Due to Cobalt elution, it cannot be used on valve seats of nuclear reactors. Ocken [8] investigated NOREM ® hardfacing alloys as a possible replacement for Stellites. Some of the reasons are:

- The low surface damage (< 3µm) generated by the pin-on-plate geometry galling wear test, with contact stresses (415 MPa) exceeding calculated average contact stresses between the valve disc and seat.
- Any number of iron-based alloys (Elmax, APM 2311, NOREM ®, Nelsit, and Everit 50 and 50 So) matches or exceeds the performance of the cobalt-base alloys (Stellites).

Processing techniques yielding finer microstructures are those with the highest resistance to galling wear. Nickel-based alloys typically showed higher values of surface damage with galling wear tests done by Ocken [8]. As Kim & Kim [9] reported, the wear resistance of NOREM 02 hardfacing alloys nearly equalled that of Stellite 6, under a contact stress of 103 MPa with a temperature range below 180°C. This is said to be, due to the oxide layers that formed during sliding. An abrupt wear mode change was noted at 190°C and galling occurred above 200°C, which can be attributed to the loss of the work hardenability. The oxide layers are however, dependent on the test conditions, therefore the results cannot be used to accurately predict how NOREM 02 would perform under operating conditions in a nuclear power plant.

Vardavoulias [12] showed how powder metallurgical (P/M) stainless steels (AISI 304L and 316L) had significantly improved wear resistance against dry sliding wear against an alumina counter body. These P/M stainless steels contained two different ceramic particles (Al_2O_3 and Y_2O_3), with BN and B_2Cr as sintering activators. The combination of Al_2O_3 as ceramic coating and B_2Cr as sintering activator provided the best results. From this study, it was deduced that sintering activators decreased porosity, while the small ceramic particles limited the plastic deformation. No oxidation wear was found to occur as would have with other ferrous materials.

Hardfacing deposit (Tristelle TS-2) on soft type 347 stainless steel was shown to have a higher threshold galling stress (TGS) than NOREM O2. The average TGS of Stellite 6 was 1200 MPa and NOREM 02 was nearly 640 MPa, while Tristelle TS-2 had a TGS of approximately 780 MPa [13]. Ni-based hardfacing alloys showed the lowest TGS. High abrasive and high adhesive wear resistance, together with low coefficients of friction ($\mu \approx 0.2$ vs. steel) could be obtained from metal-carbon films [14]. Michler et al. [14] studied the duplex coatings produced by high-pressure plasma nitriding and physical vapour deposition (PVD) of Ti-C:H hard coating on X20Cr13 ferritic stainless steel. The results showed that the critical load of Ti-C:H films on X20Cr13 could be increased by 80 N through a short time of nitriding (3 hours). Other authors [14] also showed that this duplex treatment worked well on high chromium steels such as X35CrMo17.

With sliding wear tests of Fe-20Cr-1C-1Si-xMn (x = 0 - 25 wt%) done at 25°C up to 450°C in air under contact stress of 103 MPa, the addition of manganese exceeding 10wt.%, improved the high temperature wear resistance of the Fe-20Cr-1C-1Si alloy [15]. Low friction reduced the tendency to gall, because it leads to limited growth of the contacting areas. Galling could also be reduced by factors such as high hardness, rapid work hardening, and a low surface energy. These factors were investigated by Wiklund and Hutchings [16] to eliminate the notorious susceptibility towards galling of titanium (Ti) and its alloys (e.g. Ti6Al4V (Ti-6 wt.% Al-4 wt.% V)). To eliminate galling at higher contact loads, adequate coating adhesion and cohesion played an important role, but high surface hardness and reduced ductility were a prerequisite.

2.2 Conclusion

The surveyed literature addressed the testing of different valve materials and tests conducted on hard coatings under various simulated conditions. One article dealt with the decrease in valve sealing surface contact under high temperature helium conditions (no reference to pressure indicated) [1]. No literature was found on the prevention of materials welding under

high temperature pressurised helium conditions. Therefore, a study was required to test the influence of high temperature pressurised helium on valve materials.

2.3 Purpose of the study

Taking into account the possible gain in controllability of the PBMR via "hot valves", the purpose of the study was defined.

An experimental setup was required to study the effects of high temperature pressurised helium (with T ≈ 720°C and P ≈ 52bar) on valve materials. It was envisaged that the test facility should consist of the following systems:

a. Pressure vessel (*) for simulation of high pressure and temperature conditions,
b. test specimens to simulate the contact stresses between the valve sealing surfaces, and
c. instrumentation for process control purposes.

(*) A test facility was required in which it was possible to simulate all process conditions, including hydrostatic pressure. It is reported [18] that hydrostatic pressure or triaxial compressive stress resists fracture, increases the ductility of materials, and influences crack propagation but not crack initiation. Hot isostatic pressing (HIP) also closes porosities in castings and powder metallurgy parts, and serves to improve the ductility and toughness of materials used as valve seat or part materials. Thus, material properties change with the variation of hydrostatic pressure.

This thesis deals with the design of the test facility. In a follow-up study, the abovementioned systems will be manufactured and testing of the valve materials attempted. Therefore it was a further aim of this study to develop the experimental procedure required in order to conduct tests. This material tests should be conducted according to the procedures put forward in Chapter 4.

The design of the pressure vessel is described in Chapter 3 according to the ASME VIII Boiler & Pressure Vessel Code, Division 1 of 2001 [30]. The required instrumentation is also discussed in this chapter.

The design and specification of the test setup is presented in Chapter 4. This design deals with the design of the test specimens as well as the calculations to predict the required initial

helium pressure conditions, based on the operating conditions. The testing procedure is presented in this chapter.

In Chapter 5 a finite element analysis of the pressure vessel is presented. This analysis includes the temperature and stress distribution in the vessel parts. This analysis was done to simulate the operating conditions of the pressure vessel. The stresses calculated by means of this analysis are compared with ASME VIII calculated results. The FEA is presented in a separate chapter to ensure ease of readability, and to describe the ALGOR FEA process.

All relevant calculations and drawings are shown in the Appendixes.

Chapter 3: Pressure Vessel Design

In this chapter the design of the pressure vessel is presented. The design is based on the 2001 ASME Boiler and Pressure Vessel code, Section VIII: Rules for Construction of Pressure Vessels, Division 1 [30]. Material properties were obtained from the 2001 ASME Boiler and Pressure Vessel code, Section II: Materials, Part D [31].

3.1 Conceptual design

The need for the design of a pressure vessel was mentioned previously. Conceptually the design of the pressure vessel involved a vessel capable of maintaining its strength at specific operating conditions. Provision was made for external input interfaces, such as electrical cabling, purging devices, pressure relieving devices, instrumentation, etc. The specific uses for the vessel governed the size of the vessel.

The manufacturing of parts of the pressure vessel could be done by forging, casting or rolling of the plate. Various pressure vessel parts could be of welded construction or could be seamless. The need to possibly test assembled valves in the vessel was a major contributor to the choice of the vessel size. The size of the vessel was further determined by the way in which the helium gas was heated and the amount of nozzles used for external inputs. The pressure vessel orientation could be horizontal or vertical. Two vessel concepts are shown in Figure 3-1.

The vessel was designed to simulate the operating conditions of the sealing surfaces of the proposed power turbine bypass-valve for the PBMR. These conditions included the helium pressure and temperature as well as the valve sealing contact pressure.

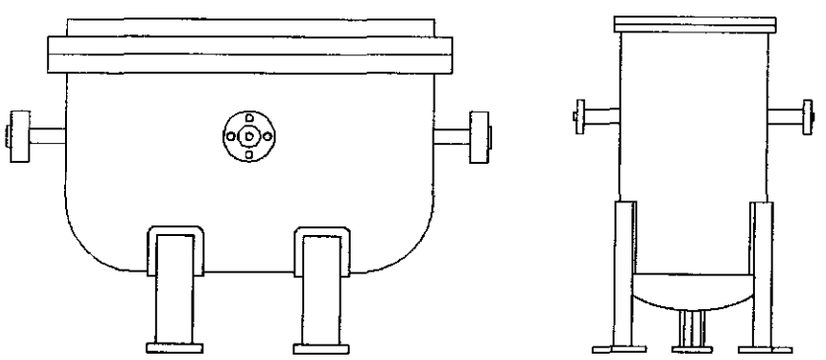

Figure 3-1: Early pressure vessel concepts

3.2 Design constraints

The low pressure turbine outlet temperature and pressure of the V704 Demonstration Plant (MPS-SS0051) were indicated as 716.7 °C and 51.48 bar by engineers from the PBMR project. Therefore, the design of the pressure vessel was done using the following design restrictions:

P_{Design} = 55 bar (Maximum operating pressure 52 bar).
T_{Design} = 732.22 °C (1350 °F) (Maximum operating temperature 720 °C).
Vessel inside diameter: 400 mm.
Vessel type: Horizontal vessel.
Operating gas: Helium.
Heater type: Resistance heating.

The pressure vessel was divided into the following components:

- Vessel shell.
- Heads (Ellipsoidal and/or flat).
- Flanges (ASME B16.5 and Appendix 2) and gaskets.
- Heater.
- Insulation.
- Saddle.
- Instrumentation.

3.3 Detail pressure vessel design

The design started with a material selection for the various pressure vessel parts from ASME II, Part D. There are only a limited number of materials that can be used at and above 720°C. The heat input control will ensure that the helium temperature will not exceed 722°C (§ 3.3.7). Therefore a design temperature of 1350°F (732.22°C) was selected.

Materials listed in ASME II, Part D are divided into ferrous and nonferrous materials. The first criterion of the search was to identify materials usable at the design temperature. The following tables list various usable materials at this temperature. Table 3-1 lists the usable ferrous materials while the usable nonferrous materials are listed in Table 3-2 for the aforementioned design conditions. Bolt materials for the pressure vessel are listed in Table 3-3, which includes ferrous and nonferrous materials.

Table 3-1: Usable ferrous materials according to Table 1A of ASME II, Part D [31] for the design condition of 1350 °F

Form	Spec No.	Type/ Grade	UNS No.	Group No.	S (bar) @ 1350 °F
Forging	SA-182	F304H	S30409	1	199.95
Casting	SA-351	CF8	J92600	1	186.16
Plate	SA-240	304H	S30409	1	199.95
Forging	SA-182	F316H	S31609	1	213.74
Casting	SA-351	CF8M	J92900	1	193.05
Plate	SA-240	316H	S31609	1	213.74

where: S is the maximum allowable stress in the material at design conditions.

Table 3-2: Usable nonferrous materials according to Table 1B of ASME II, Part D for the design condition of 1350 °F

Form	Spec No.	Commercial name	Type/ Grade	UNS No.	Class/ Cond./ Temper	S (bar) @ 1350 °F
Forging	SB-564	Haynes 230	-	N06230	Solution ann.	579.16
Plate / sheet	SB-435	Haynes 230	-	N06230	Solution ann.	579.16
Bar	SB-572	Haynes 230	-	N06230	Solution ann.	579.16
Seamless pipe	SB-622	Haynes 230	-	N06230	Solution ann.	579.16
Forging	SB-564	Inconel 625	1	N06625	Annealed	Max temp 1200°F
Plate / sheet	SB-443	Inconel 625	2	N06625	Solution ann.	586.05
Bar	SB-446	Inconel 625	2	N06625	Solution ann.	586.05
Seamless pipe	SB-444	Inconel 625	2	N06625	Solution ann.	586.05

where: S is the maximum allowable stress in the material at design conditions.

Table 3-3: Usable bolt materials according to Table 3 of ASME II, Part D for the design condition of 1350 °F

Requirements	Spec No.	Type/ Grade	UNS No.	Class/ Cond./ Temper	S (bar) @ 1350 °F
Ferrous metal					
-	SA-193	B8P	S30500	1	199.95
Carbon > 0.04%	SA-193	B8M	S31600	1	213.74
Carbon > 0.04%	SA-193	B8	S30400	1	199.95
Nonferrous metal					
-	SB-572	-	N06002	Annealed	420.58
-	SB-408	-	N08800	Annealed	110.32
-	SB-408	-	N08810	Annealed	262
-	SB-572	-	R30556	Annealed	482.63

where: S is the maximum allowable stress for bolt materials at design conditions.

To determine which type of material to use for the vessel, a shell thickness calculation (equation (3.1)) for a shell under internal pressure was done, using the equation from ASME VIII Div. 1 part UG-27 [30].

$$t = \frac{PR}{SE - 0.6P} \tag{3.1}$$

where: P = internal design pressure (bar)
R = inside radius of shell (mm)
S = maximum allowable stress value at 732.22°C (bar)
E = joint efficiency (E = 1, based on full radiographic examination, typical)

The shell (effectively a pipe) that can be blanked on the sides to contain the pressurised gas inside the vessel is a first option. To be able to insert the test specimens into the vessel, flanges are required on the shell ends.

Subsection B of ASME VIII deals with the requirements pertaining to the methods of fabrication of pressure vessels. The requirements for pressure vessels fabricated by welding are described in Part UW of ASME VIII. Welded pressure vessel joints are divided into four categories. Figure 3-2 illustrates typical joint locations included in these categories.

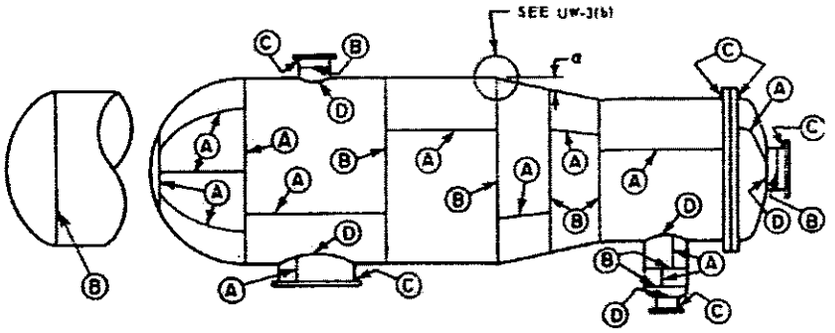

Figure 3-2: Locations typical of Categories A, B, C, and D welded joints (extracted from ASME VIII - Part UW [30]).

Category A joints include: longitudinal welded joints within the main shell, transitions in diameter, or nozzles; any welded joint within a formed or flat head; circumferential welded joints connecting hemispherical heads to abovementioned parts.

Category B joints include: circumferential welded joints within the main shell, nozzles, or transitions in diameter; circumferential welded joints connecting formed heads excluding hemispherical to abovementioned parts.

Category C joints include: welded joints connecting flanges, tubesheets, or flat heads to main shell, to formed heads, transitions in diameter or nozzles.

Category D joints include: welded joints connecting nozzles to main shell, transitions in diameter or heads.

The weld joint categories are further related to the joint efficiency through the joint types. UNF-56 of ASME VIII states that no postweld heat treatment is required for a pressure vessel constructed through welding, from nonferrous material UNS. N06230. Radiographic examination of welded butt joints, in vessels constructed of nonferrous materials, should be done for their full length when the vessel wall thickness exceeds 10 mm (UNF-57 of ASME VIII). Therefore, full radiographic examination is required. This in turn determines the joint efficiency, E. Joint efficiency depends only on the type of joint and the degree of examination of the joint. All full radiographic examined joint categories have a joint efficiency, E of 1, when the joints are of Type No. 1 from Table UW-12 of ASME VIII. The design of the vessel was based on full radiographic examined joints of Type No. 1 (joint efficiency, E = 1).

Using the aforementioned design constraints the minimum shell thickness for ferrous and nonferrous materials was calculated. The minimum required shell thickness for a ferrous material vessel is 66 mm. The minimum required shell thickness for a nonferrous material vessel is 20 mm. This calculation showed that the vessel and all its components should be designed and manufactured from nonferrous materials (thinner vessel parts relate to a lower vessel weight, and allowable material stress for nonferrous materials are higher).

Accordingly, the pressure vessel was designed using the data for nonferrous materials with UNS No. N06230 in all available forms (Table 3-2). UNF-12 of ASME VIII states that nonferrous bolts should be used with a nonferrous pressure vessel. SB-572 with UNS No. R30556 was therefore chosen as the bolt material used in this design.

The design of the components of the pressure vessel is discussed below.

3.3.1 Vessel shell

The thickness of the vessel shell under internal pressure was calculated using equations from UG-27 of ASME VIII. The material form is a seamless pipe. Material properties used for the shell are ASME SB-622 with UNS no. N06230 (Commercially: Haynes ® Alloy 230). The required shell thickness is the larger of the longitudinal (equation (3.2)) and circumferential (equation (3.3)) stress thicknesses based on ASME VIII UG-27,

$$t_{longitudinal} = \frac{PR_i}{2SE + 0.4P} = 9.32\ mm \tag{3.2}$$

$$t_{circumferential} = \frac{PR_i}{SE - 0.6P} = 20.141\ \text{mm} \tag{3.3}$$

where: P = internal design pressure (bar)
R_i = inside radius of shell (mm)
S = maximum allowable stress value at 732.22°C (bar)
E = joint efficiency (E = 1, based on full radiographic examination, typical)

Adding a corrosion allowance of 3 mm, the required shell thickness is accordingly 23.141 mm. The nominal specified thickness to be used is 25 mm.

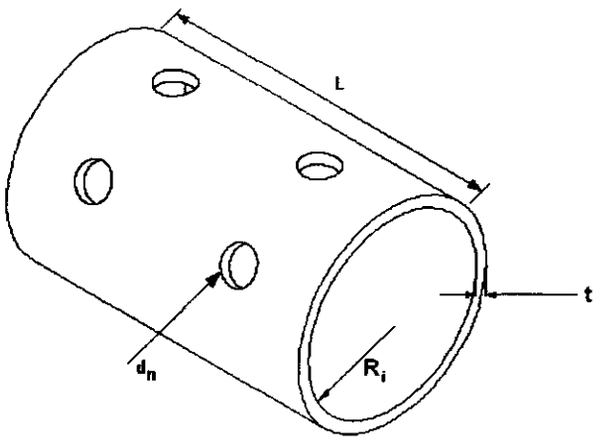

where: t = 25 mm
(nominal shell thickness)
L = 700 mm
(length of pressure vessel shell)
R_i = 400 mm
(inner pressure vessel shell radius)
d_n = 79.2 mm
(nozzle hole diameter)

Figure 3-3: Shell dimensions (Appendix 7: drawing VS_SHELL)

3.3.2 Heads

The shell ends are closed with heads. The left head (ellipsoidal 2:1) could be welded onto the shell, while the right head could be a flat head, bolted to an ASME VIII Appendix 2 flange as shown in Figure 3-4(a). This configuration was changed to a shell with two ASME VIII Appendix 2 flanges with bolted flat heads (shown in Figure 3-4(b)). This flange-head arrangement (Figure 3-4(b)) was chosen to enable entry to the vessel from both sides (inserting test specimens from one side and for heating system lead-outs on other side).

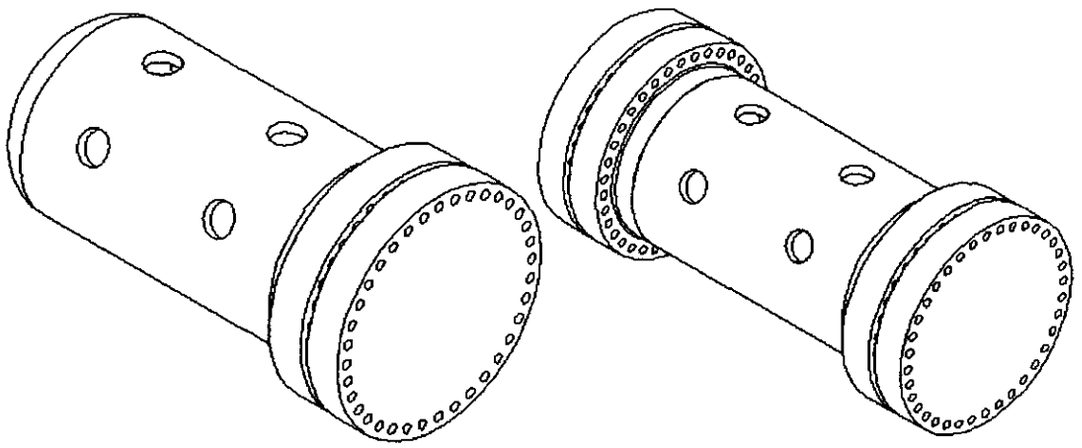

(a) (b)

Figure 3-4: Pressure vessel shell with heads

The following section describes the design of the flat head.

The thickness of the unstayed flat head under internal pressure was calculated using equations from UG-34 of ASME VIII. The type of head is described in Figure UG-34(j) of ASME VIII. The material form is a normalised plate. The flat head can be machined or forged. Material used for the flat head is ASME SB-435 with UNS no. N06230 (Commercially: Haynes ® Alloy 230). The required head thickness was calculated using equation (3.4).

$$t_{head} = d\sqrt{\frac{CP}{SE} + \frac{1.9Wh_{gg}}{SEd^3}} = 87.63 \text{ mm} \qquad (3.4)$$

where: P = internal design pressure (bar)

C = factor depending on method of attachment (from ASME VIII, Figure UG-34(j))

d = outer diameter of shell (mm)

S = maximum allowable stress value at 732.22°C (bar)

E = joint efficiency

W = total bolt load for circular heads (kN)

h_{gg} = gasket moment arm (mm) (see Figure 3-5) (see Appendix 4)

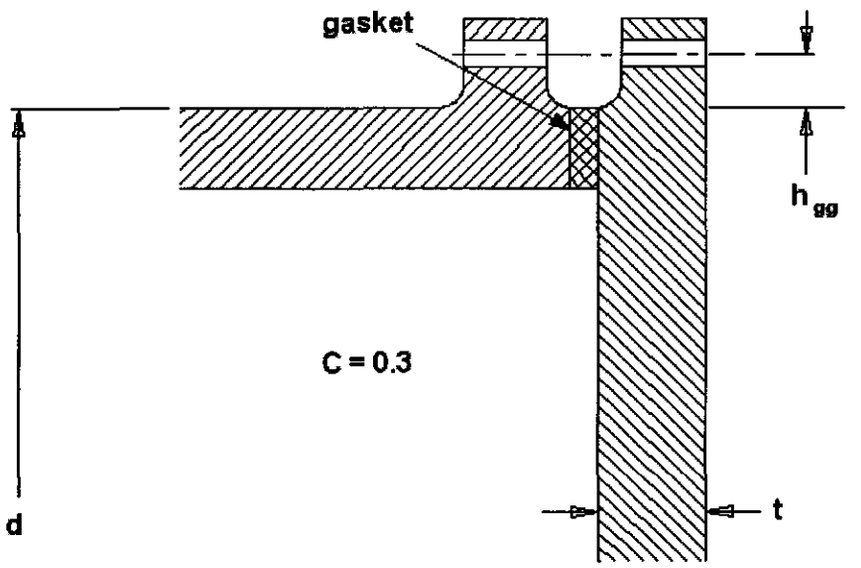

Figure 3-5: Flat head dimensions (Appendix 7: drawing VS_HEAD)

Including a corrosion allowance of 3 mm, the required head thickness is 90.63 mm. The nominal specified thickness to be used, is 92 mm. The worked calculations are presented in Appendix 2.

3.3.3 Flanges

The design of the flanges under internal pressure was done according to ASME B16.5 and Appendix 2 of ASME VIII Div. 1. The material form is a forging. Material used for the flanges is ASME SB-564 with UNS no. N06230 (Commercially: Haynes ® Alloy 230).

Standard Class 2500 long welding neck flanges, according to ASME B16.5, are used for the instrumentation and other outlets of the pressure vessel. The flanges for the unstayed flat heads were designed according to Appendix 2 of ASME VIII because ASME B16.5 does not cover this size.

- Class 2500 long welding neck flanges

These flanges' dimensions were obtained from the book of E.F. Megyesy [22] (not listed in referred version of ASME B16.5). The dimensions are shown in Figure 3-6 and listed in Table 3-4.

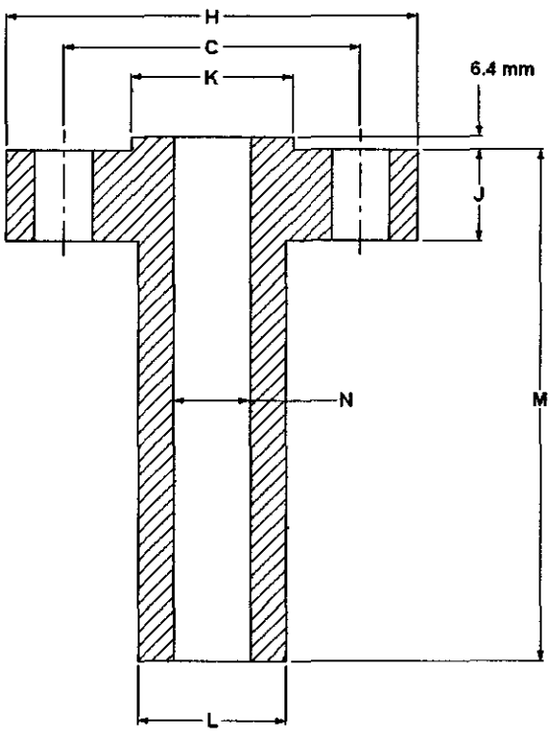

Figure 3-6: ASME B16.5 Class 2500 long welding neck flange (Appendix 7: drawing FL_LWN_DETAIL)

Table 3-4: Dimensions of ASME B16.5 Class 2500 long welding neck flanges (refer to Figure 3-6)*

Nominal pipe size	C	H	J	K	L	M	N	Bolt diam.	Bolt hole diam.	No. of bolts
1½"	146.05	203.2	44.45	73.025	79.375	304.8	38.1	30	32	4
2"	171.45	234.95	50.8	92.075	95.25	304.8	50.8	26	29	8
2½"	196.85	266.7	57.15	104.775	127	304.8	63.5	30	32	8
3"	228.6	304.8	66.68	127	133.35	304.8	76.2	32	35	8

* Dimensions in mm unless otherwise stated

Reinforcement calculations are required for openings in the vessel shell and/or heads if nozzles are used. The reinforcing calculations were done according to UG-37 (shell and formed heads) and UG-39 (flat heads) of ASME VIII Div. 1. In these calculations the available area of reinforcement must exceed the required area of reinforcement (A). Figure 3-7 defines the dimensions for the calculations. The complete reinforcement calculations are given in Appendix 3.

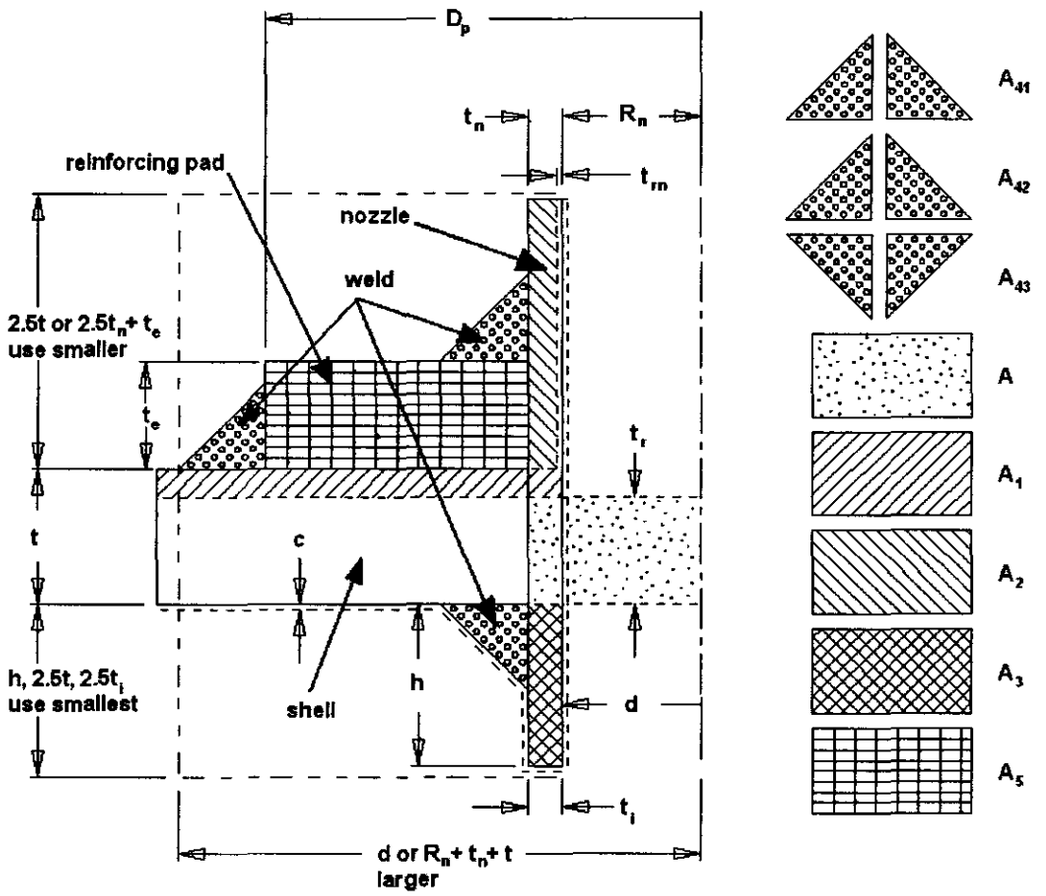

Figure 3-7: Nomenclature for reinforced openings

where: A is total cross-sectional area of reinforcement required, in plane under consideration,

A_1 is area in excess thickness in the vessel wall, available for reinforcement,

A_2 is area in excess thickness in the nozzle wall, available for reinforcement,

A_3 is area available for reinforcement when the nozzle extends into the vessel wall,

A_{41} is area available in outward weld for reinforcement,

A_{42} is area available in outer weld for reinforcement,

A_{43} is area available in inward weld for reinforcement and

A_5 is cross-sectional area of material, which is added as reinforcement.

For openings without a reinforcement pad (UG-37) equation (3.5) must be met for adequate reinforcement of an opening:

$$A_1 + A_2 + A_3 + A_{41} + A_{43} \geq A \tag{3.5}$$

For openings with a reinforcement pad (UG-37) equation (3.6) must be met for adequate reinforcement of an opening:

$$A_1 + A_2 + A_3 + A_{41} + A_{42} + A_{43} + A_5 \geq A \tag{3.6}$$

For an opening in a shell or formed head under internal pressure the total cross-sectional area for required reinforcement (UG-37) is:

$$A = dt_r F + 2t_n t_r F(1 - f_{r1}) \tag{3.7}$$

For an opening in a flat head, not exceeding one-half of the head diameter (UG-39), equation (3.8) defines the total cross-sectional area of required reinforcement:

$$A = 0.5dt + tt_n(1 - f_{r1}) \tag{3.8}$$

where d is finished diameter of circular opening,
t_n is nozzle wall thickness and
f_{r1} is a strength reduction factor.

- Appendix 2 flange

The maximum size of Class 2500 flanges covered by ASME B16.5 is 12" (304.8 mm). The outer diameter of the pressure vessel is 450 mm. Therefore, a flange had to be designed for this application. The selected type of flange is described in Figure 2-4(6) of ASME VIII. Due to the high temperature and pressure, an integral type flange was selected (personal communication with various pressure vessel designers).

Gaskets are an integral part of the flange design process set forth in Appendix 2 of ASME VIII. Flange design is done for two load cases: (a) operating conditions, and (b) gasket seating conditions. To calculate the minimum required bolt load for either operating or gasket seating condition, two gasket factors are required. Table 2-5.1 of Appendix 2 of ASME VIII lists values for m and y for different types of gaskets, to use in the design of the flange. Factor m is used to determine the required bolt load for flange operating conditions, while factor y is used to calculate the required bolt load for flange seating conditions. Due to the possible high surface temperature, the gasket material was carefully selected from this list. Two types of gaskets were investigated; (a) spiral-wound metal, asbestos filled group and (b) corrugated metal, asbestos inserted, or (c) corrugated metal, jacketed asbestos filled. The

gasket factors, m and the minimum design seating stresses, y for different gasket material options are shown in Table 3-5.

Table 3-5: Gasket materials and factors m and y [30]

Gasket material	Gasket factor m	Min. design seating stress y, (MPa)	Sketch
Spiral-wound metal, asbestos filled:			
Carbon	2.50	69	
Stainless, Monel, and Nickel-base alloys	3.00	69	
Corrugated metal, asbestos inserted, or corrugated metal, jacketed asbestos filled:			
Soft aluminium	2.50	20	
Soft copper or brass	2.75	26	
Iron or soft steel	3.00	31	
Monel or 4% - 6% chrome	3.25	38	
Stainless steel and nickel-base alloys	3.50	45	

The gasket selection process was based on the minimum required bolt load for the two abovementioned flange conditions. A corrugated metal, asbestos inserted, or corrugated metal, jacketed asbestos filled soft aluminium gasket was selected as the required gasket type. The gasket has an outer diameter of 465.5 mm, a contact width of 15 mm, and a thickness of 5 mm.

Repetitive flange calculations were done to define the dimensions of the flange. The final flange dimensions as shown in Figure 3-8, are defined in Table 3-6. The worked calculations are presented in Appendix 4.

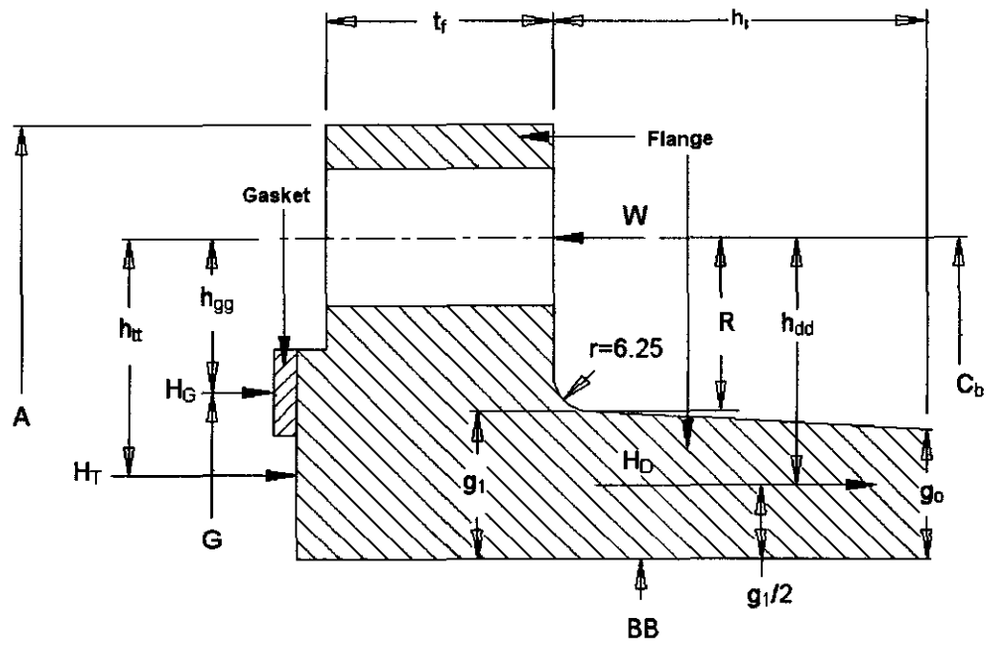

Figure 3-8: ASME VIII Appendix 2 sectioned flange (Appendix 7: drawing FL_APP2)

Table 3-6: ASME VIII Appendix 2 flange calculated design dimensions (refer to Figure 3-8)

Dimension	Description	Value
A	Outer diameter of flange (mm)	570
BB	Inside diameter of flange (mm)	400
C_b	Bolt circle diameter (mm)	516.25
G	Gasket load reaction diameter (mm)	462.76
g_1	Thickness of hub at back of flange (mm)	26.5
g_0	Thickness of hub at small end (mm)	25
H_D	Hydrostatic end force on area inside of flange (kN)	690.8
h_{dd}	Radial distance from bolt circle to circle on which H_D acts (mm)	44.88
H_G	Gasket load (kN)	846.5
h_{gg}	Radial distance from gasket load reaction to bolt circle (mm)	26.74
h_l	Hub length (mm)	60
H_T	Difference between total hydrostatic end force and hydrostatic end force on area inside of flange (kN)	233.8
h_{tt}	Radial distance from bolt circle to circle on which H_T acts (mm)	42.43
r	Fillet radius, at least $0.25g_1$ but larger than 4.76 mm (mm)	6.25
R	Radial distance from bolt circle to point of intersection of hub and back of flange (mm)	31.63
t_f	Flange thickness (mm)	90

The design results of this flange included the total bolt load required for adequate sealing of the pressure vessel. This bolt load was calculated for gasket seating conditions and operating conditions. The maximum of the aforementioned bolt loads was used to calculate the flange bolt preload. The required preload torque for the bolts used with this flange was 275 N·m. The flat unstayed head is to be bolted to this flange with 36, M20 x 250 mm (fine pitch series), SB-572 (UNS No. R30556) bolts.

3.3.4 Heater design

Various types of electrical heaters were considered for heating the helium gas. The first was a flanged immersion type heater, another was a heater with resistance heating alloy wound around ceramic tubes inserted directly into the helium atmosphere, and the last was a heater fitted inside a thermowell. The first two heater type concepts are shown in Figure 3-9.

The maximum usable design temperature for flanged immersion type heaters (Figure 3-9(a)) is about 600°C with an Inconel sheath. No standard designed Class 2500 flanged immersion heaters were available. Therefore, another type of heater was required.

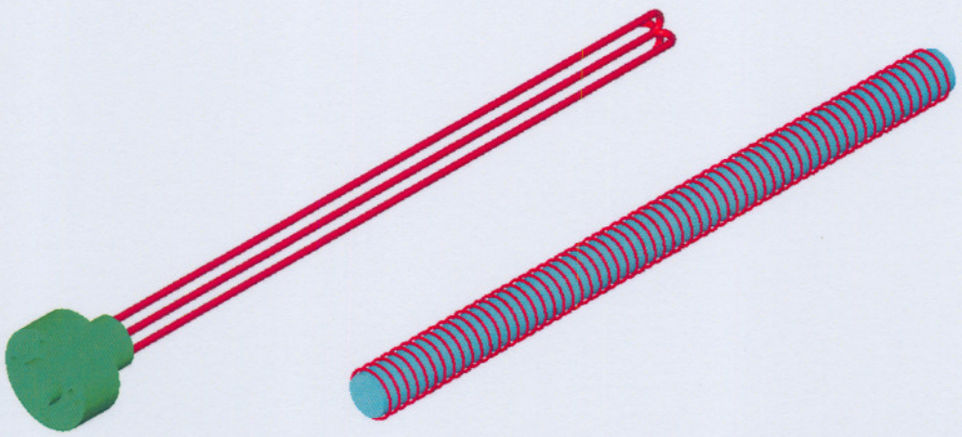

(a) **(b)**

Figure 3-9: Heater type concepts

An alternative heater design was done with assistance from Kanthal SA. Two ceramic heater tube configuration concepts were generated (see Figure 3-10). Figure 3-10(a) shows the ceramic tubes in a radial direction (horizontally) inside the vessel. Figure 3-10(b) shows the ceramic tubes placed longitudinally inside the vessel. The ceramic tubes are fitted with larger diameter ceramic stoppers at the end of the tubes. This was done because the element wires lengthen during operation and could cause an unwanted electrical short.

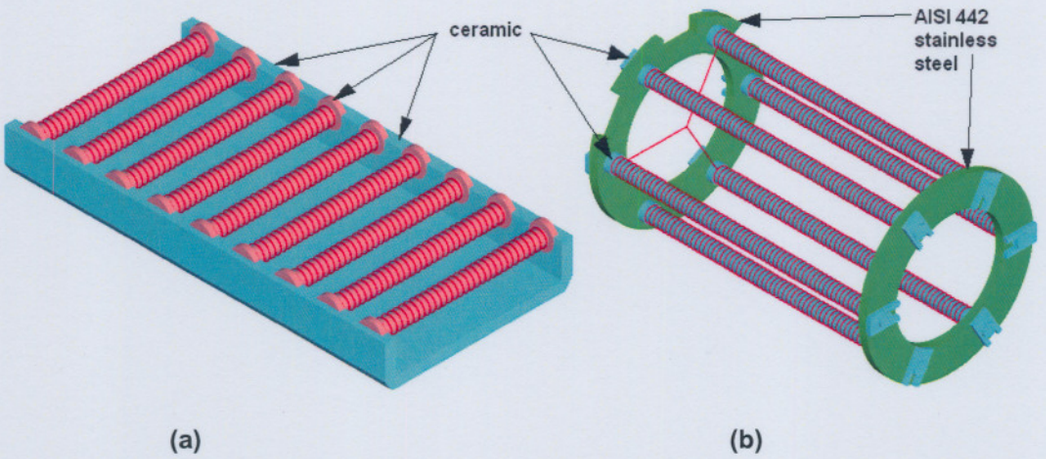

Figure 3-10: Ceramic heater tube configuration concepts

Configuration b of Figure 3-10 uses ceramic tubes inserted through two metal rings made from AISI 442 stainless steel (described below). One of these rings has portions removed, as can be seen in Figure 3-10(b), to be able to insert the assembled heater into the vessel after the long welding neck flanges has been welded into the shell. Configuration b uses less space in the vessel, while allowing space for a platform for test specimens. It was envisaged that this configuration would also heat the gas more efficiently.

The design shown in Figure 3-10(b) was modified by using hollow ceramic tubes. In this design threaded bars were inserted through the tubes and fastened to the metal rings with nuts on either side of the rings. The end of the tubes, made use of larger diameter ceramic rings to stop any contact between the expanding element wires and metal parts (See Figure 3-11).

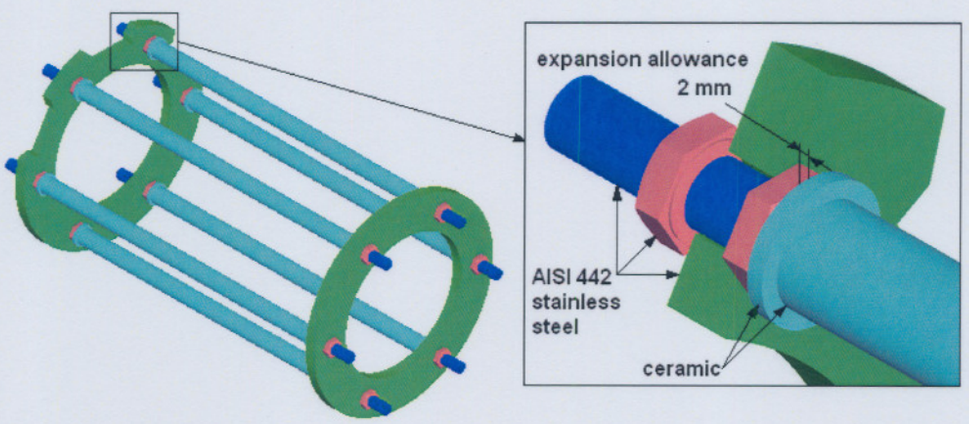

Figure 3-11: Modified heater concept (Appendix 7: drawing group INST_HEA)

A material search for the heater rings was done using CES (Cambridge Engineering Selector) software based on two graph selection stages. Stage 1 plotted thermal expansion (μstrain/°C) of the metal subset against price (ZAR/kg), while stage 2 plotted endurance limit (MPa) against maximum service temperature (°C). From this two-stage search AISI 442 stainless steel was selected as adequate.

This design further boasts a platform fitted in the heater assembly. Two holding rings are to be welded to the inside of each of the heater metal rings (Figure 3-12, Figure 3-13(a)). A metal rod insulated with a ceramic tube is then connected to these rings (Figure 3-13(b)). The ceramic platform is then placed on top of the ceramic tubes (Figure 3-13(c)). Ceramic tubes are used to ensure no unwanted electrical contact can occur.

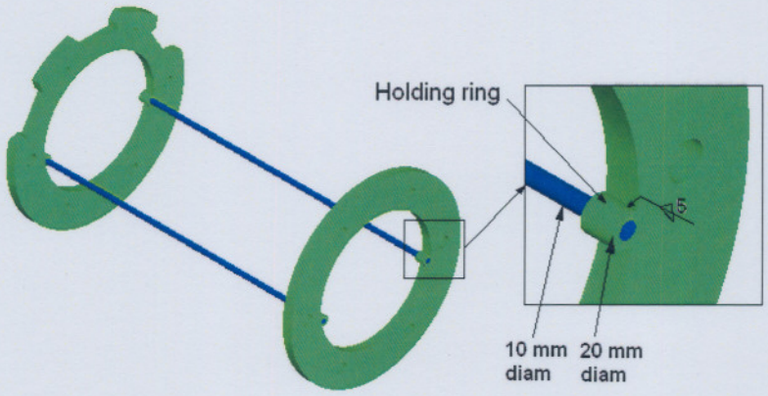

Figure 3-12: Heater platform holding ring (Appendix 7: drawing group INST_HEA_PLAT)

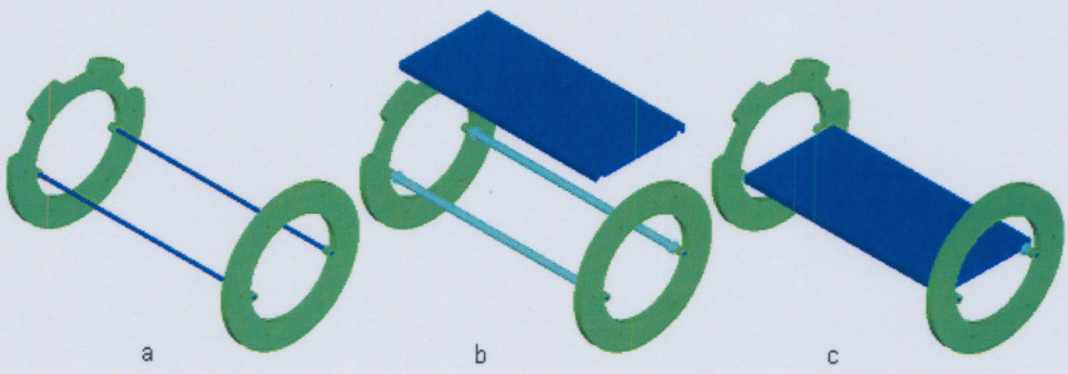

Figure 3-13: Heater platform assembly (Appendix 7: drawing group INST_HEA_PLAT)

Standard Kanthal APM ® heating element needs to be oxidised before use, therefore NiCr elements (Nikrothal ®) [36] must to be used. When used in an inert environment (He), APM elements cannot oxidise and form Al_2O_3, which is needed for the protective layer around the element wire. There are three element wires required for heating the gas. One end of each

element wire has to leave the pressure vessel for connection to the electric supply. The remaining three ends of the element wires are connected to each other (star point) and remain inside the pressure vessel. Small ceramic tubes (10 mm long) should be fitted over the wires, which will ensure that the wire could hang in its normal flexed position.

The calculations of the required power and time needed to heat the gas and pressure vessel were based on a heater heat transfer efficiency of 70%. The time to heat the vessel was based on the mass of the pressure vessel to be heated to 720°C. The specifications of the heater are summarised in Table 3-7.

Table 3-7: Heater specifications

Description	
Ceramic tube diameter	30 mm
Ceramic tube length	600 mm
Number of ceramic tubes	6
Diameter of element wire	2 mm
Pitch of element wire	4 mm
Element material	NiCr element (Nikrothal ®)
Electrical supply	400 V (3 phase)
Rated power consumption	15 kW (18 kW MAX)
Vessel heating time	4 hours

The three electrical lead-outs would have to exit the vessel through a specifically designed nozzle.

Using the information given in this table, the copper lead-outs were sized. The maximum power required for the heater was 18kW. For the following design a power requirement of 20kW was used.

To calculate the current per phase, equation (3.9) was used:

$$I = \frac{P}{\sqrt{3} \cdot V \cos\theta} = \frac{20000}{\sqrt{3} \cdot 400 \cdot 0.9} = 32\ Amp \qquad (3.9)$$

where: $\cos\theta$ = power factor of load

Using this calculated current the required wire diameter was 2.5 mm [28]. For the rated power consumption (Table 3-7), the current per phase would be 24 Amp (further decrease in required wire diameter). The required wire diameter was also calculated based on the wire resistivity.

As shown in the ASM Metals Handbook [25] the resistivity (ρ) of a metal increases with an increase in temperature. Generally, the resistivity of metal varies with temperature as given in equation (3.10) [25]:

$$\rho_T = \rho_{273}\left[1+0.005(T_K - 273)\right] \tag{3.10}$$

where: T_K = Temperature in Kelvin

Benedict [27] states the resistivity of copper at 273 K as 1.56×10^{-6} Ω.cm. The resistivity of copper at various temperatures was calculated using the previous equation. The results are shown in Table 3-8.

Table 3-8: Resistivity (ρ) of 0.04% oxide copper alloy at various temperatures

T (°C)	0	20	200	720
ρ (μΩ.cm)	1.56	1.716*	3.12	7.176

* The calculated resistivity of 0.04% oxide copper at 20°C related well to the tabulated value of 1.72 μΩ.cm [25]. 0.04% Oxide copper (UNS C11000) has an IACS conductivity rating of 100% [25].

The total length of the copper lead-out can be approximated from the total length (367.05 mm) of a Class 2500 1½" blind flange bolted to a Class 2500 1½" long weld neck flange. The maximum length of the lead-out would be 410 mm, which included adequate length for cable connections to the treaded ends of the lead-out. The lead-out was divided into different anticipated temperature zones. The first zone was the part inside the vessel in contact with the helium gas. The second zone of the lead-out was the length inside the nozzle, while the third zone was the piece connected to the external electrical supply. The proposed temperature zone lengths are shown in Table 3-9.

Table 3-9: Lead-out temperature zone lengths

	Length (mm)	Zone Temperature (°C)
Zone 1	24	720
Zone 2	361	200*
Zone 3	25	20

(* Prescribed temperature with cooling system)

The relation between the resistance (R) and the resistivity (ρ) of an electrical conductor with length ℓ and cross sectional area A is:

$$R = \rho \frac{\ell}{A} \tag{3.11}$$

Thus, the electrical resistance of each of the lead-out temperature zones could be calculated. Using the simple relation of Ohm's law:

$$V = I \cdot R \tag{3.12}$$

For the specified design power requirement of 20 kW, the current was previously calculated from a three phase electrical supply of 400 V as 32 Amp (equation (3.9)). Substituting (3.11) into (3.12) we obtain an expression for the diameter of the conductor:

$$D = \sqrt{\frac{4\rho I \ell}{\pi V}} \tag{3.13}$$

The minimum required diameter, based on conductor resistivity and constant resistance of the various temperature zones of the lead-out, is shown in Table 3-10.

Table 3-10: Minimum required lead-out zone diameters

	Zone 1	Zone 2	Zone 3
Minimum required diameter (mm)	0.013	0.034	0.0063
Zone length (mm)	24	361	25
Zone temperature (°C)	720	200	20

From this table the minimum required diameter for the lead-out should exceed 0.034 mm. As shown in drawing INST_ELO_CRR of Appendix 7 the minimum diameter used for the lead-out was 2.5 mm.

A standard Class 2500 1½" blind flange was used as holder for the lead-outs (Figure 3-14). Three taper holes are to be machined into the flange as lead-out exits (Entry diameter: 13 mm, exit diameter: 5.5 mm, which related to a taper angle of $\alpha = 1.909°$). Under operating conditions, the lead-out will press against the surfaces of the tapered hole, sealing the flange exit from leaking helium gas. The lead-out material is 0.04% oxide copper (UNS C11000).

R-1600 RTV Silicone rubber from NuSil Technology [26] can be used as a pressure and electrical contact sealant. The maximum allowable service temperature of this RTV rubber is 260°C. The copper lead-outs were designed with a ribbed cross section (CRR) as shown in Figure 3-14. The RTV rubber could therefore flow into all possible holes and serve as interfaces between the long welding neck flange and three electrical lead-outs. The interface between the inner most 140 mm of the long weld neck flange and the lead-out should be insulating material (Zircar - Alumina ZAL 15) [35], to delay the heat transfer from the gas to the RTV rubber (Figure 3-15). The CRR and RTV rubber would then be inserted into the long welding neck flange as per NuSil recommended procedure. The end of the lead-out would exit the blind flange and be held in position by another blind flange (Figure 3-14 - end), which should be bolted to the 1½" blind flange (holder).

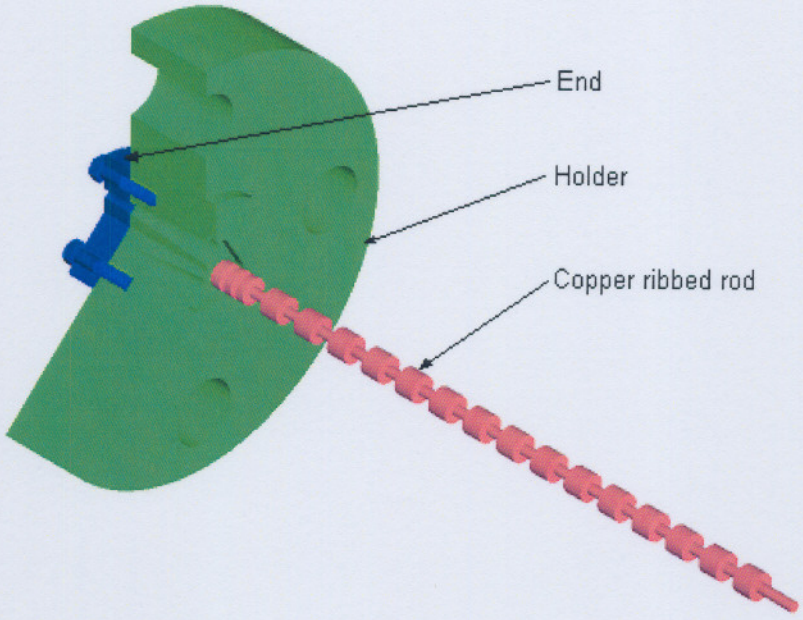

Figure 3-14: Electrical lead-out assembly (Appendix 7: drawing INST_ELO)

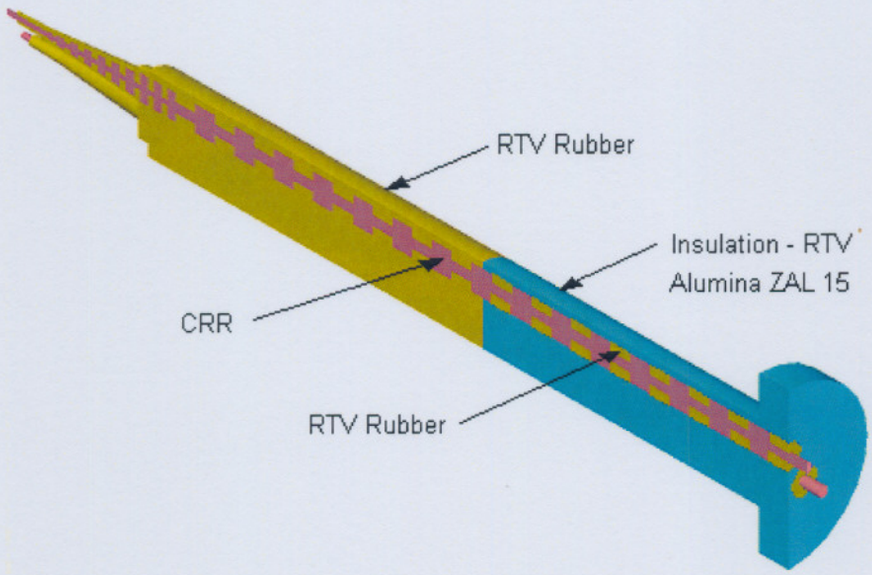

Figure 3-15: Insulation of copper ribbed rod and RTV Rubber

External cooling for the lead-out assembly nozzles required the design of a cooling tower system. The cooling water requirement design was not done in this study; the cooling water system of the PBMM plant could be modified for temporary use for the experiments.

To eliminate this design another type of heater was investigated. The proposed layout was inserting a thermowell into the pressure vessel. An electric heater would then be inserted into the thermowell. The heater would then heat the thermowell, which would heat the helium. Thus, no electrical lead-outs from the pressure vessel would be necessary. The thermowell design was done as a pressure vessel shell under external pressure using equations from UG-28(c)(2) of ASME VIII [30]. Calculations were based on 3" Class 2500 long weld neck flanges. The thermowell would fit into the flange, thus the outer diameter of the thermowell was equal to the inner diameter of the long weld neck flange. The calculation iterations are listed in Table 3-11.

Table 3-11: Calculated properties of proposed thermowell

Nominal pipe size	Thermowell wall thickness (mm)	Inner diameter (mm)	Maximum allowable external pressure (bar)
3"	3	70.2	40.8
3"	7	62.2	117.8
3"	5.6	65	91.5
3"	4.1	68	62.8

The thermowell has an outer diameter of 76.2 mm, an inner diameter of 68 mm with an immersion length of 900 mm. A presentation of the thermowell inside the flanges is shown in Figure 3-16. The design of the thermowell heater installation was stopped due to problems with the availability of small high-energy output heaters. These heaters would also occupy too large a volume of the vessel to insert a test specimen platform of usable size.

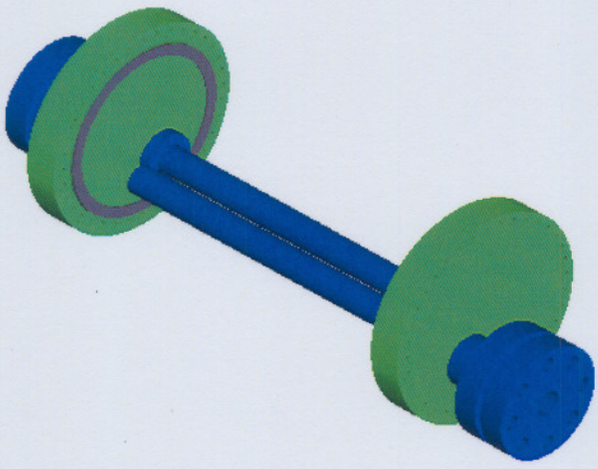

Figure 3-16: Thermowell heater assembly

3.3.5 Insulation of pressure vessel

As discussed in the previous section, the heater was designed for an efficiency of 70%, which is equivalent to an allowable heat loss of 4.5 kW through the vessel wall. The vessel had to be insulated for operator safety reasons. A Silica Blanket [32] (density: 170 kg/m^3) supplied by Intersource USA was selected as a suitable insulation material at the design temperature for the pressure vessel. Another suitable medium of insulation is Alumina Blanket type AB [33] (density: 100 kg/m^3) as supplied by Zircar Ceramics. The standard thickness of both types of blankets is 25 mm. Therefore, if four layers of blanket is used, the total thickness would be 100 mm. The blankets could be held in place with an outer sheet of AISI 316 stainless steel (1 mm thick). Various properties of these insulation blankets are listed in Table 3-12.

Table 3-12: Properties of insulation blankets

Property	Silica blanket (Intersource USA)	Alumina blanket (Zircar Ceramics)
Density (kg/m^3)	170	100
Max. operating temperature (°C)	1100	1600
Thermal conductivity @ 720°C (W/m·K)	0.10213	0.1227

The standard radial heat conduction equation (equation (3.14)) was used to calculate the required insulation thickness for the vessel shell.

$$q_r = \frac{T - T_o}{\frac{\ln\left(r_2/r_1\right)}{2\pi k_{SB-622} L} + \frac{\ln\left(r_3/r_2\right)}{2\pi k_{insulation} L} + \frac{\ln\left(r_4/r_3\right)}{2\pi k_{316\_SS} L}} \qquad (3.14)$$

where: q_r = heat loss through vessel wall

T = vessel wall temperature

T_o = constant surface temperature of insulation holder

k_{SB-622} = coefficient of thermal conductivity of ASME SB-622 (UNS No. N06230)

$k_{insulation}$ = coefficient of thermal conductivity of Silica Blanket from Intersource USA

k_{316_ss} = coefficient of thermal conductivity of AISI 316 stainless steel

L = length of shell

r_i = radial distances as defined in Figure 3-17

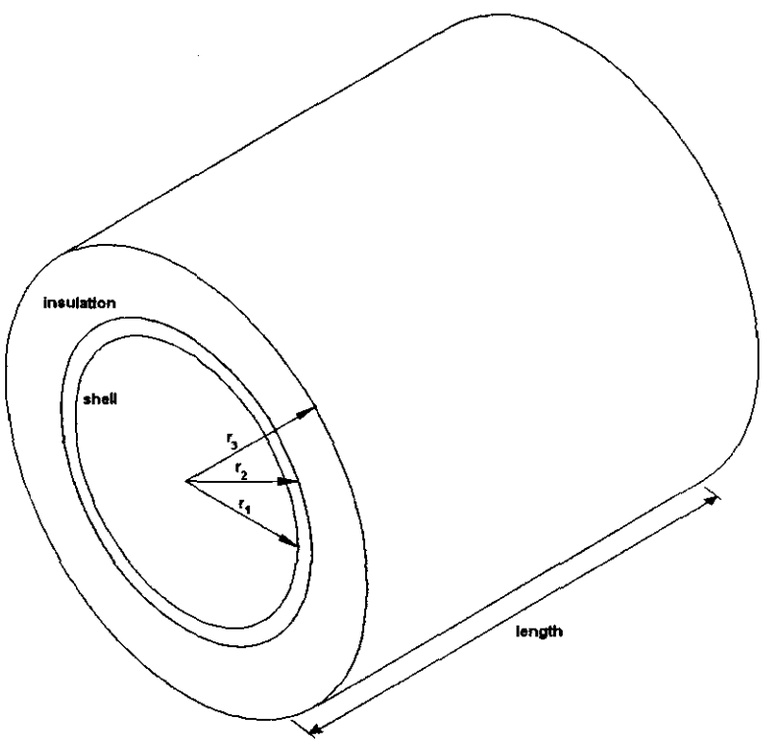

Figure 3-17: Shell and insulation dimensions (Appendix 7: drawing INSU_SHL)

The insulation thickness was calculated using different amounts of heat loss with the maximum heat loss of 4.5 kW. These values are presented in Table A5-2. The results show that the minimum insulation thickness is 15 mm (heat loss: 4.5 kW), while the maximum calculated insulation thickness is 76.14 mm (heat loss: 1 kW) for silica blanket insulation. The

results from this table also show that the minimum insulation thickness is 18 mm (heat loss: 4.5 kW), while the maximum calculated insulation thickness is 94.35 mm (heat loss: 1 kW) for alumina blanket insulation. A standard insulation thickness of 100 mm (4 layers) was therefore selected as sufficient to decrease the heat loss significantly, for a more efficient heating system. Detailed calculations are presented in Appendix 5.

The insulation for the unstayed flat heads was calculated using the standard composite wall heat conduction equation (equation (3.15)):

$$q_x = \frac{T - T_o}{\frac{t_{head}}{k_{SB-622}A} + \frac{t_{insulation}}{k_{insulation}A_{ins}} + \frac{t_{316\_SS}}{k_{316\_SS}A_{SS}}} \tag{3.15}$$

where: q_x = heat loss through head
T = vessel wall temperature
T_o = constant surface temperature of insulation holder
k_{SB-622} = coefficient of thermal conductivity of ASME SB-622 (UNS No. N06230)
$k_{insulation}$ = coefficient of thermal conductivity of Silica Blanket from Intersource USA
k_{316_ss} = coefficient of thermal conductivity of AISI 316 stainless steel
A = cross section area of head
A_{ins} = A + cross section area of thickness of insulation on shell
A_{SS} = A + cross section area of thickness of insulation on shell

The insulation thickness was calculated using different amounts of heat loss with the maximum heat loss of 4.5 kW. These values are presented in Table A5-4. The results from this table show that the minimum insulation thickness is 4.9 mm (heat loss: 4.5 kW), while the maximum calculated insulation thickness is 24.2 mm (heat loss: 1 kW) for Silica blanket insulation. The results also indicate that the minimum insulation thickness is 5.9 mm (heat loss: 4.5 kW), while the maximum calculated insulation thickness is 29 mm (heat loss: 1 kW) for Alumina blanket insulation. An insulation thickness of 25 mm was therefore selected as sufficient to decrease the heat loss significantly, for a more efficient heating system. Detailed calculations are shown in Appendix 5.

3.3.6 Saddle design

Standard designed saddle properties were obtained from E.F. Megyesy [22]. These designs include dimensions and the maximum allowable weight of a vessel. The specified outer diameter of the vessel shell for the selected saddle has to be 457.2 mm. The design calls for

the attachment of a wear plate with a thickness of 3.6 mm to the outside of the vessel shell. This will increase this part of the shell outer diameter from 450 mm to 457.2 mm, which will make it possible to use the selected size saddle.

The specified dimensions as presented in Figure 3-18 are given in Table 3-13. Material used for the parts of the saddle is ASME SB-622 with UNS no. N06230 (Commercially: Haynes ® Alloy 230). The saddle is a welded assembly.

Using the Mass Properties Verification function of CADKEY 99, the pressure vessel weight excluding the saddle was calculated to be approximately 2000 kg (density 8.608 g/cm^3). As shown in Table 3-13 the weight limit of the given saddle is 28122 kg [22].

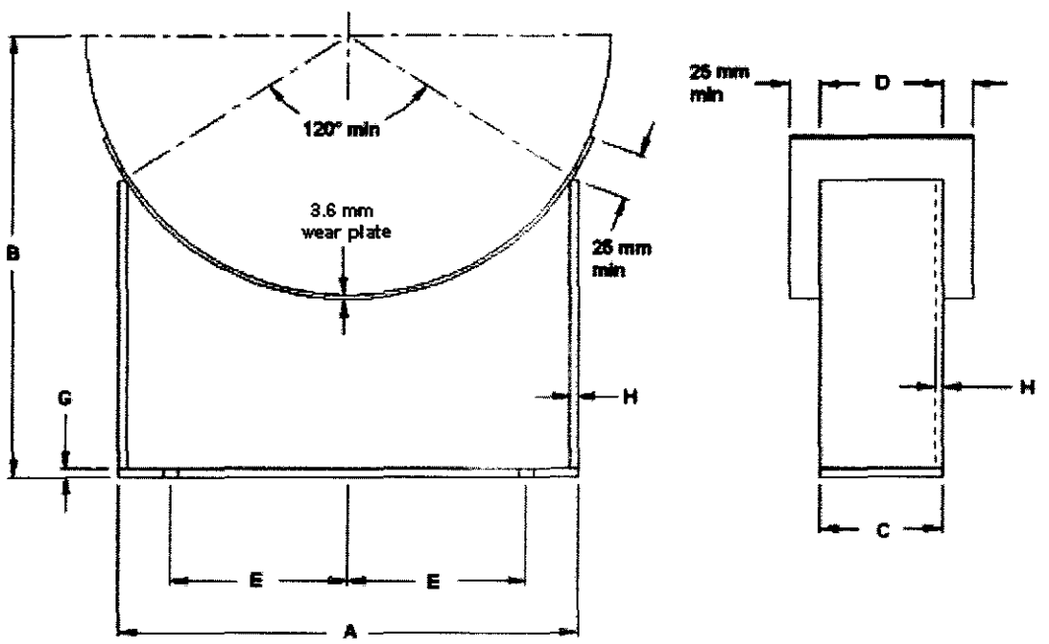

Figure 3-18: Horizontal pressure vessel standard saddle dimensions [22] (Appendix 7: drawing VS_SADDLE)

Table 3-13: Horizontal pressure vessel saddle dimensions [22] (refer to Figure 3-18)

Nominal vessel diam. (mm)	Dimensions (mm)						No. of ribs	Saddle plate thickness		Max. vessel weight (kg)
	A	B	C	D	E	Bolt diam.		Base G	Web, Flange, Ribs H	
457.2	393.7	381	101.6	101.6	152.4	M 12	0	6.35	6.35	28122

3.3.7 Instrumentation

- Temperature control

The temperature inside the vessel could be controlled in two ways. Figure 3-19 shows the first method. In this method, a temperature instrument controller (TIC) receives a signal from the thermocouple (EC). For a process set value, this controller will switch the relay switch on or off to control the temperature of the gas. This method has an effective bandwidth of 2°C (personal communication - WIKA Instrumentation).

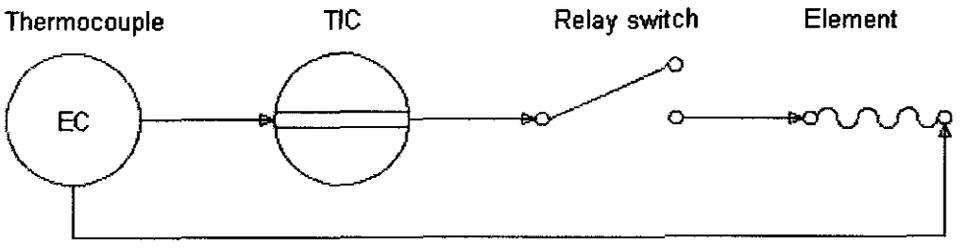

Figure 3-19: Temperature control using a relay switch

Figure 3-20 shows the method of controlling the gas temperature with a variable speed drive. In this method, a temperature instrument controller (TIC) receives a signal from the thermocouple (EC). The variable speed drive will then, for a set process value, integrate or differentiate the signal and control the temperature with a bandwidth of 0.2°C (personal communication - WIKA Instrumentation).

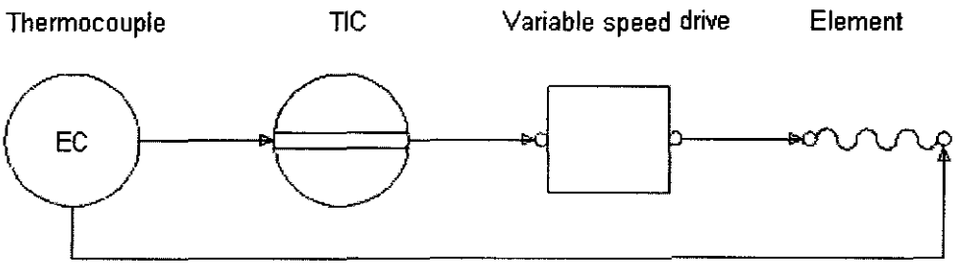

Figure 3-20: Temperature control using a variable speed drive controller

A Type K thermocouple is required to withstand the gas temperature. The thermocouple should be inserted into a standard solid drilled Class 2500 1½" flanged thermowell (Appendix 7: drawing INST_THW).

- Pressure control

A standard Class 2500 1½" capillary tube diaphragm was selected for the pressure sensor extension. The diaphragm flange body material should be stainless steel (DIN specification code DIN 1.4571). This diaphragm can withstand temperatures of up to 400°C [29]; therefore, the long weld neck flange to which the diaphragm flange is attached must be water-cooled. This study does not attend in detail to the method of cooling, but use can be made of coiled copper tubing to circulate water around the flange neck in order to cool the flange. FEM should be conducted on all water-cooled long weld neck flanges, to investigate the material stresses at the nozzle-vessel interfaces. A pressure transmitter with local display should be connected to the end of the capillary tube.

- Vacuum pump

A vacuum pump is needed to extract the air from the vessel. The pump should be connected to a shut-off valve. This valve should be connected to the vessel's applicable water-cooled long weld neck flange (Appendix 7: drawing FL_LWN – nozzle G).

- Helium supply

A standard helium supply cylinder (Afrox: Helium Research Grade N6.0 - Cylinder size ZZ) can be used to supply the system with helium. The supply should be fitted with a shut-off valve between supply and vessel. The vessel side of the supply line should be water-cooled.

- Pressure relief valve

None of the identified possible commercial type pressure relief valves (PRV) can withstand the helium design temperature. Therefore, a relief valve had to be designed. The valve was designed with a standard Class 2500 1½" blind flange as the base. A hole in this flange with a diameter of 15 mm related to a force (with end pressure of 52 bar) of 918 N. This design makes use of a BeCu spring to hold a glider inside the housing in the sealing position with this force (refer to Figure 3-21). The spring is preloaded by applying the necessary amount of turns to the spring preload bolt. To achieve the required spring preload deflection the bolt has to be rotated 5.41 times after contact between the bolt and spring was achieved. The bolt should be locked in position with an additional nut. The top of the relief valve is machined with a M36 nut interface. Two longitudinal holes should be machined in the sides of the main hole. If the internal vessel pressure exceeds 52 bar, the glider will move upwards and the gas will then escape through these two holes. Figure 3-21 shows the sectioned pressure relief valve. The spring design is shown in Appendix 6.

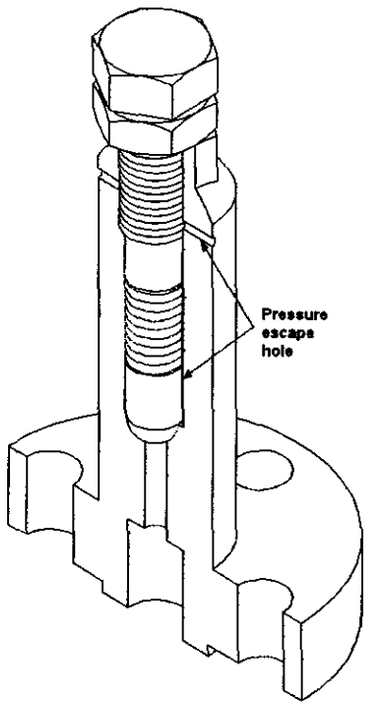

Figure 3-21: Sectioned pressure relief valve model (Appendix 7: drawing group INST_PRV)

3.4 Conclusion

The study was aimed at verifying whether the specified valve contact materials would weld when subjected to the defined operating conditions. In this chapter a pressure vessel was designed in accordance with ASME VIII Div. 1. This design was done to be able to simulate the hydrostatic pressure on the valve contact materials. The pressure vessel design conditions are shown in Table 3-14. The material specification of the pressure vessel is shown in Table 3-15.

Table 3-14: Pressure vessel design conditions

Condition	Value
Design pressure	55 bar
Design temperature	732.22°C
Max. Operating pressure	52 bar
Max. Operating temperature	720°C
Medium	Helium
Vessel ID	400 mm
Vessel orientation	Horizontal

Table 3-15: Pressure vessel material specification

Component	Material specification
Shell	SB-622 (UNS N06230)
Flat heads	SB-435 (UNS N06230)
Body flanges	SB-564 (UNS N06230)
Nozzles	SB-564 (UNS N06230)
Saddle	SB-435 (UNS N06230)
Bolting	SB-572 (UNS R30556)
Gasket	Corrugated metal, asbestos inserted, or Corrugated metal, jacketed asbestos filled
Insulation	Silica blanket (170kg/m^3)

The material selected for the pressure vessel is UNS N06230 (Commercially: Haynes ® Alloy 230) [34], in its various forms. An internal heater was designed. The heater lead-outs were designed to be electrically and pressure isolated by using R-1600 RTV Rubber from NuSil [26]. All the long weld neck flanges, except the thermocouple flange, should be cooled externally by a water-cooling system (temporary use of PBMM water-cooling system).

Based on the facility designed in this chapter (pressure vessel), the experimental design is presented in the following chapter.

Chapter 4: Design and Specification of the Test Setup

In this chapter, the design of the test specimens and the experimental procedures are presented. The design of the test specimens is divided into conceptual, intermediate, and detail design. Although the pressure vessel was designed to accommodate an assembled valve, the experimental procedure is given for a simplified test specimen.

4.1 Design of test specimen

4.1.1 Conceptual design

Hydrostatic helium pressure might play an important part as stated in § 2.3, but the pressure can also be simulated by superimposed stresses in a helium atmosphere at the required temperature in a vacuum gas oven. A test specimen design was required to simulate the possible contact welding conditions, which can be expected during normal operating conditions. As stated previously, the welding phenomenon can occur between the sealing surfaces of the butterfly valves when used under high temperature pressurised helium conditions. For the simulation, the following information is needed:

- Typical butterfly valve dimensions, as well as
- proposed operating conditions of these valves.

The following information, concerning the sealing surfaces of the proposed PBMR power turbine bypass butterfly valve (Personal communication - PBMR personnel), was available:

Table 4-1: Typical dimensions and operating conditions for power turbine bypass-valve

Property	
Diameter of sealing surface	65 mm
Width of sealing surface	1 mm
Contact force between sealing surfaces	25000 N up to 35000 N
Material of disc and seat	Material with DIN specification number DIN 1.2365 (AISI H10)
Temperature at sealing surface	720 °C
Pressure difference at sealing surface	52 bar

The sealing surfaces of these valves are machined in an elliptical shape and therefore have a slanted profile. Due to limited available information regarding the profile of the sealing

surfaces, the contact pressure was calculated as an average on a non-slanted surface. The specific profile of the sealing surfaces is not of great importance, due to the small contact area concerned. From this information, the maximum sealing surface contact pressure (equation (4.1)) was calculated as follows:

$$P_{contact} = \frac{F_{contact}}{A_{contact}} \tag{4.1}$$

where: $F_{contact}$ = 35000 N (maximum contact force) and

$A_{contact}$ = π.d.t (circumferential area)

= 204.29 mm^2

Giving

$$P_{contact} = 171.4 \text{ MPa}$$

The experimental setup was designed to simulate this calculated maximum contact pressure. For the remainder of the calculations a rounded off value of 175 MPa was used for the maximum contact pressure.

4.1.2 Intermediate design

To minimise the manufacturing costs of the test specimens a simple contacting profile is suggested. A bolted joint is the easiest way to convey pressure between two surfaces. In this phase of the test specimen design, the following concepts were considered:

Figure 4-1 shows two blind flanges with a machined recess in which the test specimens are inserted. The flanges are bolted together with the correct bolt preload to obtain the necessary contact pressure between the contact surfaces of the test specimens.

The use of two blind flanges as a bolted joint holds a couple of unwanted problems. The biggest problem is that of misalignment of the contact pressure between test specimen surfaces, due to the uncertainty of equal bolt preload distribution. Therefore, a much simpler design was considered to overcome this problem. Figure 4-2 shows an alternative design using a single bolt to convey the necessary contact pressure between the two rings. This design uses less parts and the uncertainty of unequal bolt preload distribution is eliminated.

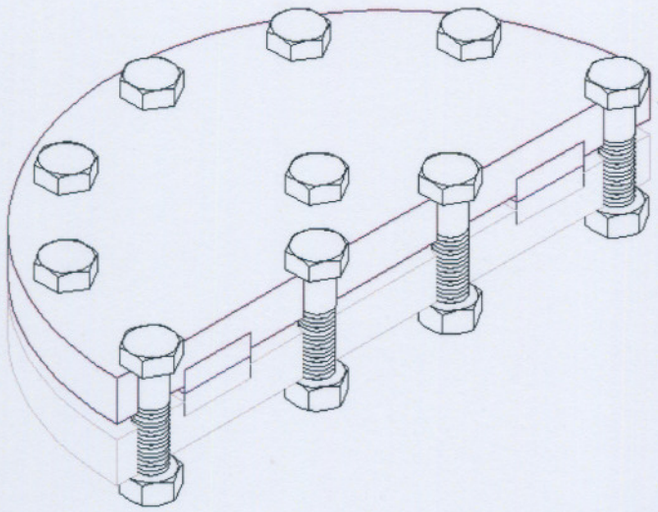

Figure 4-1: Blind flange bolted joint concept

The bolt, nut, and rings are made of the same material (AISI H10, Commercially – Böhler W320 or UTOP33 ESR EFS) to ensure constant thermal expansion and equal stress distribution in all parts. Thus, preloading at room temperature is possible if all parts are of the same material. The precise required preload is calculated in the next section.

Figure 4-2: Single bolt-joint concept

4.1.3 Detail design

The detail design of the test specimen setup is divided into two parts, namely the ring design and the bolt design.

4.1.3.1 Ring design

Using the data available for the valve dimensions the maximum sealing contact pressure was previously calculated as 175 MPa. To simulate this contact pressure between two surfaces, two rings are proposed. The rings have a thickness of 10 mm each. With an outer diameter (d_o) of 20 mm, the inner diameter (d_i) was calculated using equation (4.2):

$$A_{contact} = \pi \frac{d_o^2 - d_i^2}{4} \tag{4.2}$$

where: $A_{contact}$ = 200 mm^2 (refer to equation (4.1) - where $P_{contact}$ = 175 MPa)

Solving from equation (4.2) we get d_i *=12.06 mm.* Figure 4-3 shows the calculated size of rings.

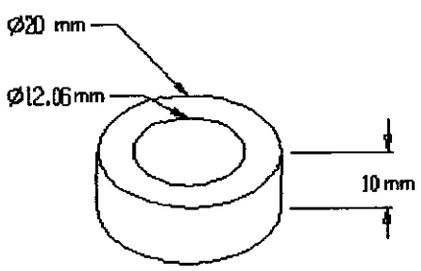

Figure 4-3: Ring dimensions

With the size of the rings fixed, the size of the bolt and nut were determined.

4.1.3.2 Bolt design

The selection of the bolt is based on the fixed inner diameter of the test specimen ring. The specifications of the selected bolts are listed in Table 4-2.

Table 4-2: Specification of M12 x 1.25 test specimen bolt

Property	
Nominal major diameter (d)	12 mm
Pitch (p)	1.25 mm
Tensile stress area (A_t)	92.1 mm^2
Minor diameter area (A_r)	86.0 mm^2
Treaded length (l_t)	50 mm (full length)
Bolt material	DIN 1.2365 (AISI H10)

Using a shaft tolerance, the tolerance between the bolt and test specimen ring is 12D9/h9. The bolt preload was calculated by calculating the bolt elongation, because the use of torque calculations to determine preloads is inaccurate [20]. Bolt elongation δ_l, has the following relation to bolt stress:

$$\delta_l = \frac{F_i \cdot l_t}{A_t \cdot E} \tag{4.3}$$

Table 4-3: Variables for bolt preload calculations (Refer to equation (4.3))

Variable	Description	Value
F_i	Preload force	35 000 N
l_t	Threaded length	20 mm
A_t	Tensile stress area	92.1 mm^2
E	Young's Modulus @ 25°C (Böhler W320) [38]	215 GPa
α	Coefficient of thermal expansion [38,39]	$13.775x10^{-6}$ m/(m·K)

Using the information in Table 4-3 δ_l was calculated to have the following value:

$$\delta_l\big|_{25°C} = 35.35\mu m$$

This means the test specimen setup is elongated $35.35\,\mu m$ to obtain the required bolt preload of 35 000 N (at room temperature), which in turn produces a contact stress between the two rings of 175 MPa. The use of the same material for all parts of the test specimen assembly enables the preloading to be done at room temperature (constant thermal expansion in all parts). The natural increase in threaded bolt length caused by the temperature rise was calculated as follows [40]:

$$\begin{aligned}\delta_l\big|_{720°C} &= \alpha \cdot l_t \cdot \Delta T \\ &= 15.775x10^{-6} m/(m \cdot K) \cdot 0.02 \cdot 700°C \\ &= 192.85\mu m\end{aligned}$$

Therefore the bolt should be preloaded (elongated @ 25°C) by $228.2\,\mu m$ ($35.35\,\mu m$ + $192.85\,\mu m$), to ensure an elongation of $35.35\,\mu m$ @ 720°C, to simulate the contact stresses of the valve sealing surfaces.

4.2 Definition of operating conditions

The ideal gas law can be used to determine specified states of gases. The relation between pressure, specific volume, and temperature characteristics of gases with low densities was shown [23] to be given by equation (4.4) (Ideal gas law):

$$P\bar{v} = \bar{R}T \tag{4.4}$$

Rewritten in terms of the total volume, (4.4) gives:

$$PV = mRT \tag{4.5}$$

The use of this law however has limits when predicting states at high temperatures and pressures, where the temperature is more than twice the critical gas temperature (T_C) and the pressure is more than five times the critical gas pressure (P_C). Table 4-4 compares the values of the critical temperature and pressure to the operating conditions.

Table 4-4: Comparison between critical gas constants of helium and operating conditions

	Critical value	**Operating conditions**
Temperature (K)	5.19	993.15
Pressure (MPa)	0.227	5.2

The operating temperature and pressure are respectively approximately 191 times the critical temperature and 23 times the critical pressure of helium. This indicates that the use of the ideal gas law for state calculations may result in unwanted state deviations.

AFROX South Africa recommended the use of the Benedict-Webb-Rubin (BWR) [24] equation of state (equation (4.6)) for the prediction of gas conditions. This equation contains eight constants and when solving for density, it can have up to six roots.

$$P = RT\rho + \left(B_0RT - A_0 - \frac{C_0}{T^2}\right)\cdot\rho^2 + (bRT - a)\cdot\rho^3 + a\alpha\rho^6 + \left(\frac{c\rho^3}{T^2}\right)\left(1+\gamma\rho^2\right)\cdot\exp\left(-\gamma\rho^2\right) \tag{4.6}$$

Another way to obtain specified states of gases is from empirical values. Tsederberg, Popov et al. [24] published tables giving the specific volume, enthalpy, and entropy for saturated and superheated helium. These tabulated values were used to calculate the specific states of helium.

The abovementioned methods to predict gas states were investigated to determine the relation between them. Using the BWR equation of state as reference, the following relations were found. In each case, the final operating condition was specified to simulate the conditions of the proposed power turbine bypass-valve. With this state specified, the initial state was calculated.

4.2.1 Ideal gas law

Equation (4.5) can be rewritten for the final operating condition as:

$$m_2 = \frac{P_2 V_2}{R T_2}$$

The pressure vessel has a constant volume; therefore, the mass was calculated for this condition using the abovementioned equation. With the gas mass remaining constant throughout the tests, the initial pressure was calculated by setting $m_1 = m_2$ and $V_1 = V_2$.

The calculated values using the ideal gas law are shown in Table 4-5.

Table 4-5: Ideal gas law; initial and operating conditions

Initial conditions	**Value**	**Operating conditions**	**Value**
P_1	15.6107 bar	**P_2**	52 bar
V_1	115 litre	**V_2**	115 litre
m_1	0.2899 kg	**m_2**	0.2899 kg
R	2.07723 kJ/kg·K	**R**	2.07723 kJ/kg·K
T_1	25°C	**T_2**	720°C

4.2.2 Empirical thermodynamic properties of helium

Relevant empirically determined thermodynamic properties of helium [24] are listed in Table 4-6.

Table 4-6: Empirical thermodynamic properties (specific volume (v)) of superheated helium

Pressure (bar)	**v (m^3/kg) @ Temperature (°C)**	
	600	800
50	0.3652	0.4481
100	0.1838	0.2252

This paragraph explains the composition of Table 4-7. Using linear interpolation over temperature, the specific volume of helium at 720°C was calculated at both 50 and 100 bar. Further interpolation over pressure resulted in the specific volume of superheated helium at 720°C, 52 bar [(1)]. With the specific volume of the final operating condition known (equal to initial specific volume [(2)]), the initial pressure was calculated as follows. Interpolation calculations over temperature for 0°C and 100°C and pressure were done to determine the initial pressure [(3)] for the pre-calculated constant specific volume at 25°C.

Table 4-7: Interpolation results of empirical initial and operating conditions

Pressure (bar)	***Specific volume*** **(m^3/kg) @ Temperature (°C)**			
	600	720	800	25
10	1.816	-	2.232	0.62280
16.96742 [(3)]	-	-	-	**0.406688** [(2)]
20	1.1169	-	1.3245	0.312625
50	0.3652	0.41494	0.4481	0.126775
52	-	**0.406688** [(1)]	-	-
100	0.1838	0.20864	0.2252	0.064850

4.2.3 BWR equation of state

Using EES this equation of state was solved. The final operating condition information was firstly entered, which produced a helium density (ρ) of 2.396 kg/m^3 at 720°C, 52 bar. This density remains constant due to the constant volume of the pressure vessel. The constant density was then entered, which yielded the initial helium pressure of 15.45 bar at 25°C. The constants used for the state calculation using the BWR equation of state are given in Table 4-8. The results calculated by the BWR equation of state are shown in Table 4-9.

Table 4-8: Constants of BWR equation of state for helium [24]

Constant	**Value**
B_0	23.661×10^{-3}
A_0	4150.475
C_0	16442.01
b	-197.27×10^{-9}
a	-58.09874
c	-559.4153
α	7.2673×10^{-6}
γ	779.42×10^{-6}

Table 4-9: Initial and operating conditions (density) calculated with BWR equation of state

Pressure (bar)	ρ (kg/ m^3) @ Temperature (°C)	
	720	25
52	**2.396**	-
15.4495	-	**2.396**

A comparison of the calculated values suggested for the initial pressure by the three methods of calculations is shown in Figure 4-4. This figure compares the three methods of predicting the states of gases. From the figure it is clear that the ideal gas law predicted the specified state of helium in close relation to the BWR equation of state, while the experimental data found in the thermodynamic tables varies significantly from the BWR-calculated gas states. The percentage deviation shown in this figure was calculated using the BWR equation of state as reference. The need for the abovementioned calculations is discussed in the following section.

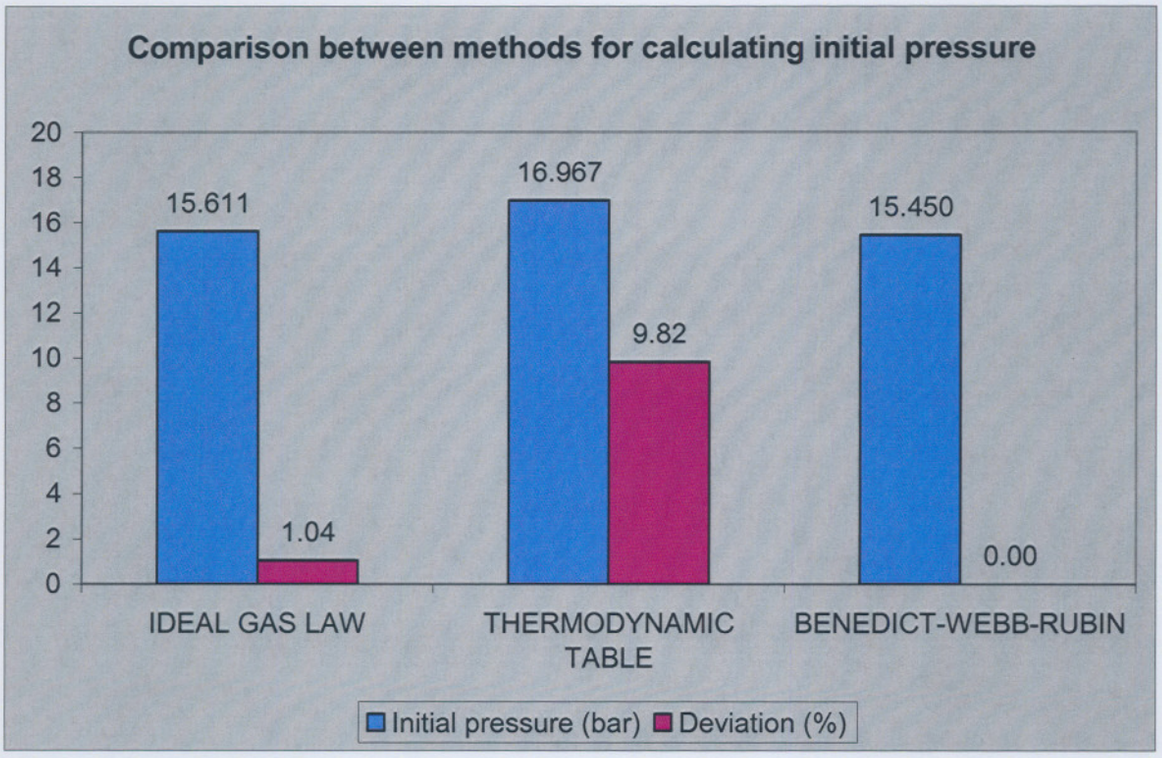

Figure 4-4: Comparison between methods for calculating initial pressure

4.2.4 Calculated initial operating conditions

According to AFROX South Africa (personal communication), the BWR equation of state is the most accurate equation to predict states for helium gas. The calculated operating conditions (for constant vessel volume) using this equation of state are shown in Table 4-10.

Table 4-10: Calculated operating conditions

Condition	Initial	Operating
Temperature (°C)	25	720
Pressure (bar)	15.45	52
Mass (kg)	0.276	0.276
Specific volume (m^3/kg)	0.417	0.417
Density (kg/m^3)	2.396	2.396

If the temperature of the helium supply differs from the one given in Table 4-10 (25°C), a set of usable temperature-pressure correction combinations is given in Appendix 1 that needs to be implemented before testing starts.

4.3 Experimental procedure

The experimental procedure set out here must be followed as a guide to the correct experimental sequence. This procedure does not in detail specify all the steps required for testing. If deemed necessary additional steps may be added.

The experimental procedure was divided into the following sub procedures:

a. Start-up procedure.
b. Operating condition simulation procedure.
c. Material evaluation procedure.
d. Material coating procedure.

4.3.1 Start-up procedure

This procedure describes all the necessary steps of preparation for the testing of the test specimens. This includes the testing of instrumentation, preloading the test specimens, and other activities, before the testing and simulation phases of the experimental procedure commence.

Required activities can be summarized as follows:

a. Preload test specimens -

These activities are done at room temperature. Fit the two specimen rings over the bolt. Hand fasten the nut onto the bolt until further fastening by hand is impossible. Hand fasten second nut to bolt. Insert test specimen setup into hydraulic bolt preloading device. Preload the bolt until the elongation of the bolt is 228.2 μm. Fasten second nut to secure the bolt preload.

b. Insert test specimens into pressure vessel.

c. Close pressure vessel -

Fasten pressure vessel flange bolts to close pressure vessel. The bolts should be fastened to the larger of the required gasket seating bolt torque and the required operating condition bolt torque requirement as calculated in Chapter 3. The required torque was shown to be 275 N·m.

4.3.2 Operating condition simulation procedure

In this procedure, the simulation of the operating conditions of the proposed power turbine bypass-valve is described. The operating conditions include the gas temperature and pressure, the loads on the contacting surfaces, the selected valve materials, and the use of helium gas.

Required activities can be summarized as follows:

a. Draw vacuum in pressure vessel -

Engage vacuum pump to extract the air from the pressure vessel. After acceptable level of vacuum (0.1 kPa) is obtained, close vacuum pump seal valve.

b. Helium gas inlet -

Open helium gas regulated one-way inlet valve. Fill vessel with helium. Ensure the initial operating condition of 15.45 bar at 25°C is reached before helium gas inlet valve is closed. If the gas inlet temperature has a different value, refer to Appendix 1 for corresponding initial pressure.

c. Heat gas to final operating condition -

Start cooling water system for long weld neck flanges and helium supply line. Turn on gas heating elements. Heat gas up to operating condition of 52 bar at 720°C.

d. Regulate this operating condition for the proposed three-hour testing period.

e. Power down system -

Turn off heating elements. Slowly release warm helium gas through blow off pipe.

4.3.3 Material evaluation procedure

In this procedure, the materials subjected to the various operating conditions are examined. The specimens are sectioned and studied for contact surface adhesion (welding). The outcome of this procedure may lead to the next procedure or the end of testing.

Required activities can be summarized as follows:

a. Remove test specimens from pressure vessel -
   Open pressure vessel flange by loosening flange bolts. Inspect gasket after removal of flange for visible damage, which might implicate gasket replacement. Prepare specimens for material evaluation.
b. Section specimens longitudinally -
   Attempt to loosen the bolts of the test specimen setup. Bolts might not be able to be loosened. Cut the test specimens longitudinally.
c. Examine specimen contacting surfaces -
   Examine ring-contacting surfaces with electron microscope (or other optical image evaluation equipment) for welding of these surfaces. If welding did not occur, the tests can be stopped. If surface welding (adhesion) occurred, the contacting surfaces have to be coated with the predetermined hard facing coating as described in next procedure.

4.3.4 Material coating procedure

This procedure describes the possible material coating techniques and the different coatings, those, which can be applied, and those, which should be avoided.

Required activities can be summarized as follows:

a. Determine suitable coating method -
   The following methods are recommended: PVD (Physical Vapour Deposition) and CVD (Chemical Vapour Deposition).
b. Determine suitable coating -
   The following coatings are recommended for testing: Al_2O_3, Norem 02, and Nitronic 60. The following coatings should not be used: Stellite based (Cobalt based) coatings as described in Chapter 2, Section 2.3.
c. Retesting of test specimens -
   After coating the test specimen ring contacting surfaces, the specimens are again tested, starting at the start-up procedure as described above in Section 4.3.1.

The next chapter presents the finite element analysis carried out on the designed pressure vessel.

This page has been left blank intentionally.

Chapter 5: Finite Element Analysis

In this chapter, results of the FEA on the pressure vessel are presented. This analysis was done using ALGOR FEMPRO Software. The solid CAD models were created with CADKEY and imported into FEMPRO. Steady State Heat Transfer and Static Stress with Linear Material Models analyses were done to compare material stresses with calculated and allowable ASME VIII Div. 2 material stresses.

5.1 Pressure vessel analysis - Thermal

5.1.1 Input

A longitudinally halved section solid CAD model of the pressure was created using the design drawings shown in Appendix 7, as shown in Figure 5-1. This model included the following parts:

- Pressure vessel shell.
- ASME VIII Appendix 2 girth flanges.
- UG-34 flat unstayed heads.
- Saddle wear plates.
- Nozzles with inner and outer welds.
- Gaskets.
- Vessel insulation.

Due to the symmetry of the vessel, the model was simplified to a longitudinally halved section. The CAD model was imported into FEMPRO and all parts were named. The next step was creating the meshed model. A solid meshed model was created. The mesh size of all the pressure vessel parts (shell, App 2 flanges, heads, insulation, nozzles, and welds) was set to 100% of automatic size. This coarser mesh was selected to speed up meshing and calculation time.

The part contact type was set to default as bonded. Where parts were only in contact, a surface contact pair was created. The following parts were set as surface contact:

- All part in contact with insulation.
- Nozzles in pressure vessel parts (shell, flat head).

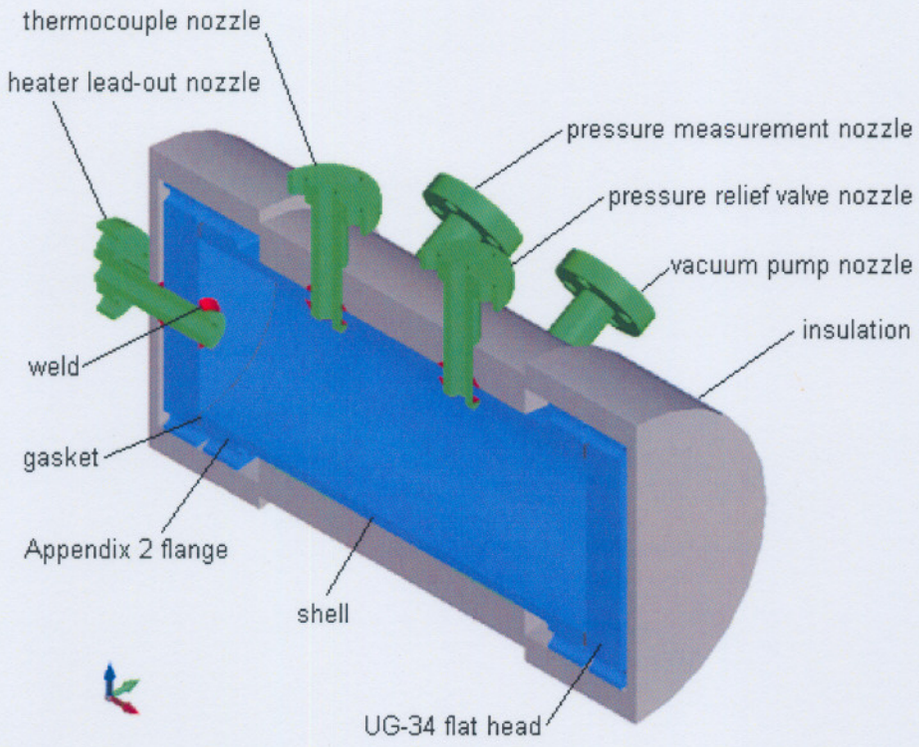

Figure 5-1: CADKEY sectioned pressure vessel model

A "Steady State Heat Transfer Analysis" was first done to calculate the model nodal temperatures. This calculation was done because material properties differ with temperature. In the FEA Editor window the material properties were set. Element definition was set as orthotropic (properties vary in x, y, and z direction, or varies with temperature). These properties were entered as temperature dependent isotropic (properties are constant in x, y, and z direction, but varies with temperature). Material properties required for the heat transfer calculations were:

- Density (ρ) (kg/m^3).
- Coefficient of thermal conduction (k - Table 5-1) (W/m·K).
- Specific heat (c_p - Table 5-1) (J/kg·K).

These properties were entered for a temperature range of 0°C to 800°C. The thermal material properties for Silica insulation blanket [32] and Haynes Alloy 230 [34] were used in the material properties input window. The properties are listed in Table 5-1.

Table 5-1: Thermal material properties used in ALGOR model

Silica insulation blanket [32]	Temperature (°C)	k (W/m·K)	c_p (J/kg·K)	Haynes Alloy 230 [34]	Temperature (°C)	k (W/m·K)	c_p (J/kg·K)
	0	0.0211	995.6		0	8.4	389.67
	25	0.0236	1004.35		25	8.9	397
	100	0.0311	1030.6		100	10.4	419
	400	0.06552	1135.6		200	12.4	435
	500	0.07622	1170.6		300	14.4	448
	600	0.08766	1196.46		400	16.4	465
	700	0.09675	1218.96		500	18.4	473
	800	0.12365	1241.46		600	20.4	486
	-	-	-		700	22.4	574
	-	-	-		800	24.4	595

The applied thermal loads (convection heat transfer) were then entered. The applicable surfaces were selected for the internal gas thermal load (T = 720°C, convection coefficient = 15 $W/m^2 \cdot K$). The applicable surfaces were selected for the external thermal load (T = 25°C, convection coefficient = 25 $W/m^2 \cdot K$). The FEA model with applied thermal loads is presented in Figure 5-2. The default nodal temperature was set to 25°C and the control of the heat rate at boundaries was set to "Temperature control". Since the problem is nonlinear, an iterative method is required for the analysis, that is, to calculate the new nodal temperature, the previous nodal temperature was used. The material properties were also based on this previous nodal temperature. A flowchart of the nonlinear equation-solving algorithm of ALGOR is presented in Figure 5-3.

The following annotation represents the thermal loads in Figure 5-2:

- Yellow arrows - Convection thermal load

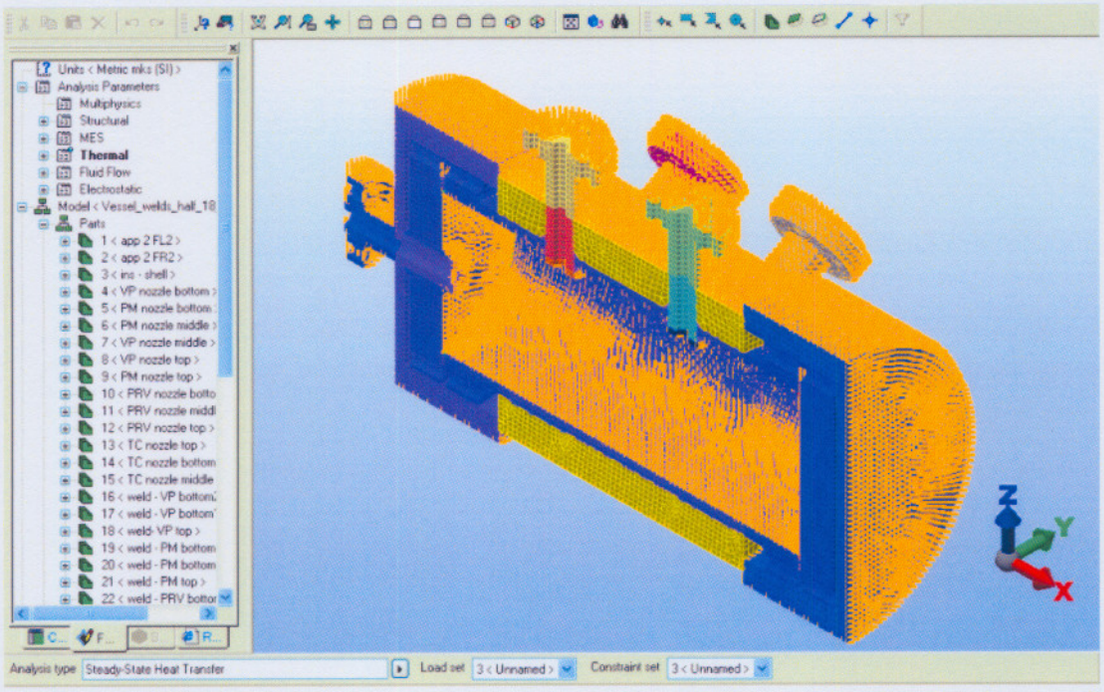

Figure 5-2: Thermally loaded FEMPRO model

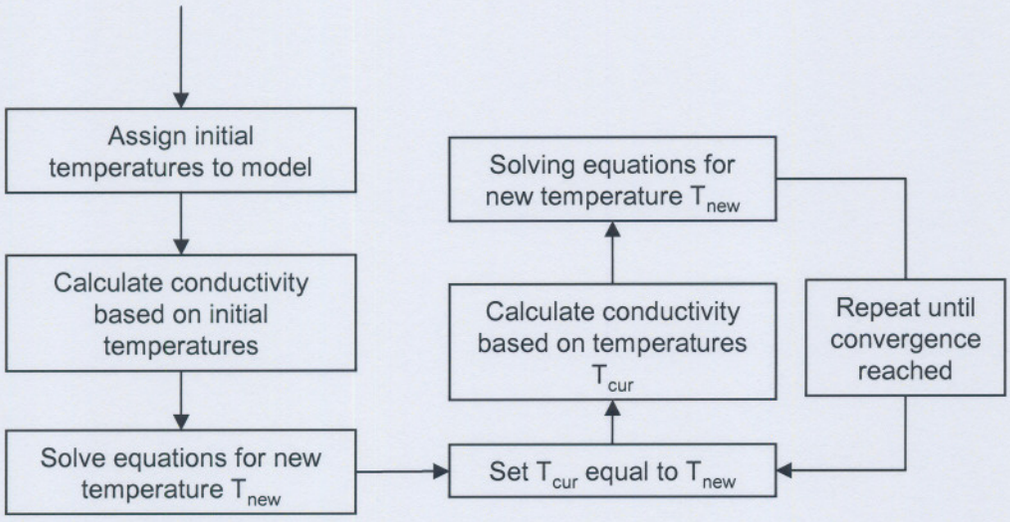

Figure 5-3: Nonlinear equation solving flowchart (modified after ALGOR User's Guide)

where: T_{cur} = current temperature

T_{new} = new temperature

5.1.2 *Output*

The Steady State Heat Transfer results are shown in Figure 5-4. This figure indicates the minimum temperature of the vessel as -97.6°C and the maximum temperature as 699.2°C. Note the large decrease in thermal conduction through the insulation (Temperature decreases from approx. 670°C to 25°C).

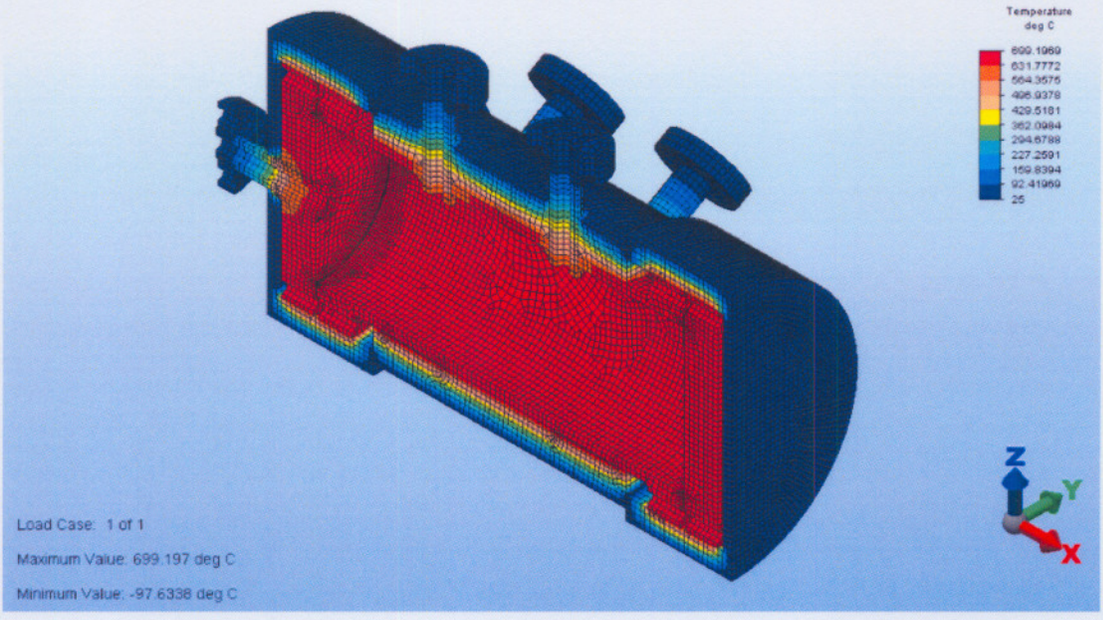

Figure 5-4: FEMPRO Steady State Heat Transfer results

5.1.3 *Conclusions*

The minimum temperature value of -97.63°C is only present at one node of the heater lead-out nozzle (Figure 5-5) interface with external surface of the flat head insulation. The minimum temperature varies between -55°C and -8°C at two other nozzle - insulation interfaces. It seemed that a discontinuity in the surface (i.e. interface between two parts) related to a calculation problem. Figure 5-5 shows the temperature distribution at the nozzle interface with the flat head insulation. Discarding these calculated errors, the correct minimum nodal temperature was approximately 25°C. A stress analysis followed, where the above calculated nodal temperatures were used to allocate the correct material properties for the relevant temperatures.

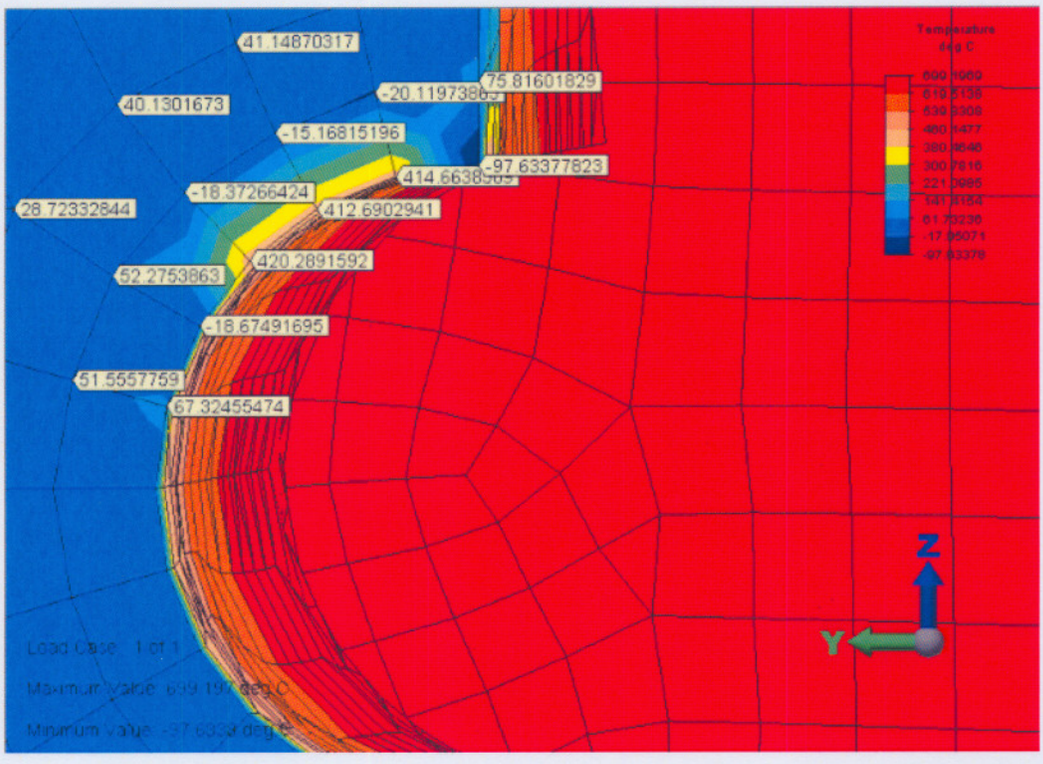

Figure 5-5: Temperature distribution at heater lead-out nozzle - flat head insulation interface

5.2 Pressure vessel analysis - Structural

5.2.1 Input

The previously defined meshed CAD model was used for the "Static Stress with Linear Material Models" simulation. The element definition was changed to "Temperature Dependent Isotropic". Material properties required for the static stress calculations were:

- Young's Modulus (E - Table 5-2) (GPa).
- Poisson's ratio (ν - Table 5-2).
- Shear Modulus (G - Table 5-2) (GPa).
- Coefficient of thermal expansion (α - Table 5-2) (m/m/°C).

These material properties were entered for a temperature range of 0°C to 1000°C.

Table 5-2: Mechanical material properties used in ALGOR model

Silica insulation blanket [32]	Temp (°C)	E * (GPa)	ν *	G * (GPa)	α * (m/m·°C)	Haynes Alloy 230 [34]	Temp (°C)	E (GPa)	ν	G (GPa)	α (m/m·°C)
	0	69	0.18	29.2	5.3×10^{-10}		0	214	0.3	82.4	0
	25	69	0.18	29.2	5.3×10^{-10}		25	211	0.3	81.2	0
	100	69	0.18	29.2	5.3×10^{-10}		100	207	0.3	79.6	11.8×10^{-6}
	200	69	0.18	29.2	5.3×10^{-10}		200	202	0.3	77.7	12.4×10^{-6}
	300	69	0.18	29.2	5.3×10^{-10}		300	196	0.3	75.4	12.8×10^{-6}
	400	69	0.18	29.2	5.3×10^{-10}		400	190	0.3	73.1	13.2×10^{-6}
	500	69	0.18	29.2	5.3×10^{-10}		500	184	0.3	70.8	13.6×10^{-6}
	600	69	0.18	29.2	5.3×10^{-10}		600	177	0.3	68.1	14.1×10^{-6}
	700	69	0.18	29.2	5.3×10^{-10}		700	171	0.3	65.8	14.7×10^{-6}
	800	69	0.18	29.2	5.3×10^{-10}		800	164	0.3	63.1	15.2×10^{-6}
	-	-	-	-	-		900	157	0.3	60.4	15.7×10^{-6}
	-	-	-	-	-		1000	150	0.3	57.7	16.1×10^{-6}

* Approximated values

The gas pressure was simulated as gauge pressure (52 bar). It was applied to the inner pressure vessel surfaces as a uniform pressure (surface load - structural). Atmospheric pressure (85 kPa - Potchefstroom, South Africa) was applied to the outer surfaces of the pressure vessel (surface load - structural). The left vertical surface of the left saddle was set as fixed (no translation or rotation possible). The boundary conditions of the right saddle were set as x anti-symmetric (x translation and y and z rotation possible). The head - flange bolt loads were simulated as surface forces applied to the inner bolt hole surfaces of the flat head and ASME VIII Appendix 2 flanges. The FEA model with applied structural loads and boundary conditions is presented in Figure 5-6. The stress free reference temperature was set to 25°C.

The following annotations represent structural loads and boundary conditions in Figure 5-6:

- Yellow arrows - Uniform pressure.
- Red arrows - Surface forces.
- Red triangles or circles - Boundary conditions.

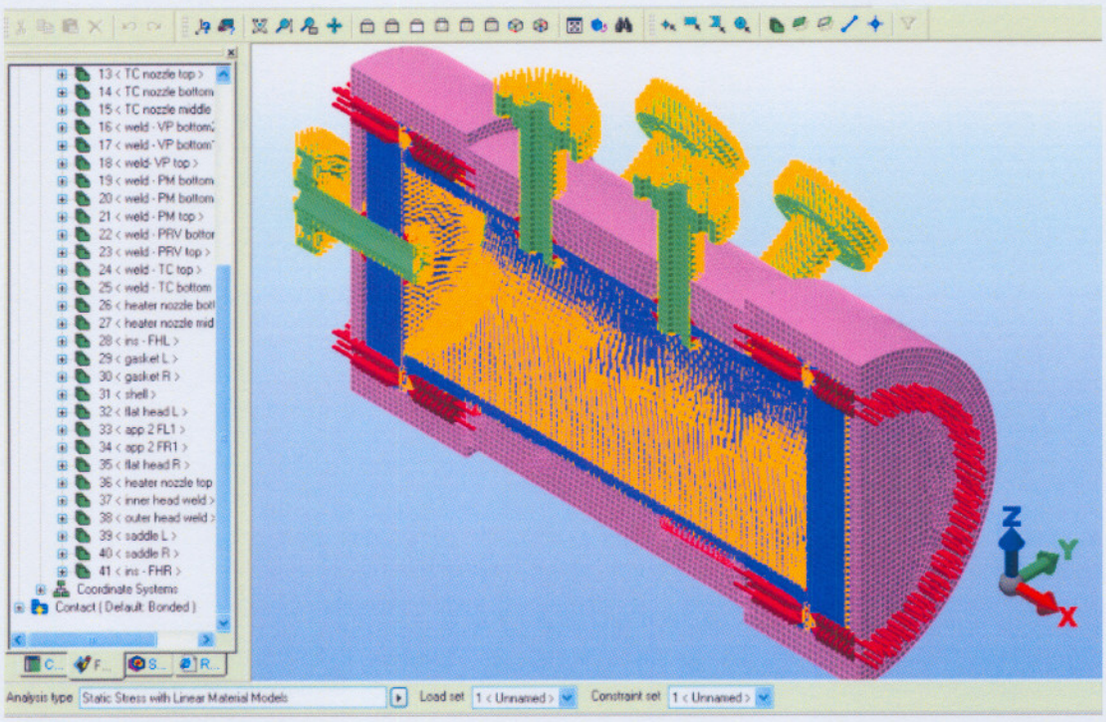

Figure 5-6: Structurally loaded FEMPRO model

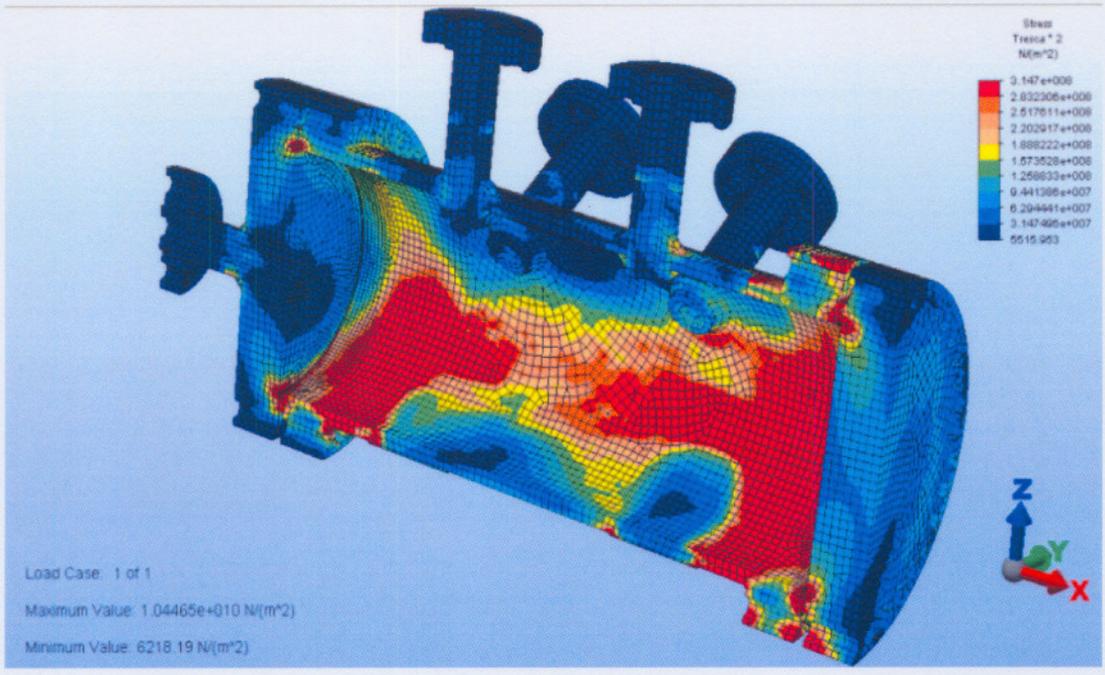

Figure 5-7: FEMPRO Tresca Effective Stress Distribution - Vessel

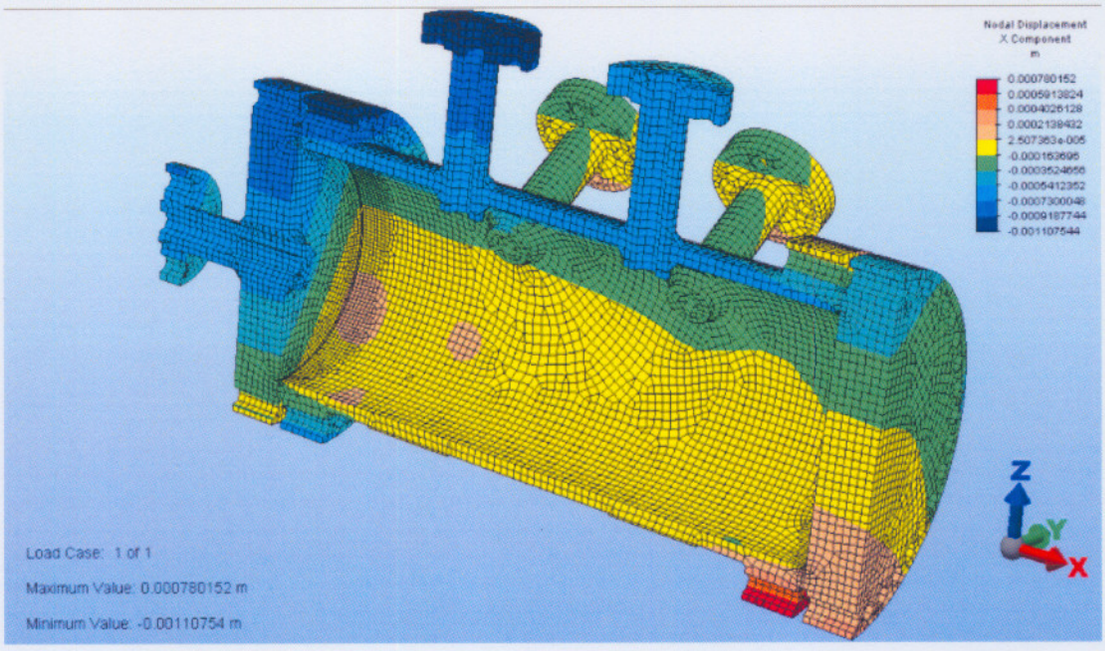

Figure 5-8: FEMPRO Nodal displacements (x-component) - Vessel

Figure 5-9: FEMPRO Tresca Effective Stress Distribution - Nozzle welds

5.2.2 Output

The Static Stress results are shown for the pressure vessel with the insulation removed. The Tresca effective stress results for the sectioned pressure vessel are shown in Figure 5-7. The maximum indicated Tresca effective stress was 10.4 GPa (FEM analysis local point stresses).

The legend was modified to indicate all stresses equal to and exceeding the 0.2% yield strength at 720°C (314.71 MPa) as red. The stress legend of this figure indicates a minimum Tresca effective stress of 6.2 kPa. The x-component of the nodal displacements is shown in Figure 5-8. The maximum calculated nodal displacement (x component) value was 780 µm. The maximum Tresca effective stress of a nozzle weld was calculated as 328.5 MPa (FEM analysis local point stresses). The Tresca effective stress range for the flanges was approximately between 160 MPa and 300 MPa.

5.2.3 Conclusions

The Tresca effective stresses shown in the above figure indicated twice the actual material stress (Algor User's Guide). When this Tresca effective stress exceeds the material yield strength for the relevant temperature, the material will yield. The 0.2% yield strength of Cold rolled and Solution annealed (1232°C) Haynes Alloy 230 [34] varies from 422 MPa at room temperature to 310.6 MPa at 700°C. Based on the abovementioned FEMPRO Tresca effective stress results, the vessel (parts in red in Figure 5-7) would yield when subjected to these operating conditions.

The maximum allowable stress value according to ASME II Part D [31, 34] for nonferrous material UNS N06230 (Commercially Haynes 230) is 57.9 MPa. Halving the Tresca effective stress for the actual internal stresses, gave the maximum stress as 5.2 GPa and the minimum stress as 6.2 kPa. ASME VIII Div. 2 [37] states that the Tresca effective stress can be compared with three times the material allowable stress at design conditions. Even at this allowable stress of approximately 180 MPa, the vessel still failed. The average Tresca effective stress for the pressure vessel nozzle welds indicated in Figure 5-9 (up to 110 MPa) was less than three times the allowable stress at 720°C.

The huge difference in allowable and calculated material stress (for specified temperature and pressure) could be attributed to the stringent limits placed on allowable material stresses by ASME. The indicated ultimate tensile strength of Haynes 230 was 609 MPa at 700°C. ASME VIII (1965) used among others the lowest of the following values for the stress allowances [37]:

- 25% of specified tensile strength at room temperature (209.5 MPa) [34]
- 25% of expected tensile strength at operating metal temperature (152.2 MPa) [34]
- 62.5% of 0.2% offset yield strength at operating metal temperature (194.13 MPa) [34]

Input errors of the operating conditions could also relate to faulty stresses. These errors included the miscalculated negative temperature values (Figure 5-5). Based on the ALGOR FEMPRO results discussed above, parts of the pressure vessel (parts in red in Figure 5-7)

designed in accordance with ASME VIII Division I could not operate under the defined conditions.

It is recommended that the same analysis be done with another FEM analysis software package, to verify the calculated material stresses. This analysis can be incorporated into the follow-up study, where the water-cooling system must also be designed. The influence on the water-cooled flange interfaces with the pressure vessel can then also be modelled. Before the manufacturing of the pressure vessel can commence, the design has to be approved by a third party inspector. Any design updates necessary from the inspector's report should also be included in the follow-up study.

References

References were obtained through searches done on the following databases:

ScienceDirect [Available on the internet:] www.sciencedirect.com
Compendex Plus [Available on the internet:] www-win2/atsite/atsiteext.dll
EbscoHost [Available on internet:] http://web20.epnet.com/selectdb.asp
http://www.google.com
http://www.aol.com and other

[1] D. Böhlo, H. Liebe, *Dichtigkeitsuntersuchungen an armaturensitzen grosser nennweite bis 900°C,* Jahrestagung Kerntechnik '88, pp. 543-546, May 1988.

[2] *SUBJECT: Selecting the correct hard face seal material 5-2,* 4p. [Available on the internet:] http://www.mcnallyinstitute.com/05-html/5-2.html [Date of access: 29 August 2002].

[3] A. Matthews, S.S. Eskildsen, *Engineering applications for diamond-like carbon,* Diamond and Related Materials, Vol. 3, pp. 902-911, 1994.

[4] J. Vetter, T. Michler, H. Steuernagel, *Hard coatings on thermochemically pretreated soft steels: application potential for ball valves,* Surface and Coatings Technology, Volume 111, pp. 210-219, 1999.

[5] A. Kawana, H. Ichimura, Y. Iwata, S. Ono, *Development of PVD ceramic coatings for valve seats,* Surface and Coatings Technology, Volume 86-87, pp. 212-217, 1996.

[6] H. Tsujikawa, et al, *Preliminary studies on large metal-sealed gate valves for the International Thermonuclear Experimental Reactor (ITER),* Vacuum, Volume 47, numbers 6-8, pp. 639-646, 1996.

[7] REMR Technical note EM-CR-1.5, *Mechanical properties and corrosion behaviour of stainless steels for lock, dam, and hydroelectric plant applications,* 9p.

[8] H. Ocken, *The galling wear resistance of new iron-base hardfacing alloys: a comparison with established cobalt- and nickel-base alloys,* Surface and Coatings Technology, Volume 76-77, pp. 456-461, 1995.

[9] J. Kim, S. Kim, *The temperature dependence of the wear resistance of iron-base NOREM 02 hardfacing alloy,* Wear, Volume 237, pp. 217-222, 2000.

[10] W. Schumacher, *Wear and galling of nitrogen-strengthened stainless steels,* Machine Design, Volume 55(19), pp. 87-88, Aug 1983.

[11] I. Inglis, E.V. Murphy, *Performance of wear-resistant iron base hardfacing alloys in valves operating under prototypical pressurized water reactor conditions,* Surface and Coatings Technology, Volume 53, pp.101-106, 1992.

[12] M. Vardavoulias, M. Jeandin, F. Velasco, J.M. Torralba, *Dry sliding wear mechanism for P/M austenitic stainless steels and their composites containing Al_2O_3 and Y_2O_3 particles,* Tribology International, Volume 29, Number 6, pp. 499-506, 1996.

[13] B.V. Cockeram, R.F. Buck, W.L. Wilson, *Laboratory galling tests of several commercial cobalt-free weld hardfacing alloys,* Surface and Coatings Technology, Volume 94-95, pp. 495-500, 1997.

[14] T. Michler, M. Grischke, K. Bewilogua, H. Dimigen, *Properties of duplex coatings prepared by plasma nitriding and PVD Ti-C:H deposition on X20Cr13 ferritic stainless steel,* Thin Solid Films, Volume 322, pp. 206-212, 1998.

[15] J. Kim, G. Kim, S. Kim, *The effect of manganese on the strain-induced martensitic transformation and high temperature wear resistance of Fe-20-Cr-1C-1Si hardfacing alloy,* Journal of Nuclear Materials, Volume 289, pp. 263-269, 2001.

[16] U. Wiklund, I.M. Hutchings, *Investigation of surface treatments for galling protection of titanium alloys,* Wear, Volume 251, pp. 1034-1041, 2001.

[17] Description of: *Performance of NOREM ™ Hardfacing Alloys,* Report summary TR-112993, 5p, 1999 [Available on internet:] http://www.epri.com [Date of access: 24 October 2002].

[18] G.E. Dieter, *Effect of high hydrostatic pressure on fracture,* Mechanical Metallurgy, Chapter 7-13, pp. 271-272, 1988.

[19] A. Koster, H.D. Matzner, D.R. Nicholsi, *PBMR design for the future,* Nuclear Engineering and Design, Volume 222, pp. 231-245, 2003.

[20] M.L. Nayyar (Editor), Chapter A7: *Gasket & bolt selection,* Piping Handbook, 7th edition, 2000.

[21] J.E. Shigley, C.R. Mischke, *Mechanical Engineering Design,* 6th edition, 1248 p, 2001.

[22] E.F. Megyesy, *Pressure vessel handbook,* 11th edition, p. 100, 101 and 355, 1998.

[23] R.E. Sonntag, C. Borgnakke, G.J. Van Wylen, *Fundamentals of thermodynamics,* 5th edition, 783 p, 1998.

[24] R.H. Perry, D.W. Green, J.O. Maloney, *Perry's Chemical engineers' handbook,* 6th edition, p. 3-192, 3-254, 3-270, 3-271, 1984.

[25] H.E. Boyer, T.L. Gall, *ASM Metals Handbook Desk Edition,* p. 2.20, 1985.

[26] NuSil Technology, *Product Profile - R-1600, Non-Corrosive RTV Silicone Adhesive Sealant,* NT/052901/REVA.

[27] R.P. Benedict, *Fundamentals of Temperature, Pressure, and Flow Measurements,* 2nd edition, p. 65, 1977.

[28] Aberdare Cable Facts & Figures - Power Cables.

[29] CS 99.04, Diaphragm-Type Chemical Seals, Flange-Type Diaphragm Seals, Model 990.27, WIKA Instruments, Technical Information Compact Disk.

[30] ASME Boiler and Pressure Vessel Committee Subcommittee on Pressure Vessels, *ASME VIII Division 1, Rules for construction of pressure vessels,* The American Society of Mechanical Engineers, New York, pp. 668, July 2001.

[31] ASME Boiler and Pressure Vessel Committee Subcommittee on Materials, *Section II: Materials, Part D - Properties,* The American Society of Mechanical Engineers, New York, pp. 789, July 2001.

[32] Intersource USA, Datasheet - Silica Blanket, [Available on internet:] http://www.intersourceusa.com [Date of access: 21 November 2003].

[33] ZIRCAR Ceramics, Alumina Blanket type AB & MB, [Available on internet:] http://www.zircarceramics.com/pages/flexible/index.htm [Date of access: 21 November 2003].

[34] HAYNES® 230® ALLOY H-3000H Product specification sheet, Haynes International High-Temperature Alloys, [Available on internet:] http://www.haynesintl.com/mini/230Site/230.htm [Date of access: 21 November 2003].

[35] ZIRCAR Ceramics, Alumina Insulation Type ZAL-15 & ZAL-15AA, [Available on internet:] http://www.zircarceramics.com/pages/rigidmaterials/aluminaproducts.htm [Date of access: 2 March 2004].

[36] Kanthal Handbook - Resistance Heating Alloys and Systems for Industrial Furnaces, Catalogue nr. 1-A-5B-3 09.2001 5000, 24 p. 2001, Kanthal AB, Sweden.

[37] ASME Boiler and Pressure Vessel Committee Subcommittee on Pressure Vessels, *ASME VIII Division 2, Alternative Rules,* The American Society of Mechanical Engineers, New York, pp. 478, July 2001.

[38] BÖHLER W320 Hot Work Tool Steel, W320 DE 01.02 - 1000 G Data brochure.

[39] UTOP33 EFS, UTOP33 ESR EFS, METAL RAVNE, [Available on internet:] http://www.sz-metal.si/products/steels/utop33.pdf [Date of access: 18 November 2002].

[40] W.C. Durney, *Worked examples in applied mechanics,* 1st edition, p. 3, 1959.

[41] P.G. Rousseau, G.P. Greyvenstein, *Conceptual Thermo-Hydraulic design of the PBMR Micro Model,* Document number: PBMM-0001, Revision 1, February 2002.

Appendix 1: Initial Operating Conditions

This Appendix contains results of helium gas conditions based on the Benedict-Webb-Rubin equation of state.

The following initial operating conditions were obtained by solving the Benedict-Webb-Rubin equation of state (equation (A1.1)). The design was done using an initial temperature of 25°C, but Table A1-1 gives alternative pressures that corresponds to the given temperatures.

$$P = RT\rho + \left(B_0 RT - A_0 - \frac{C_0}{T^2}\right)\cdot\rho^2 + (bRT - a)\cdot\rho^3 + a\alpha\rho^6 + \left(\frac{c\rho^3}{T^2}\right)\left(1+\gamma\rho^2\right)\cdot\exp\left(-\gamma\rho^2\right) \qquad \text{(A1.1)}$$

Table A1-1: Benedict-Webb-Rubin calculated initial operating conditions

T (°C)	T (K)	P_I (bar)		T (°C)	T (K)	P_I (bar)
1	274.15	14.19		16	289.15	14.98
2	275.15	14.24		17	290.15	15.03
3	276.15	14.29		18	291.15	15.08
4	277.15	14.35		19	292.15	15.13
5	278.15	14.4		20	293.15	15.19
6	279.15	14.45		21	294.15	15.24
7	280.15	14.5		22	295.15	15.29
8	281.15	14.56		23	296.15	15.34
9	282.15	14.61		24	297.15	15.4
10	283.15	14.66		**25**	**298.15**	**15.45**
11	284.15	14.71		26	299.15	15.5
12	285.15	14.77		27	300.15	15.55
13	286.15	14.82		28	301.15	15.61
14	287.15	14.87		29	302.15	15.66
15	288.15	14.92		30	303.15	15.71

The values listed above were calculated with EES (Engineering Equation Solver). The required final operating condition was entered, which calculated the helium density. This density was converted to specific volume. Because the pressure vessel volume and helium mass remains constant throughout the experiment, the specific volume also remains constant. This constant specific volume was then used to calculate the initial pressure corresponding to the initial temperature inputs.

Appendix 2: UG-34 Flat Head Design

This Appendix contains ASME VIII Div. 1 calculations for an unstayed flat head bolted to an Appendix 2 (ASME VIII) flange. Refer to Figure A2-1 *for head dimensions.*

UG-34 unstayed flat head and cover calculation:

Table A2-1: Input values for UG-34 calculations

Variable	Description	Value
C	Attachment factor	0.3
d	Shell outer diameter	450 mm
E	Joint efficiency	1
h_{gg}	Gasket moment arm from Appendix 2 flange calculation (see Appendix 4)	26.74 mm
P	Internal design pressure	5500 kPa
$S_{operating}$	Maximum allowable stress value in tension for operating condition	57.916 MPa
$S_{seating}$	Maximum allowable stress value in tension for gasket seating	189.6 MPa
t_r	Required thickness of shell	20.141 mm
t_s	Nominal thickness of shell	25 mm
$W_{operating}$	Total bolt load for circular heads for equation 3 of 2-5(e)	979.3kN
$W_{seating}$	Total bolt load for circular heads for equation 4 of 2-5(e)	1771 kN

The equations used for the flat head design:

$$m = \frac{t_r}{t_s}$$

$$t_{operating} = d\sqrt{\frac{C \cdot P}{S_{operating} \cdot E} + \frac{1.9 \cdot W_{operating} \cdot h_{gg} \cdot 10^6}{S_{operating} \cdot E \cdot d^3}}$$

$$t_{seating} = d\sqrt{\frac{1.9 \cdot W_{seating} \cdot h_{gg} \cdot 10^6}{S_{seating} \cdot E \cdot d^3}}$$

$$t = \max(t_{operating}; t_{seating})$$

The results are shown in Table A2-2.

Table A2-2: Results from UG-34 calculations

Variable	Description	Value
M	Ratio	0.8056
$t_{operating}$	Minimum required head thickness for operating conditions	87.63 mm
$t_{seating}$	Minimum required head thickness for gasket seating	32.47 mm
t	Minimum required thickness of head	87.63 mm
t_h	Nominal head thickness	92 mm

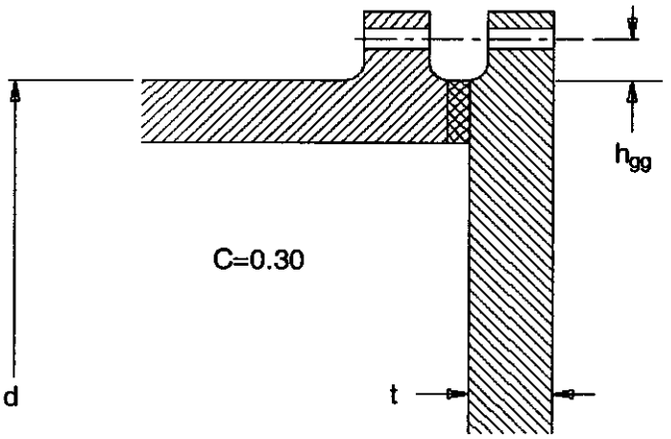

Figure A2-1: Dimensions of ASME VIII UG-34 unstayed flat head

Appendix 3: UG-37 Reinforcement Required For Openings in Shells and Formed Heads

This Appendix contains calculations of reinforcement requirements of openings in the pressure vessel shell.

The nomenclature for the reinforced opening is shown in Figure A3-1.

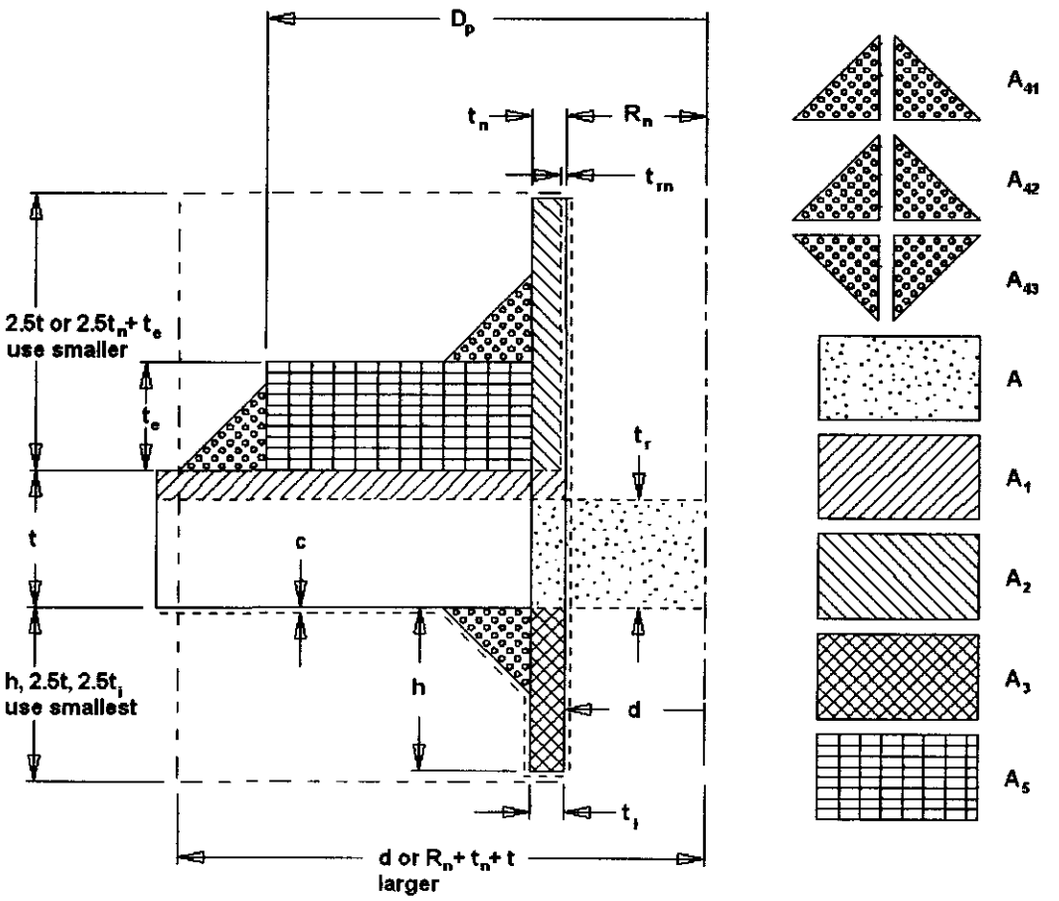

Figure A3-1: Nomenclature for reinforced openings

The calculations were done for Class 2500 long welding neck flanges (1.5", 2", 2.5", and 3"). A standard welding leg length of 17 mm was used for all welds. The nozzle extension inside the vessel wall was 30 mm. If the calculation without a reinforcing element failed, it was repeated with a reinforcing element.

A3.1 Openings in vessel shell

Example calculation of reinforcement required for an opening (1.5" Class 2500 long weld neck flange) in the vessel shell:

Area required:

$$A = dt_r F + 2t_n t_r F(1 - f_{r1})$$
$$= 38.1 * 20.141 * 1 + 2 * 3 * 20.141 * 1 * (1 - 1)$$
$$= 767.37 mm^2$$

Area available in shell; use larger value:

$$A_1 = d(E_1 t - Ft_r) - 2t_n(E_1 t - Ft_r)(1 - f_{r1})$$
$$= 38.1(1 * 25 - 1 * 20.141) - 2 * 3(1 * 25 - 1 * 20.141)(1 - 1)$$
$$= 185.13 mm^2$$
$$A_1 = 2(t + t_n)(E_1 t - Ft_r) - 2t_n(E_1 t - Ft_r)(1 - f_{r1})$$
$$= 2(25 + 3)(1 * 25 - 1 * 20.141) - 2 * 3(1 * 25 - 1 + 20.141)(1 - 1)$$
$$= 272.1 mm^2$$

Area available in nozzle projecting outward; use smaller value:

$$A_2 = 5(t_n - t_m) f_{r2} t$$
$$= 5 * (3 - 3.6323) * 1 * 25$$
$$= -79.04 mm^2$$
$$A_2 = 5(t_n - t_m) f_{r2} t_n$$
$$= 5 * (3 - 3.6323) * 1 * 3$$
$$= -9.485 mm^2$$

Area available in inward nozzle; use smallest value:

$$A_3 = 5 t t_i f_{r2}$$
$$= 5 * 25 * 3 * 1$$
$$= 375 mm^2$$
$$A_3 = 5 t_i t_i f_{r2}$$
$$= 5 * 3 * 3 * 1$$
$$= 45 mm^2$$
$$A_3 = 5 h t_i f_{r2}$$
$$= 5 * 30 * 3 * 1$$
$$= 450 mm^2$$

Area available in outward weld:

$$A_{41} = (leg)^2 f_{r2}$$
$$= 17^2 * 1$$
$$= 289 mm^2$$

Area available in inward weld:

$$A_{43} = (leg)^2 f_{r2}$$
$$= 17^2 * 1$$
$$= 289mm^2$$

The opening is adequately reinforced when

$$A_1 + A_2 + A_3 + A_{41} + A_{43} \geq A$$

thus reinforcement is sufficient because

$$(272.1 + (-79.04) + 45 + 289 + 289)\ mm^2 = 817\ mm^2 > 767.37\ mm^2.$$

Appendix 4: ASME VIII Appendix 2 Flange Design

This Appendix contains ASME VIII Appendix 2 flange design calculations.

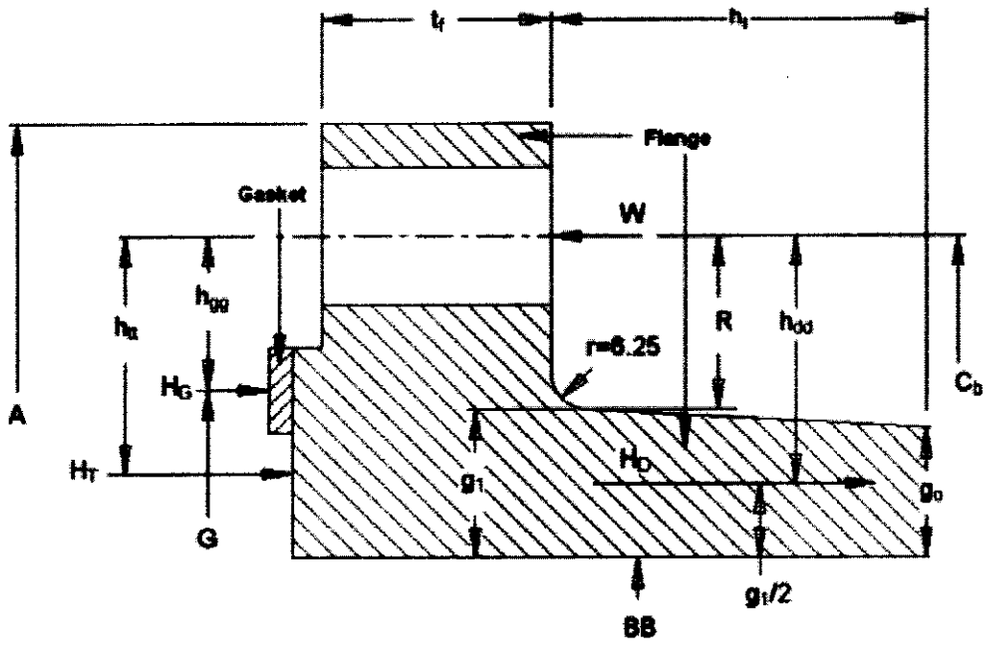

Figure A4-1:ASME VIII Appendix 2 flange dimensions

Table A4-1: Input values for Appendix 2 flange design (refer to Figure A4-1)

Dimension	Description	Value
A	Outer diameter of flange	570 mm
A_b	M20 Fine series bolt, cross-sectional root area	259 mm^2
BB	Inside diameter of flange	400 mm
C_b	Bolt circle diameter	516.25 mm
F	Factor from Figure 2-7.2 of ASME VIII Div. 1	0.90892
V	Factor from Figure 2-7.3 of ASME VIII Div. 1	0.550103
f_h	Hub stress correction factor for integral type flange	1
G	Gasket load reaction diameter	462.76 mm
g_1	Thickness of hub at back of flange	26.5 mm
g_0	Thickness of hub at small end	25 mm
h_l	Hub length	60 mm

Dimension	Description	Value
r	Fillet radius, at least $0.25g_1$ but larger than 4.76 mm	6.25 mm
S_f	Allowable design stress for flange material for either operating condition or gasket seating	57.92 MPa or 189.606 MPa
S_n	Allowable design stress for shell material for either operating condition or gasket seating	57.92 MPa or 189.606 MPa
N	Width used to determine b_o (Table 2-5.2 of ASME VIII Div. 1)	15 mm
P	Design pressure	55 bar
S_a	Allowable bolt design stress at atmospheric temperature	172.37 MPa
S_b	Allowable bolt design stress at design temperature	48.26 MPa
t_f	Flange thickness	90 mm
t_n	Shell nominal thickness	25 mm
m	Gasket factor from Table 2-5.1 of ASME VIII Div. 1	2.5
y	Gasket seating load from Table 2-51 of ASME VIII Div. 1	20 MPa

The equations used in the design of the ASME VIII Appendix 2 flange:

$$A_m = \max(A_{m1}, A_{m2}) \qquad A_{m1} = \frac{W_{m1}}{S_b}$$

$$A_{m2} = \frac{W_{m2}}{S_a} \qquad B_1 = BB + g_1$$

$$b = 0.5\sqrt{b_o} \qquad b_o = \frac{N}{2}$$

$$c = \min(t_n, t_x) \qquad d = \frac{U}{V} \cdot h_o \cdot g_o^{\,2}$$

$$e = \frac{F}{h_o} \qquad H = 0.785 \cdot G^2 \cdot P$$

$$H_D = 0.785 \cdot BB^2 \cdot P \qquad H_G = W - H$$

$$H_p = 2 \cdot b \cdot 3.14 \cdot G \cdot m \cdot P \qquad H_T = H - H_D$$

$$h_{dd} = R + 0.5 \cdot g_1 \qquad h_{gg} = \frac{C_b - G}{2}$$

$$h_o = \sqrt{BB \cdot g_o} \qquad h_{tt} = \frac{R + g_1 + h_{gg}}{2}$$

$$K = \frac{A}{BB} \qquad L = \frac{t_f \cdot e + 1}{T} + \frac{t_f^3}{d}$$

$$M_D = H_D \cdot h_{dd} \qquad M_G = H_G \cdot h_{gg}$$

$$M_T = H_T \cdot h_{tt}$$

$$M_0 = W \cdot \left[\frac{C_b - G}{2}\right] \text{ (for gasket seating)} \qquad W = \frac{(A_m + A_b) \cdot S_a}{2} \text{ (for gasket seating)}$$

$M_0 = M_D + M_G + M_T$ (for operating condition)

$W = W_{m1}$ (for operating condition)

$$R = \frac{C_b - BB}{2} - g_1$$

$$S_H = \frac{f_h \cdot M_0}{L \cdot g_1^2 \cdot B_1}$$

$$S_R = \frac{(1.33 \cdot t_f \cdot e + 1) \cdot M_0}{L \cdot t_f^2 \cdot BB}$$

$$S_T = \frac{Y \cdot M_0}{t_f^2 \cdot BB} - Z \cdot S_R$$

$$T = \frac{K^2 \cdot (1 + 8.55246 \cdot \log(K)) - 1}{(1.0472 + 1.9448 \cdot K^2) \cdot (K - 1)}$$

$$U = \frac{K^2 \cdot (1 + 8.55246 \cdot \log(K)) - 1}{1.36136 \cdot (K^2 - 1) \cdot (K - 1)}$$

$$Y = \left[\frac{1}{K-1}\right] \cdot \left[0.66845 + 5.7169 \cdot \left(\frac{K^2 \cdot \log(K)}{K^2 - 1}\right)\right]$$

$$Z = \frac{K^2 + 1}{K^2 - 1}$$

$$t_x = 2 \cdot g_o$$

$$W_{m1} = H + H_p$$

$$W_{m2} = 3.14 \cdot b \cdot G \cdot y$$

Allowable flange design stresses:

$$S_H < 1.5 \cdot S_f$$

$$S_R < S_f$$

$$S_T < S_f$$

$$\frac{(S_H + S_R)}{2} < S_f$$

$$\frac{(S_H + S_T)}{2} < S_f$$

The results of the above equations are shown in Table A4-2.

Table A4-2: Calculated Appendix 2 flange results

Dimension	Description	Value
A_{m1}	Total required cross-sectional area of bolts for operating conditions	20291mm^2
A_{m2}	Total required cross-sectional area of bolts for gasket seating	230.9 mm^2
A_m	Total required cross-sectional area of bolts	20291 mm^2
b	Effective gasket seating width	1.369 mm
B_1	-	426.5 mm
b_o	Basic gasket seating width	7.5 mm
c	Basic dimension used for minimum sizing of welds	25 mm
d	Factor	705340 mm^3
e	Factor	0.009089 mm^{-1}

Dimension	Description	Value
H	Total hydrostatic end force	924.6 kN
H_D	Hydrostatic end force on area inside of flange	690.8 kN
h_{dd}	Radial distance from bolt circle to circle on which H_D acts	44.88 mm
H_G	Gasket load	846.5 kN
h_{gg}	Radial distance from gasket load reaction to bolt circle	26.74 mm
h_o	Factor	100 mm
H_p	Total joint-contact surface compression load	54.72 kN
H_T	Difference between total hydrostatic end force and hydrostatic end force on area inside of flange	233.8 kN
h_{tt}	Radial distance from bolt circle to circle on which H_T acts	42.43 mm
K	Ratio of outside diameter to inside diameter of flange	1.425
L	Factor	2.076
M_0	Total moment acting on flange for maximum of operating condition or gasket seating	47366 kN.mm
M_D	Component of moment due to H_D	31000 kN.mm
M_G	Component of moment due to H_G	22639 kN.mm
M_T	Component of moment due to H_T	9921 kN.mm
R	Radial distance from bolt circle to point of intersection of hub and back of flange	31.63 mm
S_{a1}	Allowable flange design stresses according to section 2-8 of ASME VIII, Appendix 2	284.4 MPa
S_{a2}		14.70 MPa
S_{a3}		39.36 MPa
S_{a41}		45.43 MPa
S_{a42}		57.76 MPa
S_H	Calculated longitudinal stress in flange hub	76.16 MPa
S_R	Calculated radial stress in flange	14.70 MPa
S_T	Calculated tangential stress in flange	39.36 MPa
T	Factor	1.743
t_x	-	50 mm
U	Factor	6.208
W	Flange design bolt load for maximum of operating condition or gasket sating	1771 kN
W_{m1}	Minimum required bolt load for operating condition	979.3 kN
W_{m2}	Minimum required bolt load for gasket seating	39.79 kN
Y	Factor	5.649
Z	Factor	2.941

Appendix 5: Insulation Calculations

This Appendix contains calculations for the insulating of the pressure vessel.

The insulation calculations were done with the data for the Silica (Intersource USA) and the Alumina (Zircar Ceramics) insulation blankets. The main parts of the pressure vessel to insulate were the shell, Appendix 2 flange and flat head. From the design of the heater the allowable heat loss through the vessel is 4.5 kW. The insulation calculations however were based on values ranging from 1 kW up to and including 4.5 kW.

A5.1 Shell insulation

Table A5-1: Input values for shell insulation calculation

Variable	Description	Value
T	Internal surface temperature	720°C
T_o	Outer surface temperature	70°C
r_1	Shell internal radius	0.2 m
r_2	Shell outer radius	0.225 m
t_{ss}	Thickness of stainless steel plate	0.001 m
k_{ss}	Thermal conduction coefficient of stainless steel	14.18 W/m·K
k_{metal}	Thermal conduction coefficient of UNS N06230	22.8 W/m·K
k_{ins}	Thermal conduction coefficient of Silica blanket insulation	0.10213 W/m·K
k_{ins}	Thermal conduction coefficient of Alumina blanket insulation	0.1227 W/m·K
L	Pressure vessel shell length	0.7 m

The equations used to calculate the insulation thickness for the shell:

$$r_4 = r_3 + t_{ss} \qquad t_{ins} = r_3 - r_2$$

$$q = \frac{T - T_o}{\frac{\ln(\frac{r_2}{r_1})}{2\pi \cdot k_{metal}} + \frac{\ln(\frac{r_3}{r_2})}{2\pi \cdot k_{ins}} + \frac{\ln(\frac{r_3}{r_4})}{2\pi \cdot k_{ss} \cdot L}}$$

This calculation was done for both types of insulating materials and the results for the insulation thickness are shown in Table A5-2:

Table A5-2: Shell insulation thicknesses

q (W)	Silica blanket $t_{insulation}$ (m)	Alumina blanket $t_{insulation}$ (m)	q (W)	Silica blanket $t_{insulation}$ (m)	Alumina blanket $t_{insulation}$ (m)
1000	0.07614	0.09435	2810	0.02451	0.02976
1121	0.06682	0.08251	2931	0.02344	0.02845
1241	0.05952	0.07329	3052	0.02247	0.02726
1362	0.05365	0.06592	3172	0.02157	0.02616
1483	0.04883	0.05988	3293	0.02074	0.02514
1603	0.0448	0.05485	3414	0.01997	0.0242
1724	0.04139	0.0506	3534	0.01925	0.02333
1845	0.03845	0.04696	3655	0.01859	0.02251
1966	0.0359	0.0438	3776	0.01797	0.02176
2086	0.03367	0.04104	3897	0.01739	0.02105
2207	0.0317	0.0386	4017	0.01684	0.02038
2328	0.02994	0.03644	4138	0.01633	0.01976
2448	0.02837	0.03451	4259	0.01585	0.01917
2569	0.02696	0.03276	4379	0.01539	0.01862
2690	0.02567	0.03119	4500	0.01496	0.0181

An insulation thickness of 90 mm for the shell was selected to be sufficient to enhance the effectiveness of the heating system, which in its turn lowered the time it takes to heat the helium.

A5.2 Flat head insulation

Table A5-3: Input values for flat head and Appendix 2 flange insulation calculation

Variable	Description	Value
T	Internal surface temperature	720°C
T_o	Outer surface temperature	70°C
t_{head}	Shell internal radius	0.092 m
t_{ss}	Thickness of stainless steel plate	0.001 m
k_{metal}	Thermal conduction coefficient of UNS N06230	22.8 W/m·K
k_{ss}	Thermal conduction coefficient of stainless steel	14.18 W/m·K
k_{ins}	Thermal conduction coefficient of Silica blanket insulation	0.10213 W/m·K
k_{ins}	Thermal conduction coefficient of Alumina blanket insulation	0.1227 W/m·K
od_{head}	Flat head outer diameter	0.57 m

The equations used to calculate the insulation thicknesses for the flat head and Appendix 2 flange:

$$q = \frac{T - T_o}{\frac{t_{head}}{k_{metal} \cdot A_{metal}} + \frac{t_{ins}}{k_{ins} \cdot A_{ins}} + \frac{t_{ss}}{k_{ss} \cdot A_{ss}}} \qquad A_{metal} = \frac{\pi \cdot od_{head}^{\ 2}}{4}$$

$$A_{ins} = A_{metal} \qquad A_{ss} = A_{metal}$$

This calculation was done for both types of insulating materials and the results for the insulation thickness are shown in Table A5-4:

Table A5-4: Flat head and Appendix 2 flange insulation thicknesses

q (W)	Silica blanket $t_{insulation}$ (m)	Alumina blanket $t_{insulation}$ (m)	q (W)	Silica blanket $t_{insulation}$ (m)	Alumina blanket $t_{insulation}$ (m)
1000	0.02421	0.02909	2810	0.008222	0.009878
1121	0.02154	0.02588	2931	0.007858	0.009441
1241	0.01939	0.02329	3052	0.007523	0.009038
1362	0.01761	0.02116	3172	0.007214	0.008666
1483	0.01613	0.01938	3293	0.006927	0.008322
1603	0.01487	0.01786	3414	0.00666	0.008002
1724	0.01379	0.01656	3534	0.006412	0.007703
1845	0.01284	0.01543	3655	0.00618	0.007425
1966	0.01202	0.01444	3776	0.005963	0.007164
2086	0.01129	0.01356	3897	0.005759	0.006919
2207	0.01064	0.01278	4017	0.005568	0.006689
2328	0.01005	0.01208	4138	0.005388	0.006473
2448	0.009528	0.01145	4259	0.005218	0.006269
2569	0.009052	0.01087	4379	0.005057	0.006076
2690	0.008618	0.01035	4500	0.004905	0.005893

An insulation thickness of 25 mm for the flat head and Appendix 2 flange was selected to be sufficient to enhance the effectiveness of the heating system.

The calculations were based on the use of AISI 316 stainless steel (1 mm thickness) as outer support for the insulation blankets. The temperature of the stainless steel was fixed at 70°C for these calculations.

Appendix 6: Pressure Relief Valve

This Appendix contains calculations for the pressure relief valve.

The spring used in the pressure relief valve was designed using equations from Shigley [21], to maintain the required preload on the glider. The selected spring material was BeCu - Brush Wellman: Brush Alloy M25 - UNS C17300.

Table A6-1: Input values for PRV spring design calculations

Variable	Description	Value
F	Required spring preload	918.92 N
$spring_{od}$	Outer diameter of spring	0.03 m
$wire_{od}$	Outer diameter of spring wire	0.005 m
E	Young's Modulus	131 GPa
v	Poisson's ratio	0.285
N_e	Number of end coils	2
p	Spring wire pitch	0.01 m
L_o	Spring free length	0.07 m

The following equations were used for the spring design.

$$D = spring_{od} - wire_{od}$$

$$N_t = N_a + 2$$

$$G = \frac{E}{2 \cdot (1+v)}$$

$$L_o = p \cdot N_a + 2 \cdot wire_{od}$$

$$L_s = wire_{od} \cdot N_t$$

Stress equations:

- *Static:*

$$\tau = \frac{K_s \cdot (8FD)}{\pi \cdot wire_{od}^{\ 3}}$$

$$K_s = \frac{2C+1}{2C}$$

$$C = \frac{D}{wire_{od}}$$

- *Fatigue:*

$$\tau_{max} = K_c \cdot \tau \qquad K_c = \frac{K_B}{K_s}$$

$$K_B = \frac{4C+2}{4C-3}$$

Deflection equations:

$$y = \frac{8 \cdot F \cdot D^3 \cdot N_a}{wire_{od}^{\ 4} \cdot G} \qquad k = \frac{wire_{od}^{\ 4} \cdot G}{8 \cdot D^3 \cdot N_a}$$

Stability equations:

$$\alpha = 0.5 \qquad L_{stable} = \frac{\pi \cdot D}{\alpha}\left[\frac{2(E-G)}{2G+E}\right]^{0.5}$$

These results of the calculations shown above are shown in Table A6-2:

Table A6-2: Spring design results

Variable	Description	Value
C	Ratio	0.5
k	Spring stiffness	42.477 kN/m
K_B	Ratio	1.294
K_c	Ratio	1.176
K_s	Ratio	1.1
L_{stable}	Maximum stable spring length	0.1302 m
τ	Static stress	514.8 MPa
τ_{max}	Fatigue stress	605.6 MPa
y	Deflection	0.0216 m

Appendix 7: Drawings

This Appendix contains the pressure vessel drawings.

The pressure vessel was divided into the following categories:

- Vessel
  - Shell (VS_SHELL)
  - Heads (VS_HEAD)
  - Saddle (VS_SADDLE)
- Flanges
  - ASME VIII Appendix 2 flanges (FL_APP2)
  - Long welding neck flanges (FL_LWN_DETAIL)
  - Gasket (FL_APP2_GASKET)
- Instrumentation
  - Heater assembly (INST_HEA)
    - Structure rings (INST_HEA_STRR)
    - Tube bolts & nuts (INST_HEA_BN)
    - Ceramic tubes & washers (INST_HEA_TUBW)
    - Element wire (No detail sketch)
    - Ceramic platform (INST_HEA_PLAT)
  - Thermowell (INST_THW)
  - Pressure relief valve (INST_PRV)
    - Glider (INST_PRV_GLD)
    - Housing (INST_PRV_HOUS)
    - Spring (INST_PRV_SPR)
    - Spring preload bolt (INST_PRV_BLT)
  - Lead outs (INST_ELO)
    - Holder (INST_ELO_HLD)
    - Lead out external stop (INST_ELO_STP)
    - Copper ribbed lead out rods (INST_ELO_CRR)
- Insulation
  - Shell (INSU_SHL)
  - Heater structure rings (INSU_HEAT)
  - Heads (INSU_HEAD)
  - RTV Rubber (INSU_RTV)

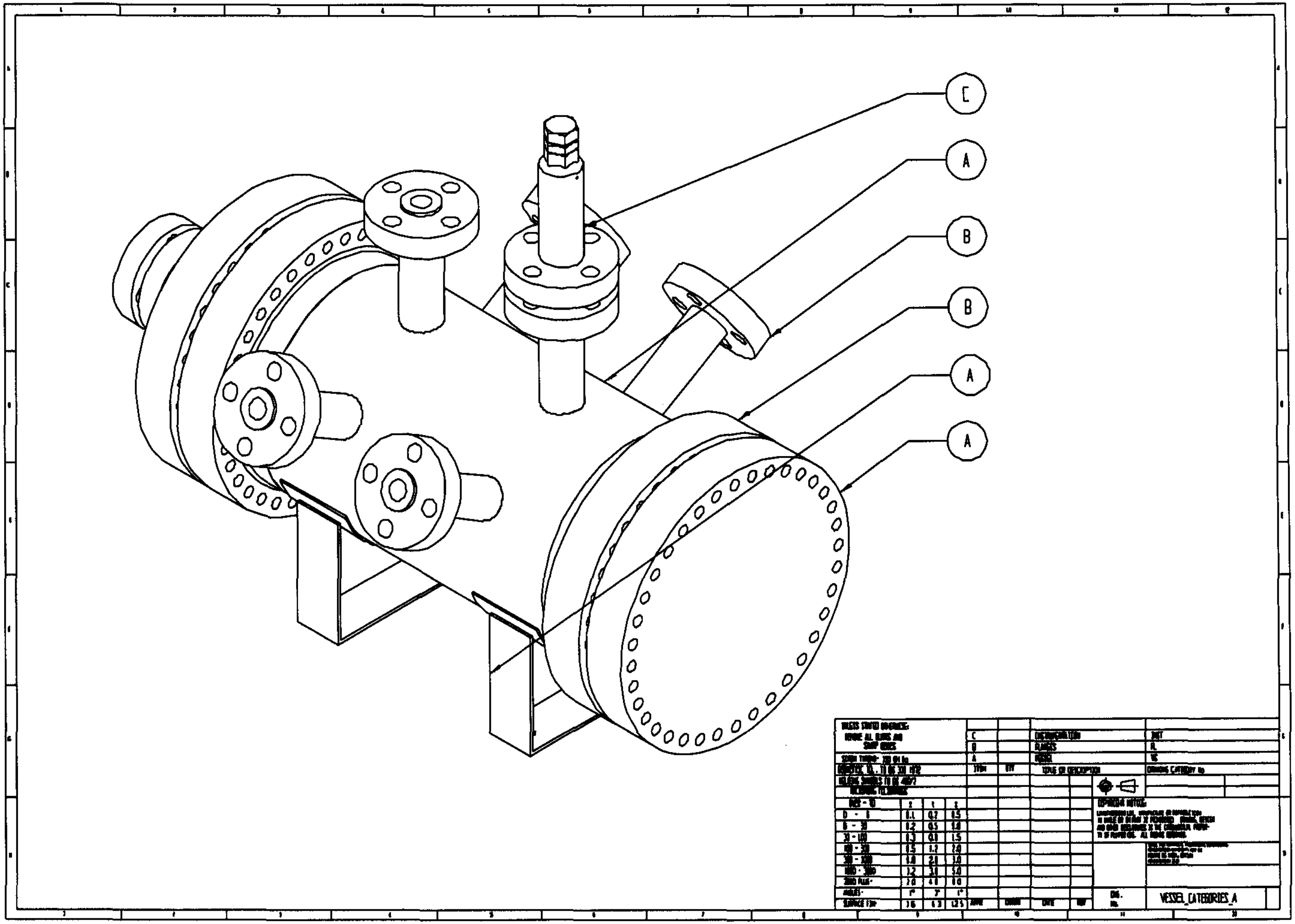

C
A
B
B
A
A
TITLE OF DESCRIPTION
VESSEL_CATEGORIES_A

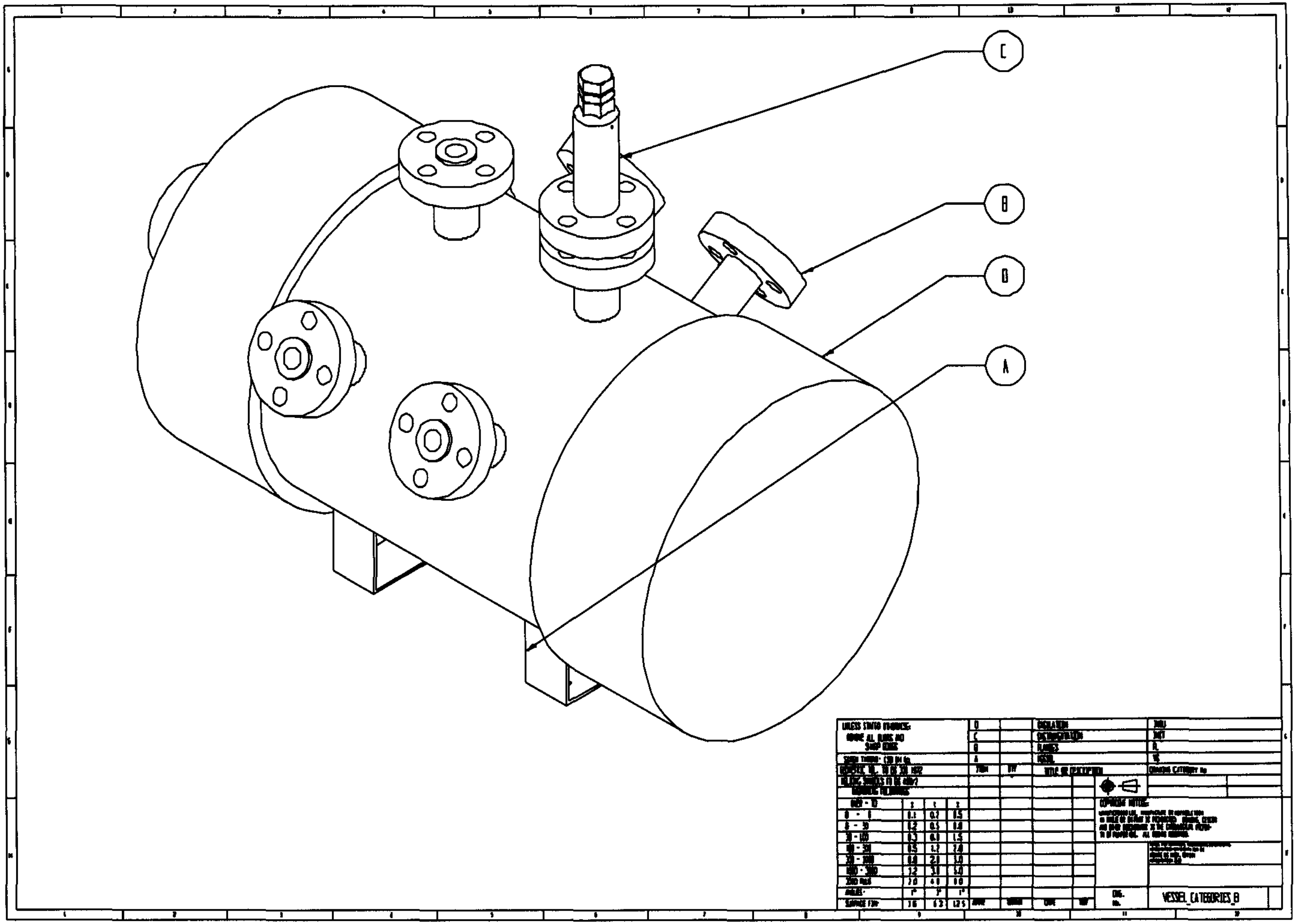
C
B
D
A
UNLESS STATED OTHERWISE:
FLANGES
VESSEL
TITLE OR DESCRIPTION
COPYRIGHT NOTICE:
DWG.
No.
VESSEL_CATEGORIES_B

A7.1: Vessel drawings

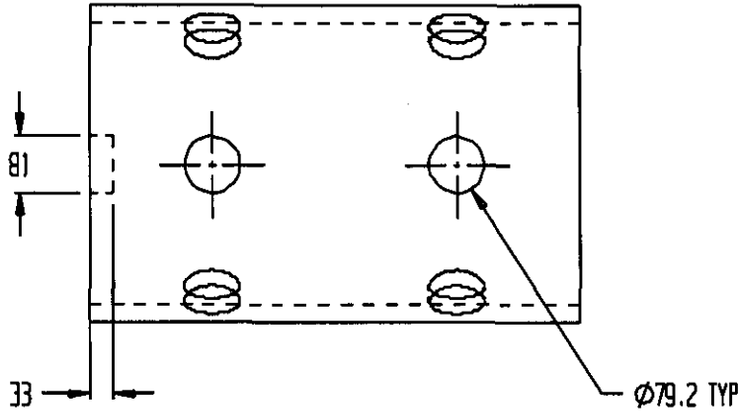

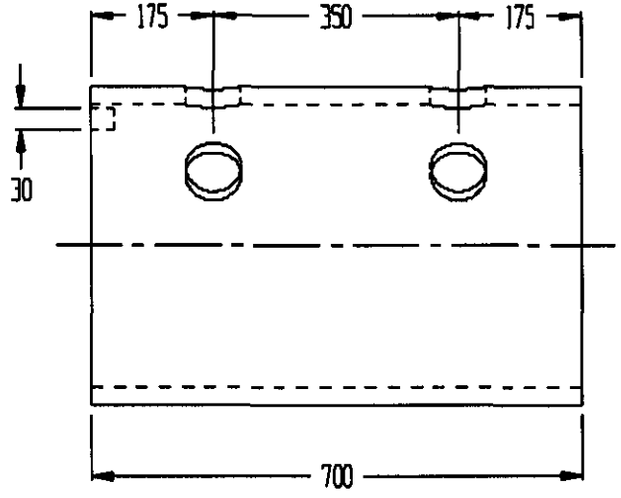

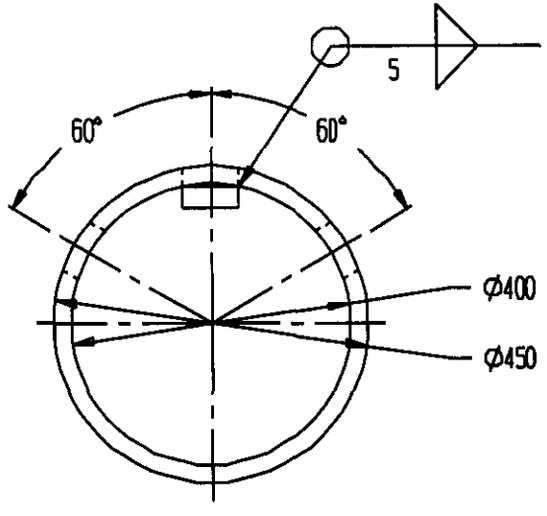

MATERIAL :	HAYNES ALLOY 230
	PRESSURE VESSEL SHELL
	VS_SHELL

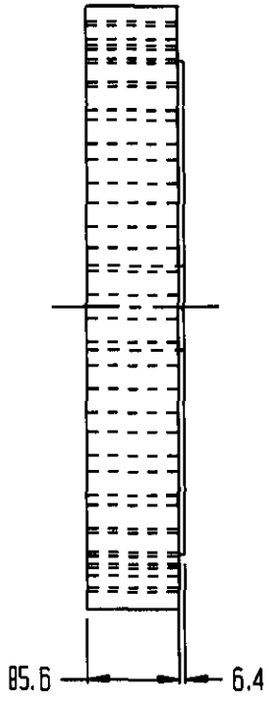

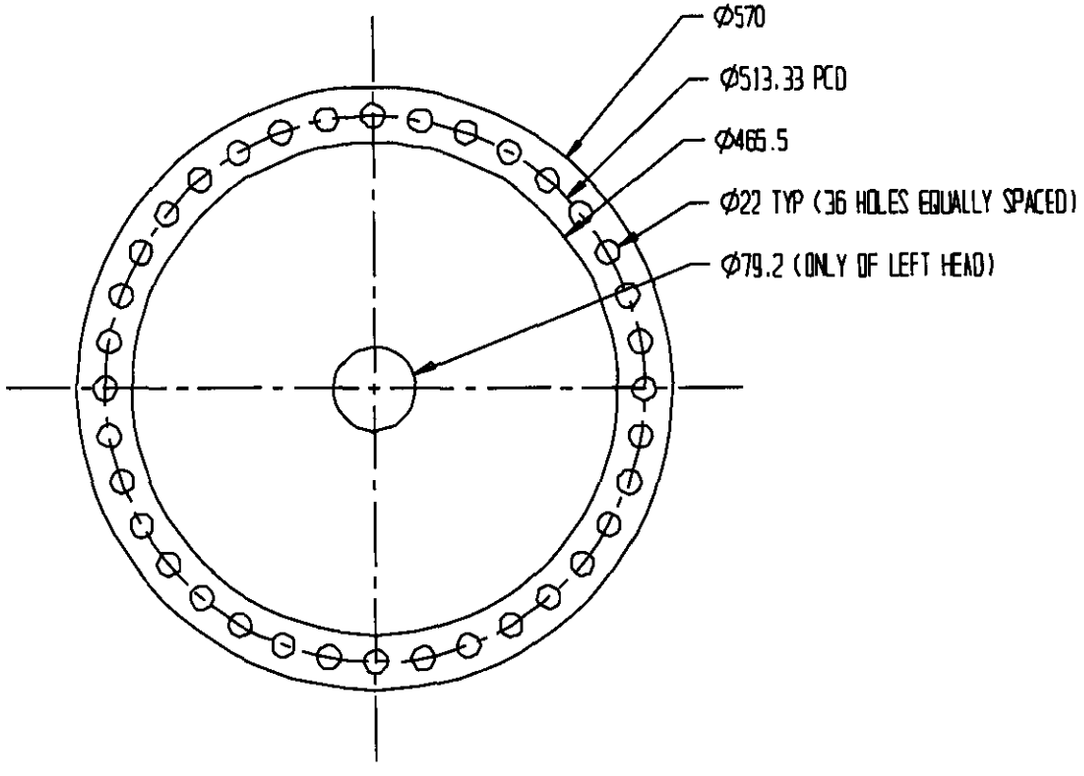

MATERIAL:	HAYNES ALLOY 230
	VESSEL FLAT HEAD
	FS_HEAD

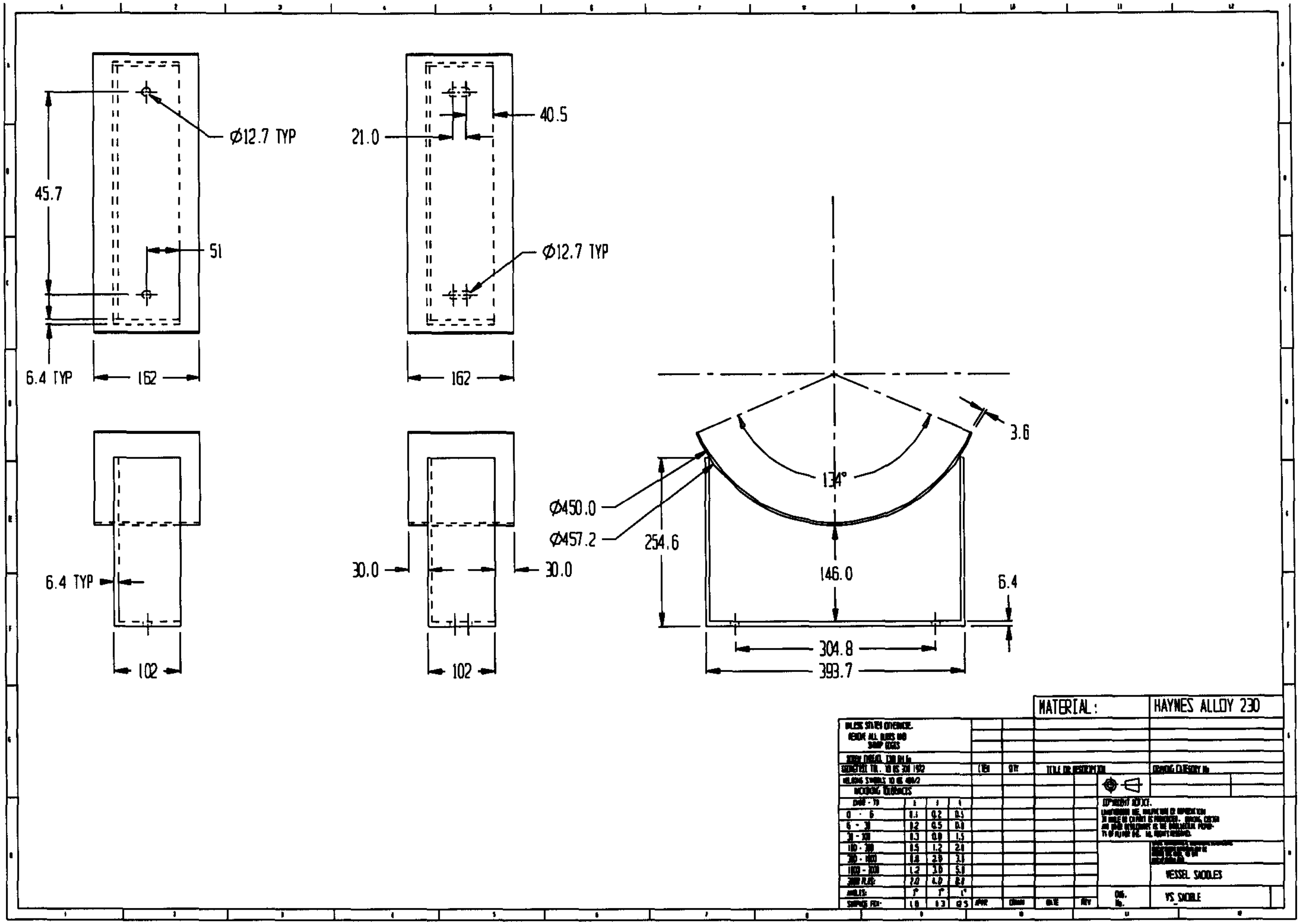

Ø12.7 TYP
45.7
51
6.4 TYP
162
40.5
21.0
Ø12.7 TYP
162
6.4 TYP
102
30.0
30.0
102
134°
3.6
Ø450.0
Ø457.2
254.6
146.0
6.4
304.8
393.7
MATERIAL:
HAYNES ALLOY 230
VESSEL SADDLES
VS_SADDLE

A7.2: Flange drawings

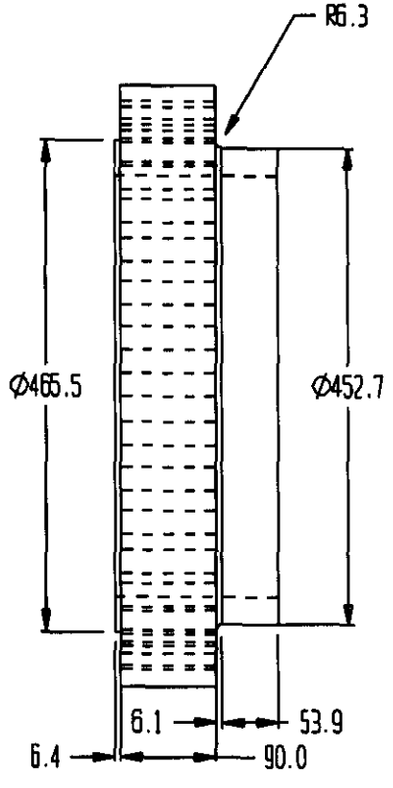

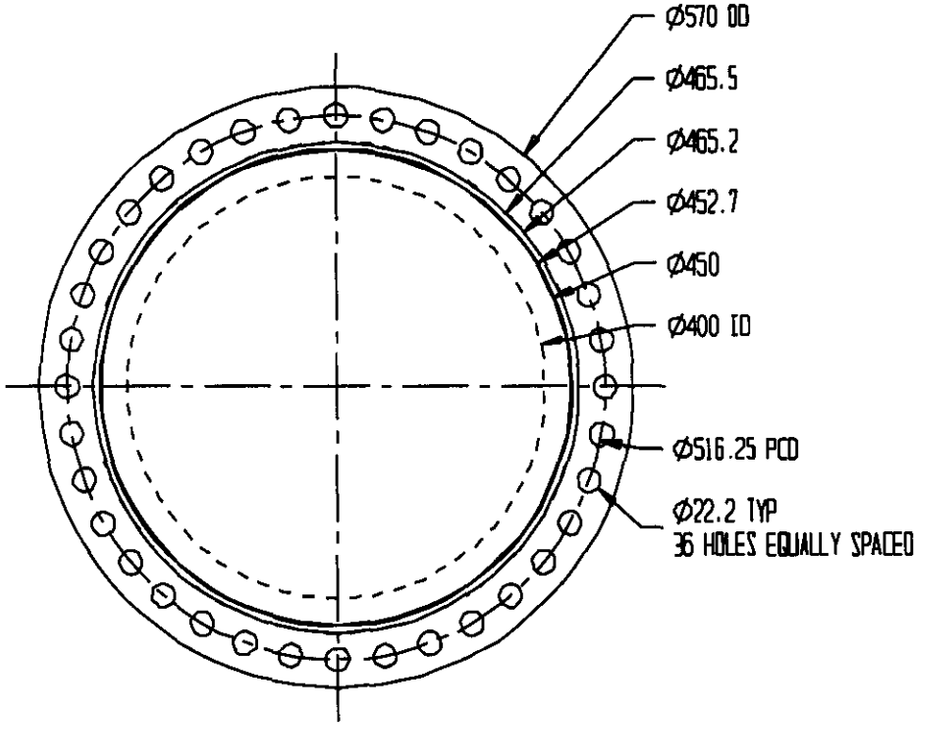

MATERIAL:	HAYNES ALLOY 230
ASME VIII APPENDIX 2 FLANGE	
DWG. No.	FL_APP2

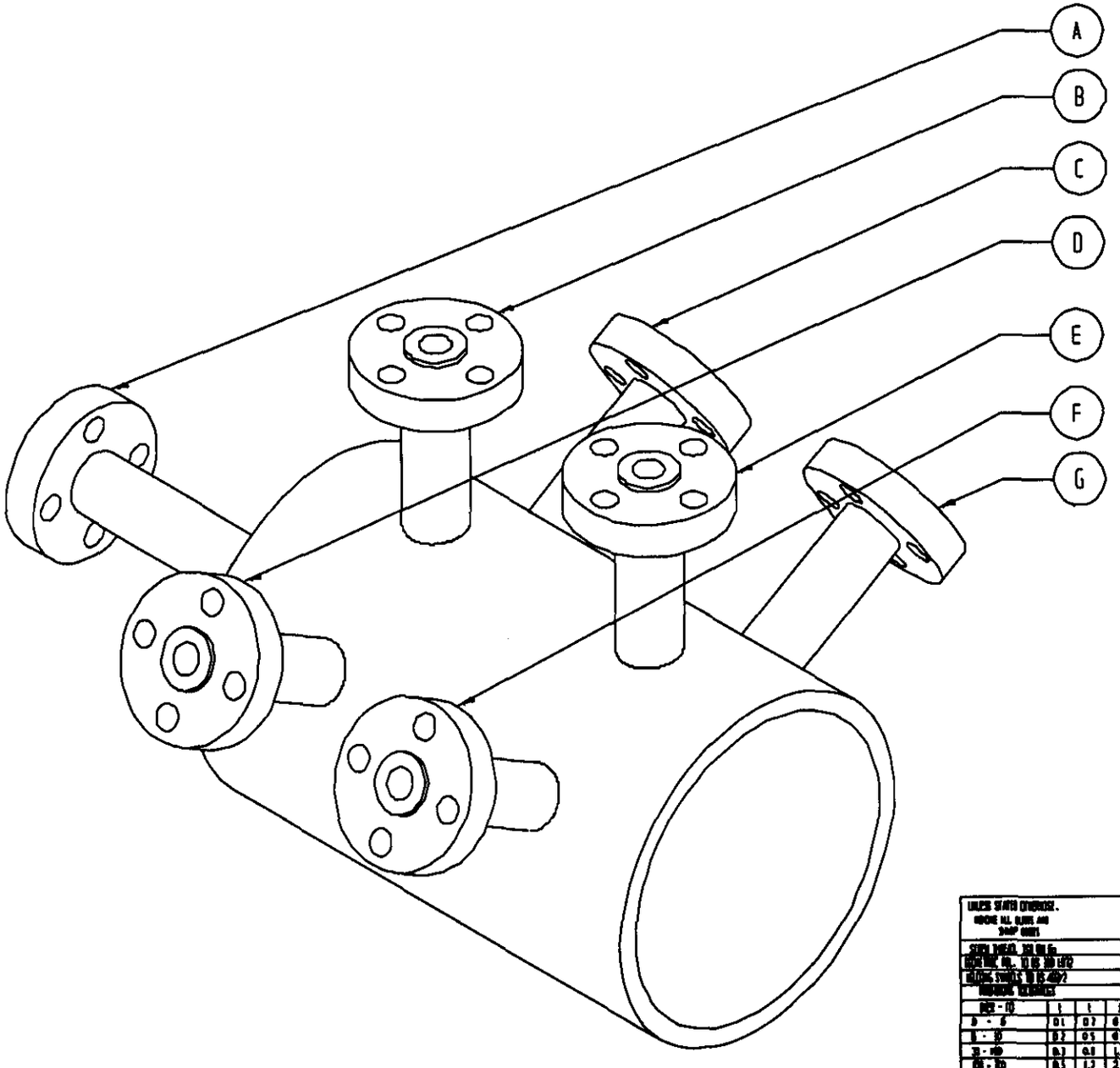

STANDARD CLASS 2500 1.5" LINE

R_LIN

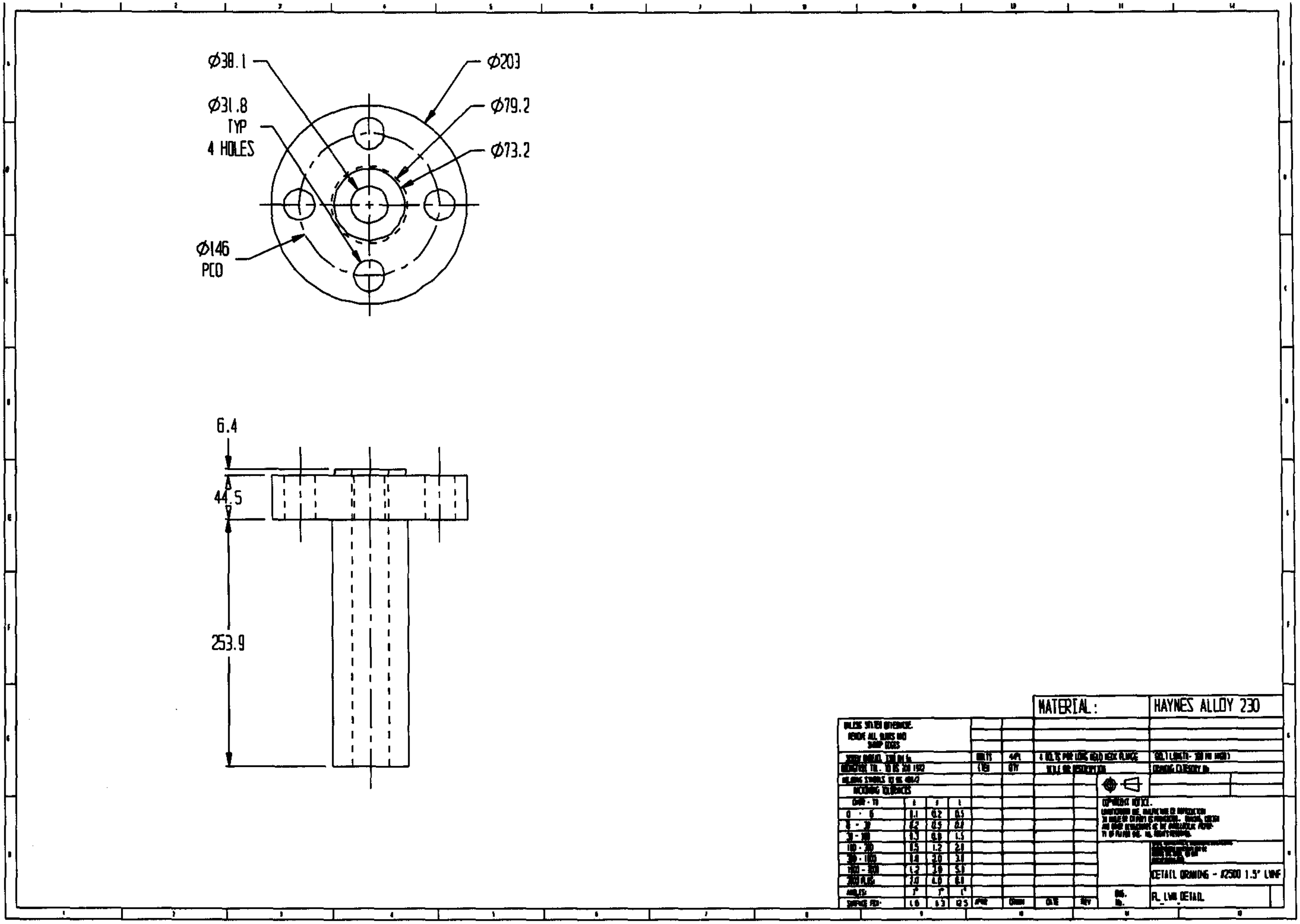

Ø38.1
Ø203
Ø31.8
TYP
4 HOLES
Ø79.2
Ø73.2
Ø146
PCD
6.4
44.5
253.9
MATERIAL :
HAYNES ALLOY 230
DETAIL DRAWING - #2500 1.5" LWNF

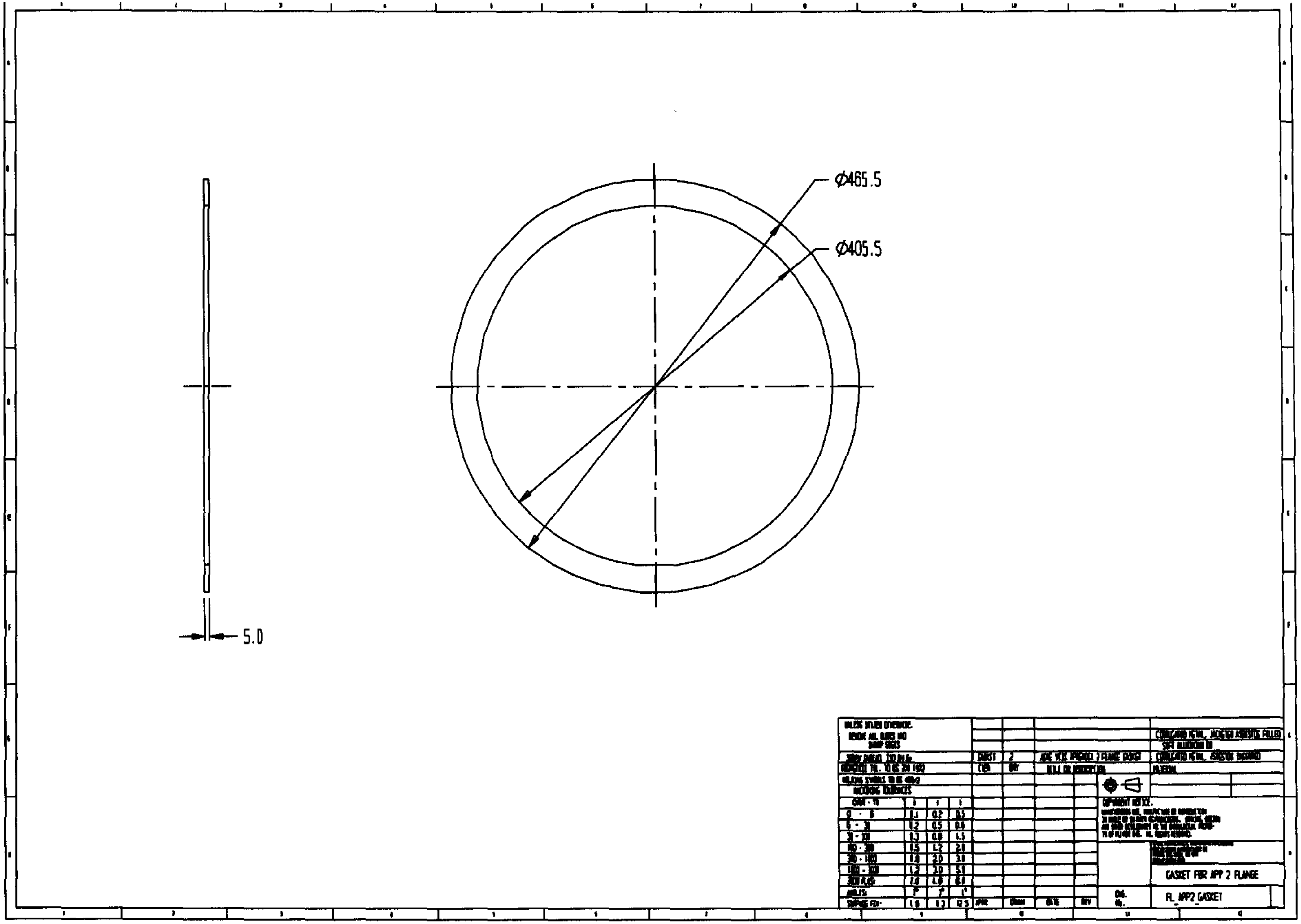
Ø465.5
Ø405.5
5.0
GASKET FOR APP 2 FLANGE
FL_APP2_GASKET

A7.3: Instrumentation drawings

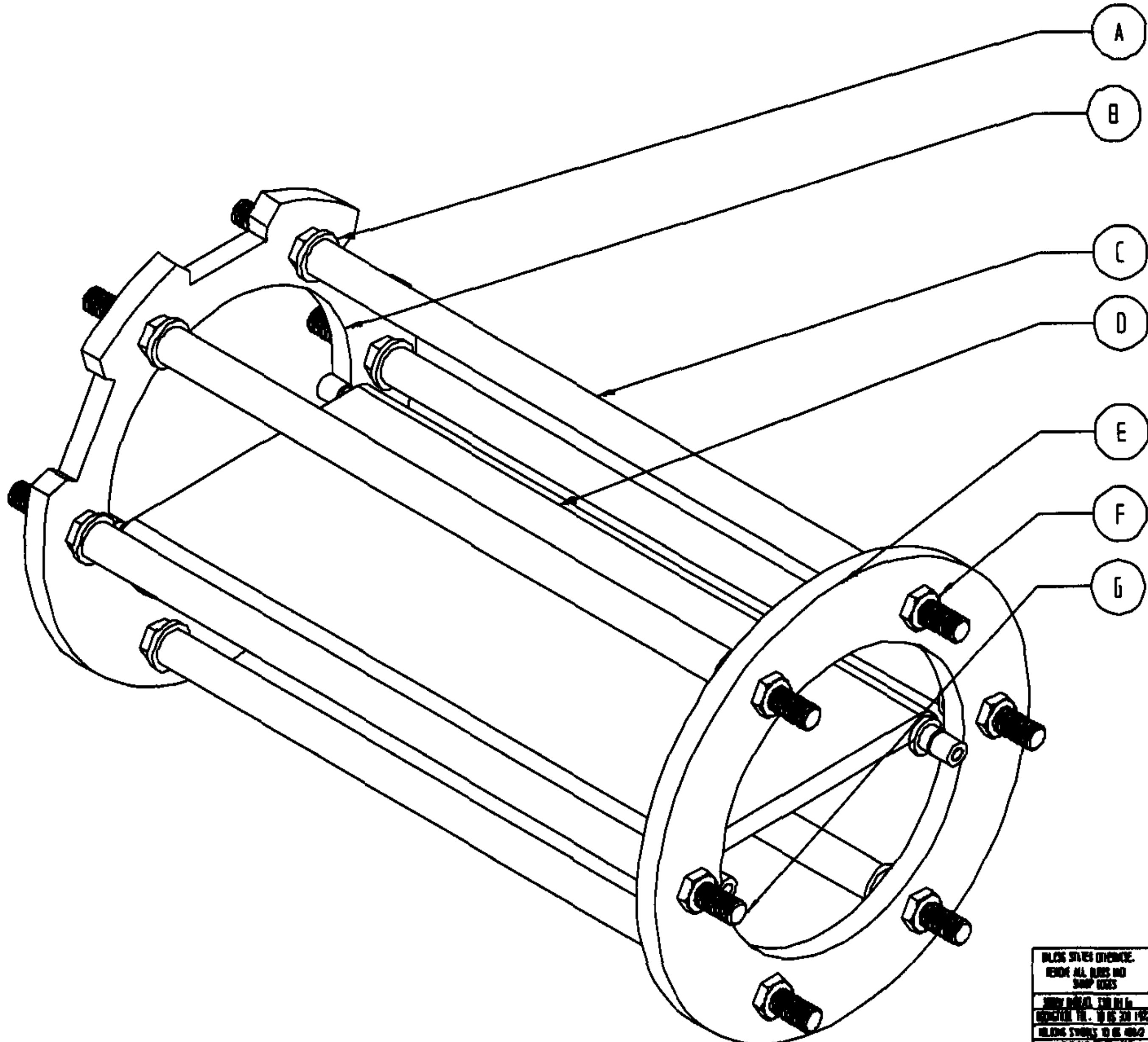

G	8	HEATER BOLT	INST HEA BO
F	24	HEATER NUT	INST HEA NU
E	1	HEATER STRUCTURE RING - RIGHT	INST HEA STR R
D	1	CERAMIC PLATFORM	INST HEA PLAT
C	8	CERAMIC HEATER TUBE	INST HEA TUBE
B	1	HEATER STRUCTURE RING - LEFT	INST HEA STR L
A	12	CERAMIC WASHER	INST HEA WASH
ITEM	QTY	TITLE OR DESCRIPTION	DRAWING CATEGORY No

UNLESS STATED OTHERWISE.
REMOVE ALL BURRS AND SHARP EDGES

DRAWING TOL. TO BS 308 1972

WELDING SYMBOLS TO BS 499/2

MACHINING TOLERANCES

0 - 6	0.1	0.2	0.5
6 - 30	0.2	0.5	0.8
30 - 120	0.3	0.8	1.5
120 - 315	0.5	1.2	2.0
315 - 1000	0.8	2.0	3.0
1000 - 2000	1.2	3.0	5.0
2000 & OVER	2.0	4.0	8.0
ANGLES			
SURFACE FIN.	1.6	6.3	12.5

APPD | DRAWN | DATE | REV

COPYRIGHT NOTICE.

HEATER ASSEMBLY

DWG. No. INST_HEA

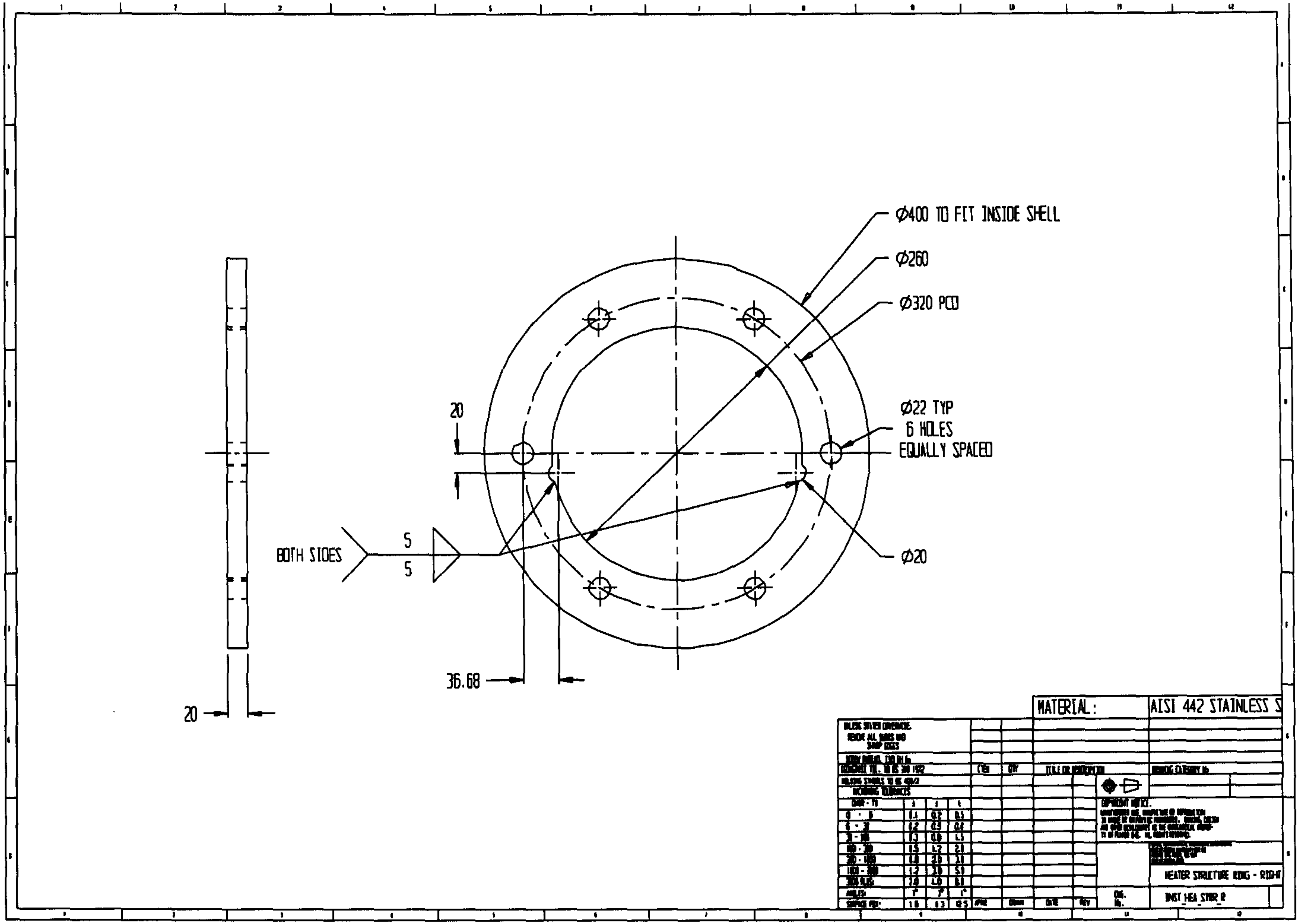

Ø400 TO FIT INSIDE SHELL
Ø260
Ø320 PCD
Ø22 TYP
6 HOLES
EQUALLY SPACED
Ø20
20
36.68
5
5
BOTH SIDES
20
MATERIAL:
AISI 442 STAINLESS S
HEATER STRUCTURE RING - RIGHT

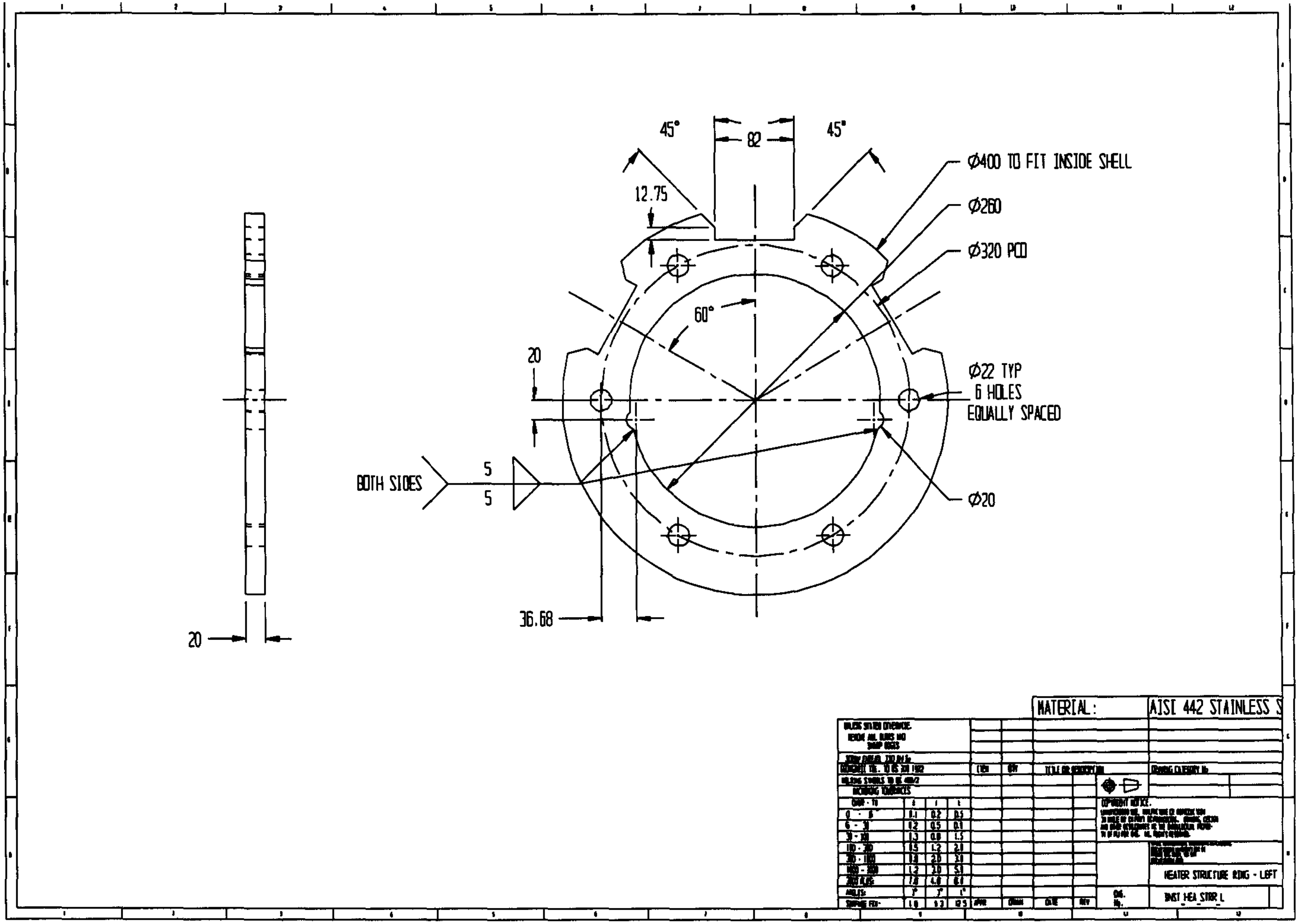
45°
82
45°
12.75
Ø400 TO FIT INSIDE SHELL
Ø260
Ø320 PCD
60°
20
Ø22 TYP
6 HOLES
EQUALLY SPACED
BOTH SIDES
5
5
Ø20
36.68
20
MATERIAL:
AISI 442 STAINLESS S
HEATER STRUCTURE RING - LEFT
INST HEA STRR L

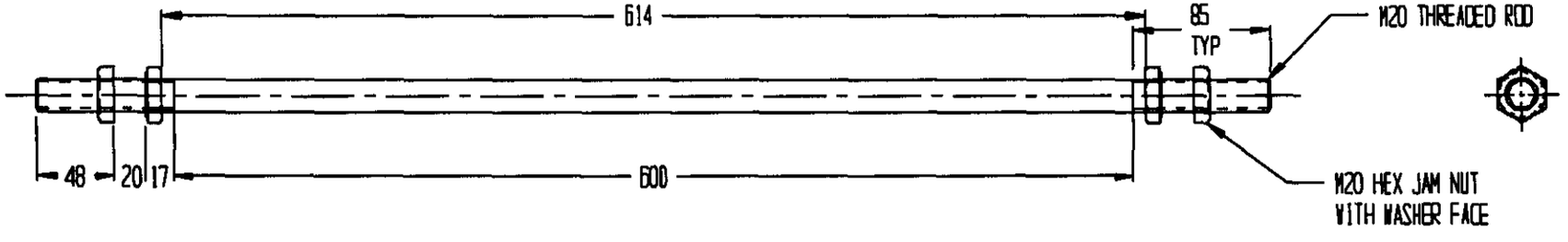

MATERIAL:	AISI 442 STAINLESS S
	CERAMIC TUBE BOLT & NUTS
	DIST HEA EN

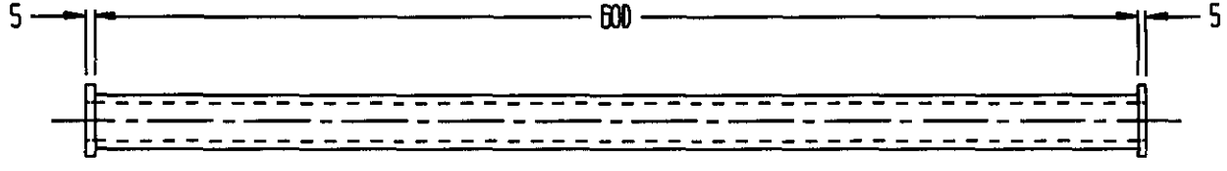

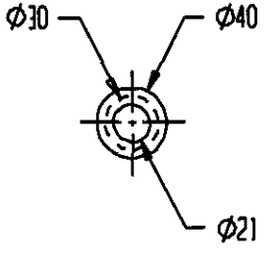

MATERIAL :	CERAMIC TUBE
	HEATER TUBE & BIOS
	INST HEA TUBV

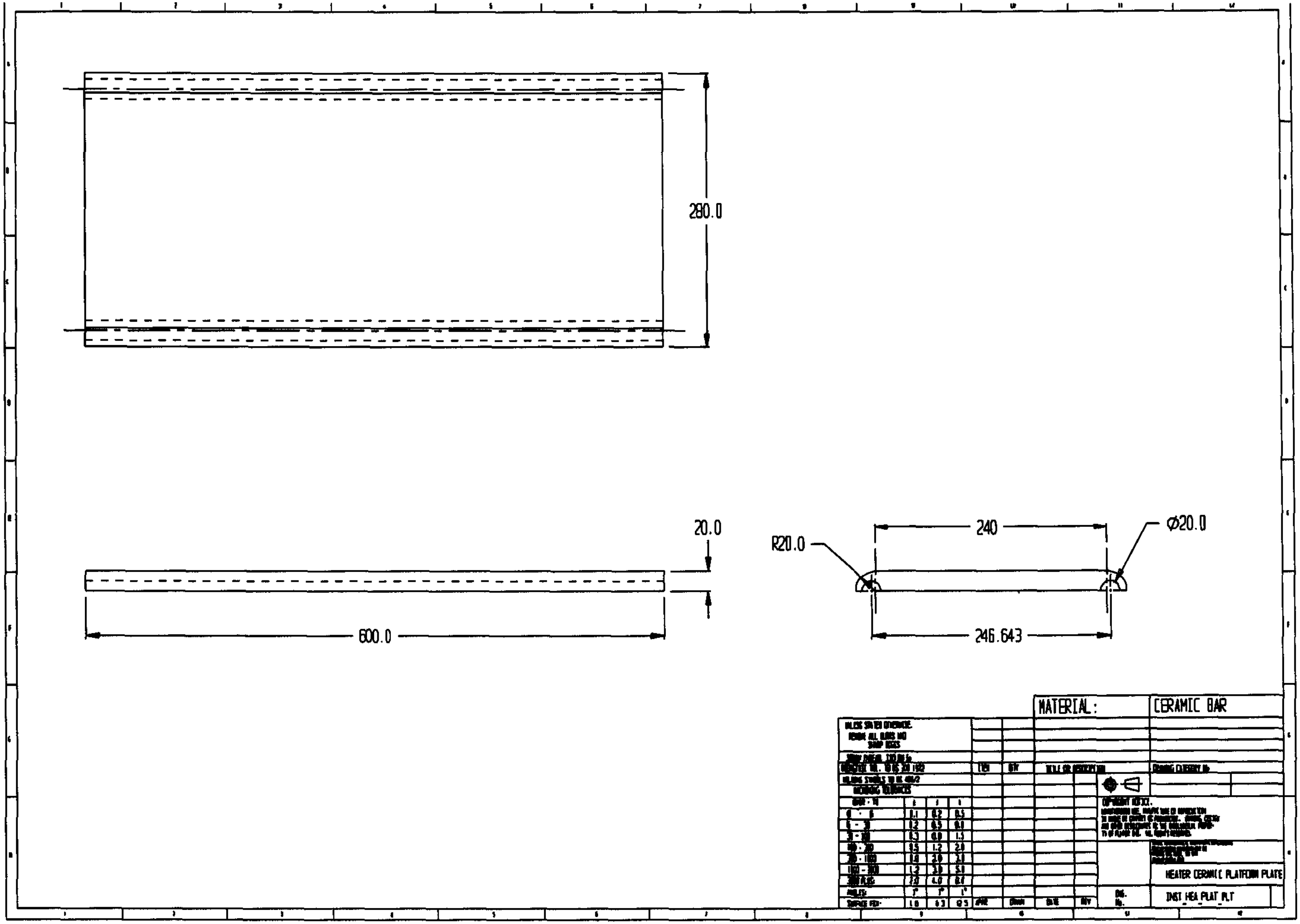
280.0
20.0
600.0
240
R20.0
Ø20.0
246.643
MATERIAL:
CERAMIC BAR
HEATER CERAMIC PLATFORM PLATE
INST HEA PLAT PLT

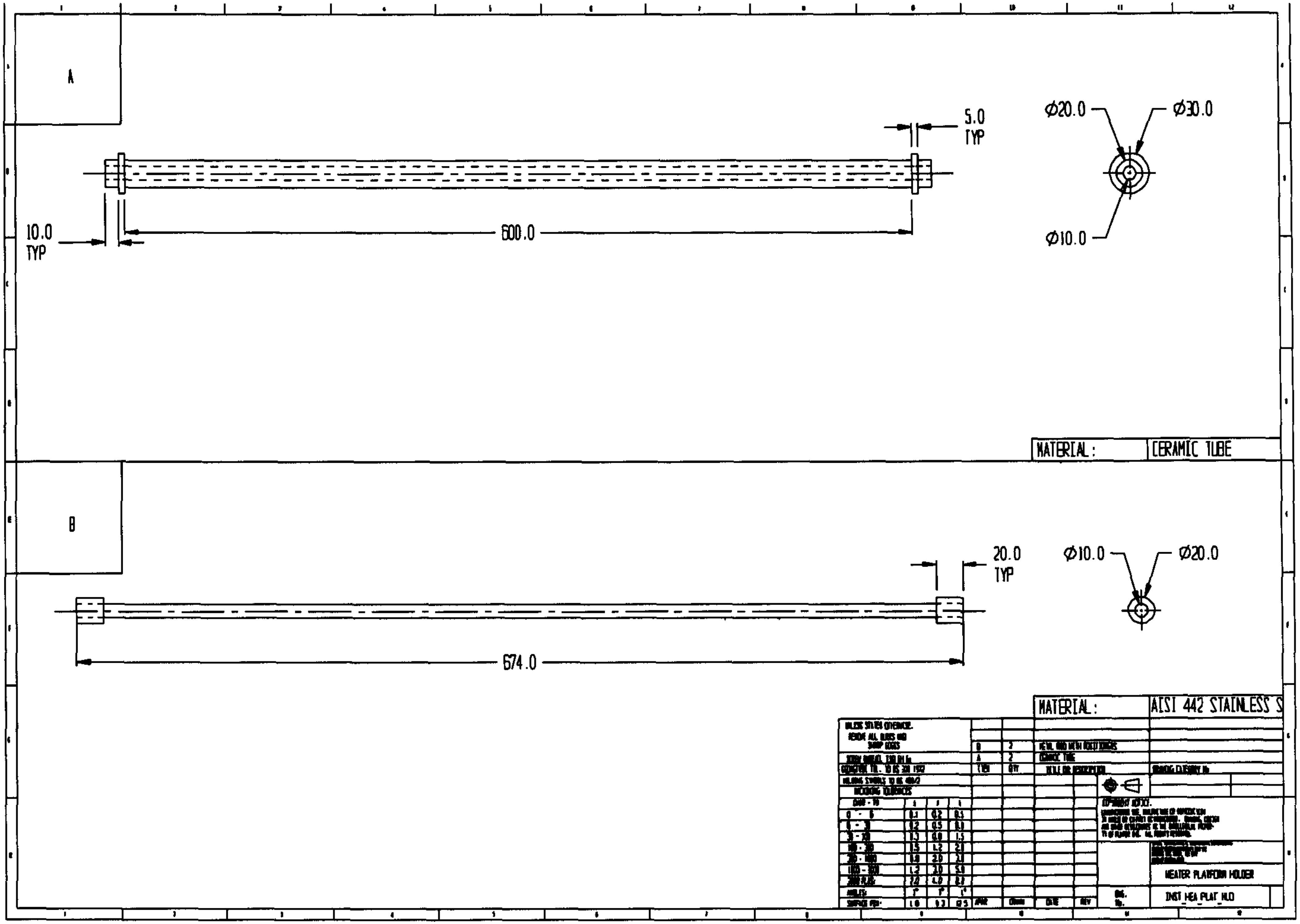
A
5.0 TYP
10.0 TYP
600.0
Ø20.0
Ø30.0
Ø10.0
MATERIAL :
CERAMIC TUBE
B
20.0 TYP
674.0
Ø10.0
Ø20.0
MATERIAL :
AISI 442 STAINLESS S
CERAMIC TUBE
ITEM
QTY
TITLE OR DESCRIPTION
COPYRIGHT NOTICE
HEATER PLATFORM HOLDER
INST_HEA_PLAT_HLD

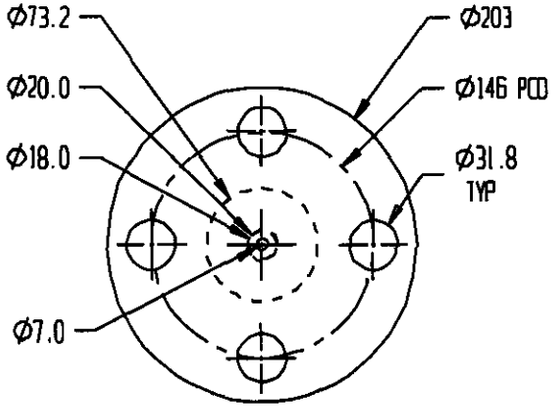

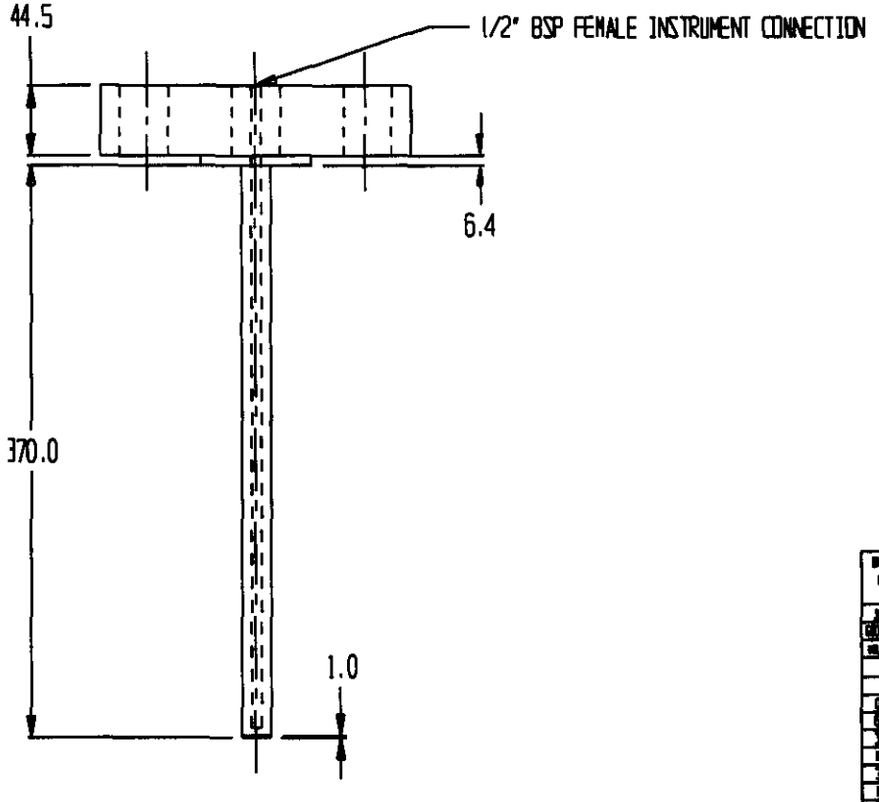

THERMOCOUPLE THERMOWELL

INST_THW

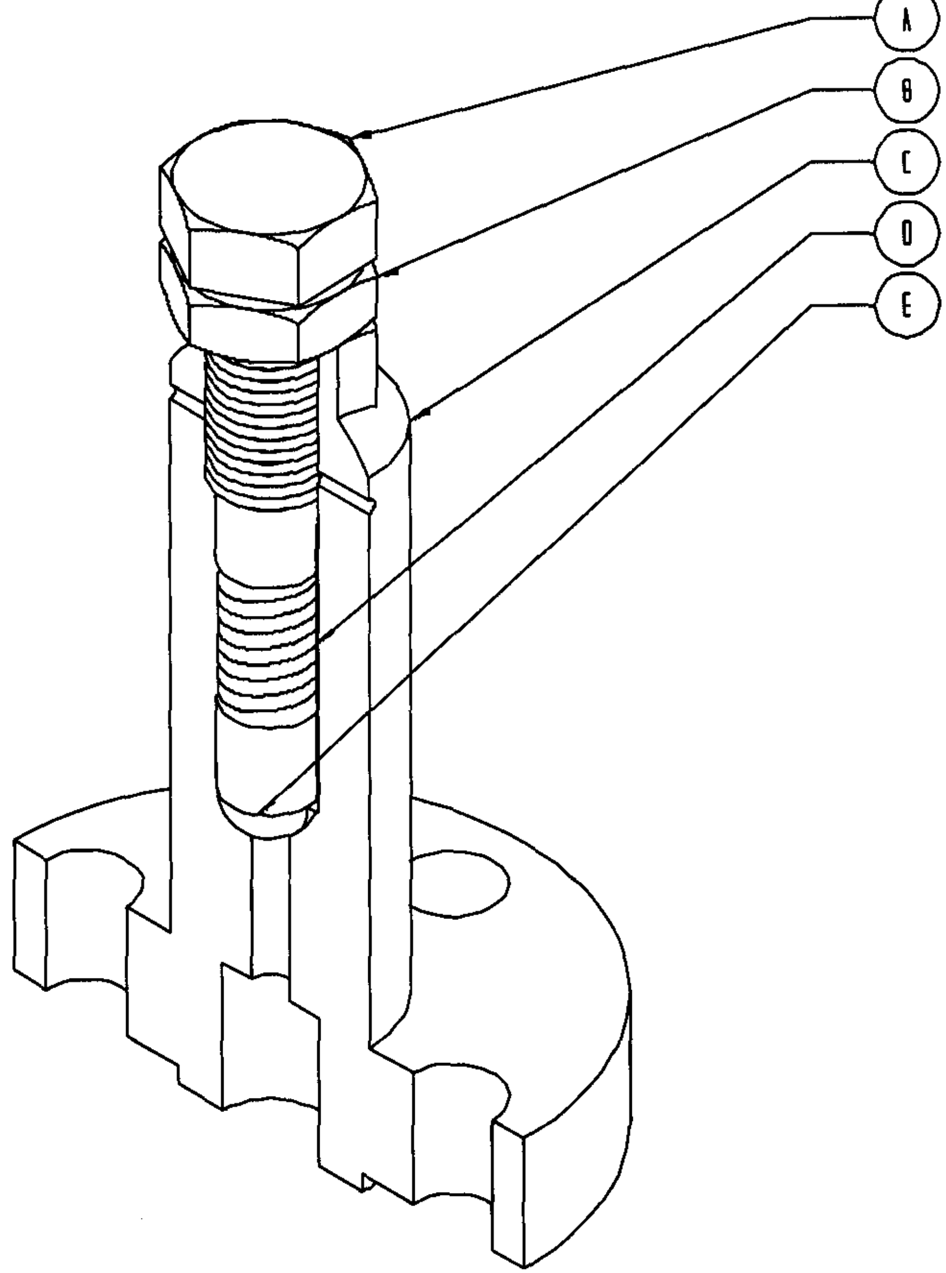

COPYRIGHT NOTICE.

PRESSURE RELIEF VALVE ASSEMBLY

DWG. No. INST_PRV

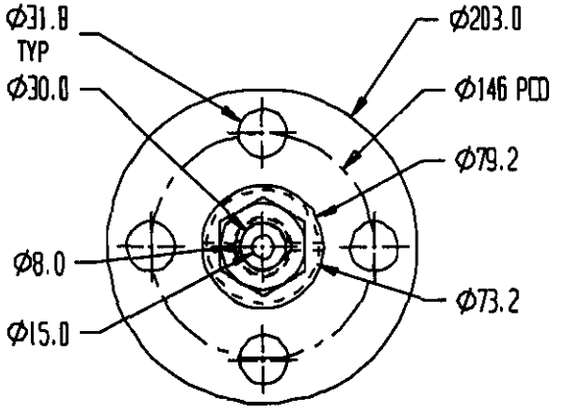

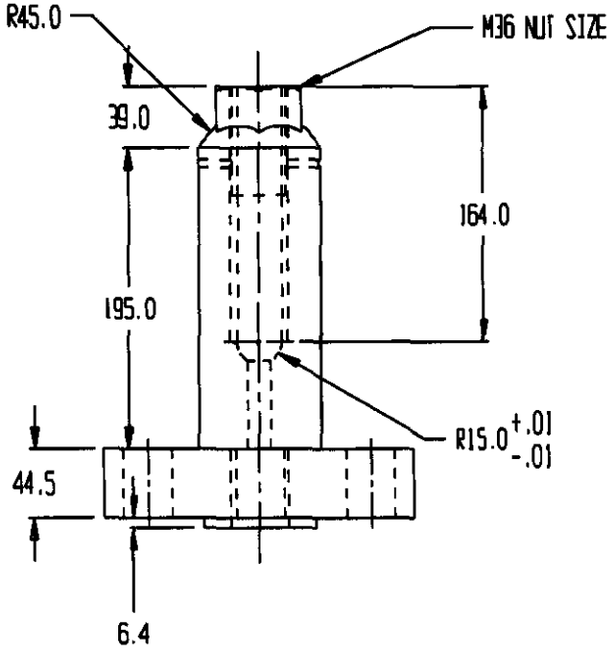

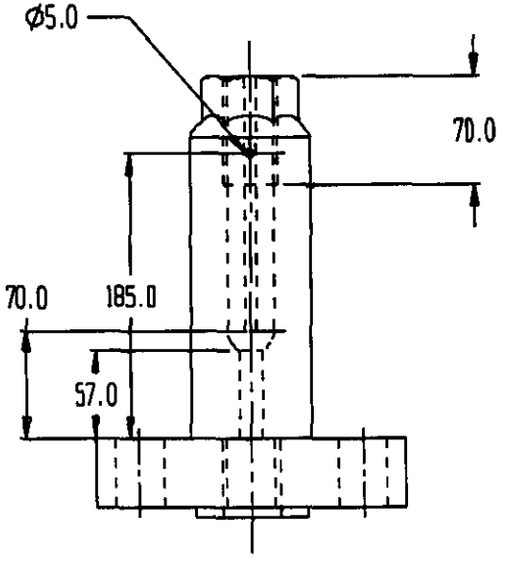

MATERIAL:	HAYNES ALLOY 230
	PRESSURE RELIEF VALVE HOUSING
DWG. No.	INST PRV HOUS

A

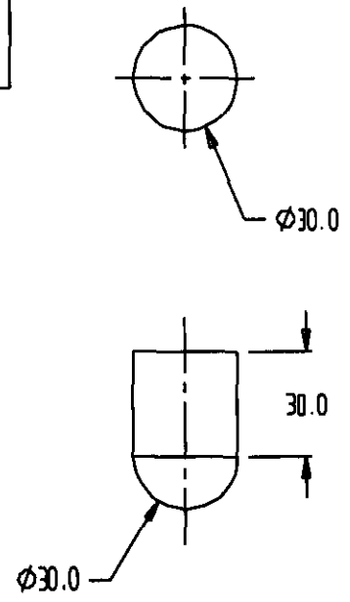

MATERIAL: 316 SS

B

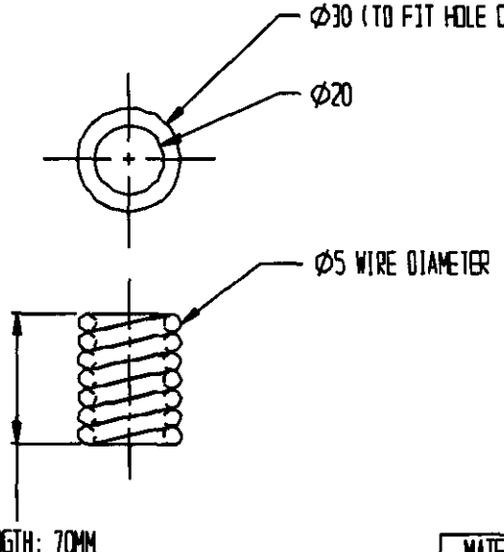

MATERIAL: BERYLLIUM COPPER
BRUSH ALLOY M25 - UNS C17300

C

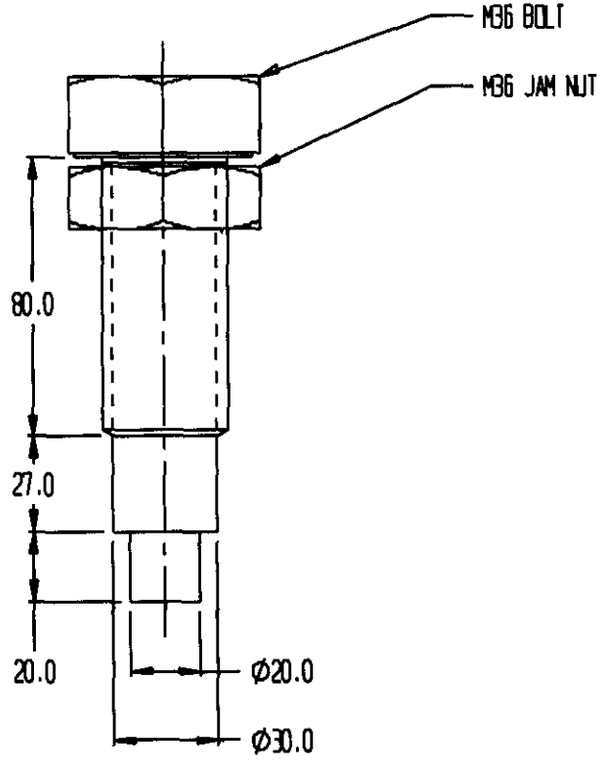

MATERIAL: 316 SS

PRESSURE RELIEF VALVE PARTS

INST PRV

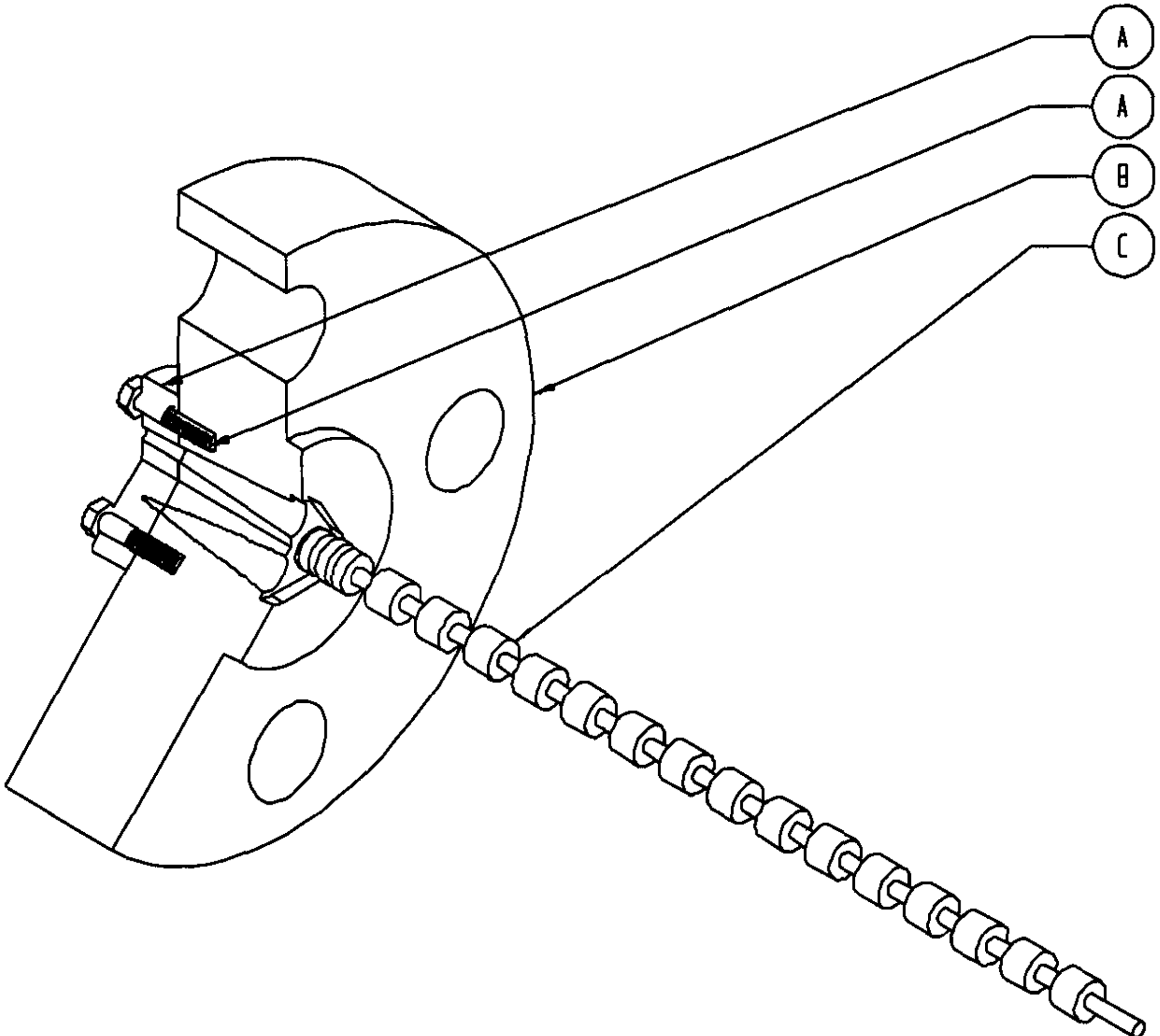

ITEM	QTY	TITLE OR DESCRIPTION	DRAWING/CATEGORY No
C		[illegible] COVER AND LEAD OUT	INST ELO CVR
B		LEAD OUT HOLDER	INST ELO HLD
A		LEAD OUT STOP BOLTS	INST ELO STP
A		LEAD OUT STOP	INST ELO STP

UNLESS STATED OTHERWISE, REMOVE ALL BURRS AND SHARP EDGES

ELECTRICAL LEAD OUT ASSEMBLY

DWG. No. INST_ELO

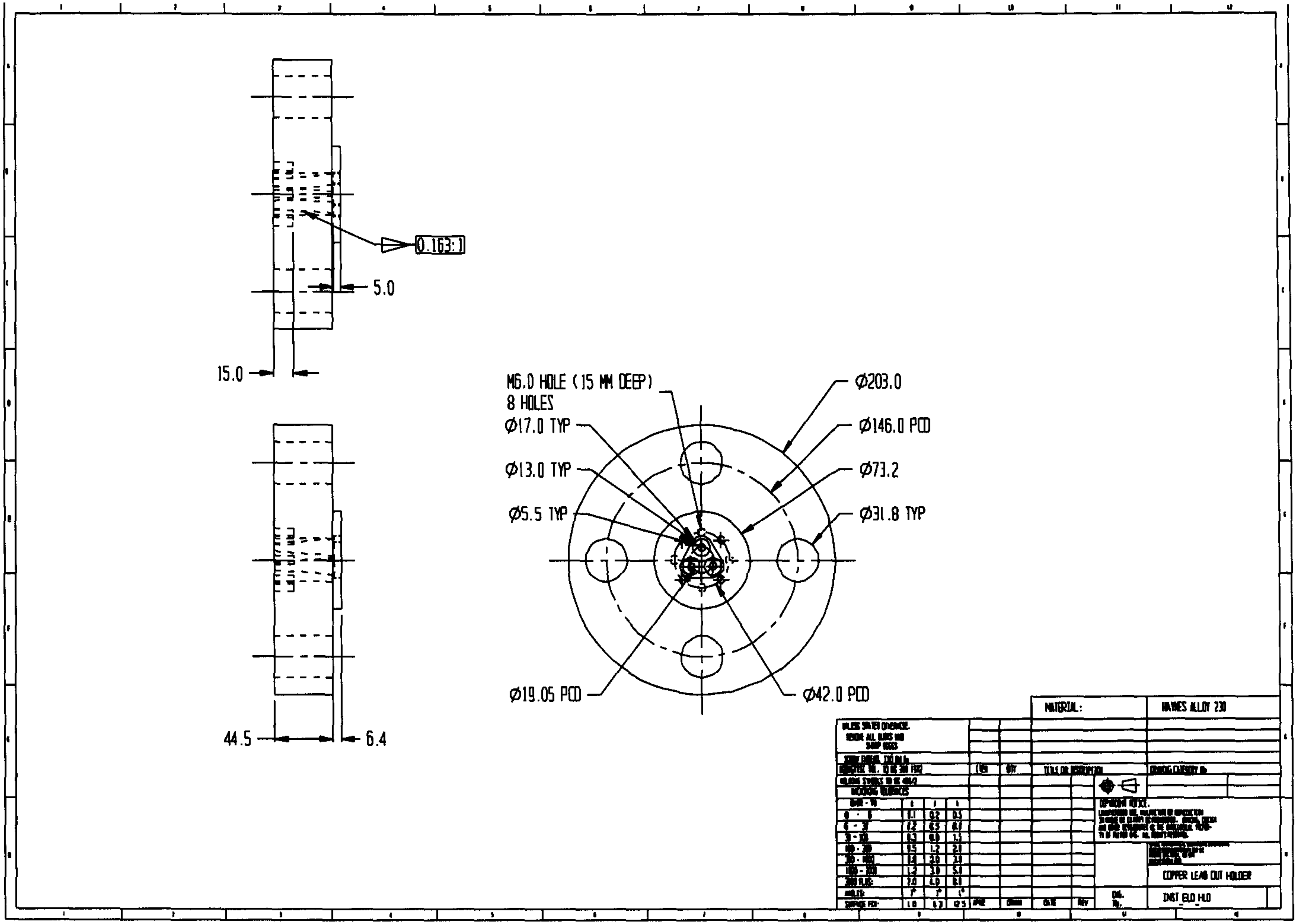

0.163:1
5.0
15.0
44.5
6.4
M6.0 HOLE (15 MM DEEP)
8 HOLES
Ø17.0 TYP
Ø13.0 TYP
Ø5.5 TYP
Ø19.05 PCD
Ø203.0
Ø146.0 PCD
Ø73.2
Ø31.8 TYP
Ø42.0 PCD
MATERIAL:
HAYNES ALLOY 230
TITLE OR DESCRIPTION
COPYRIGHT NOTICE.
COPPER LEAD OUT HOLDER
DWG. No.
INST ELD HLD

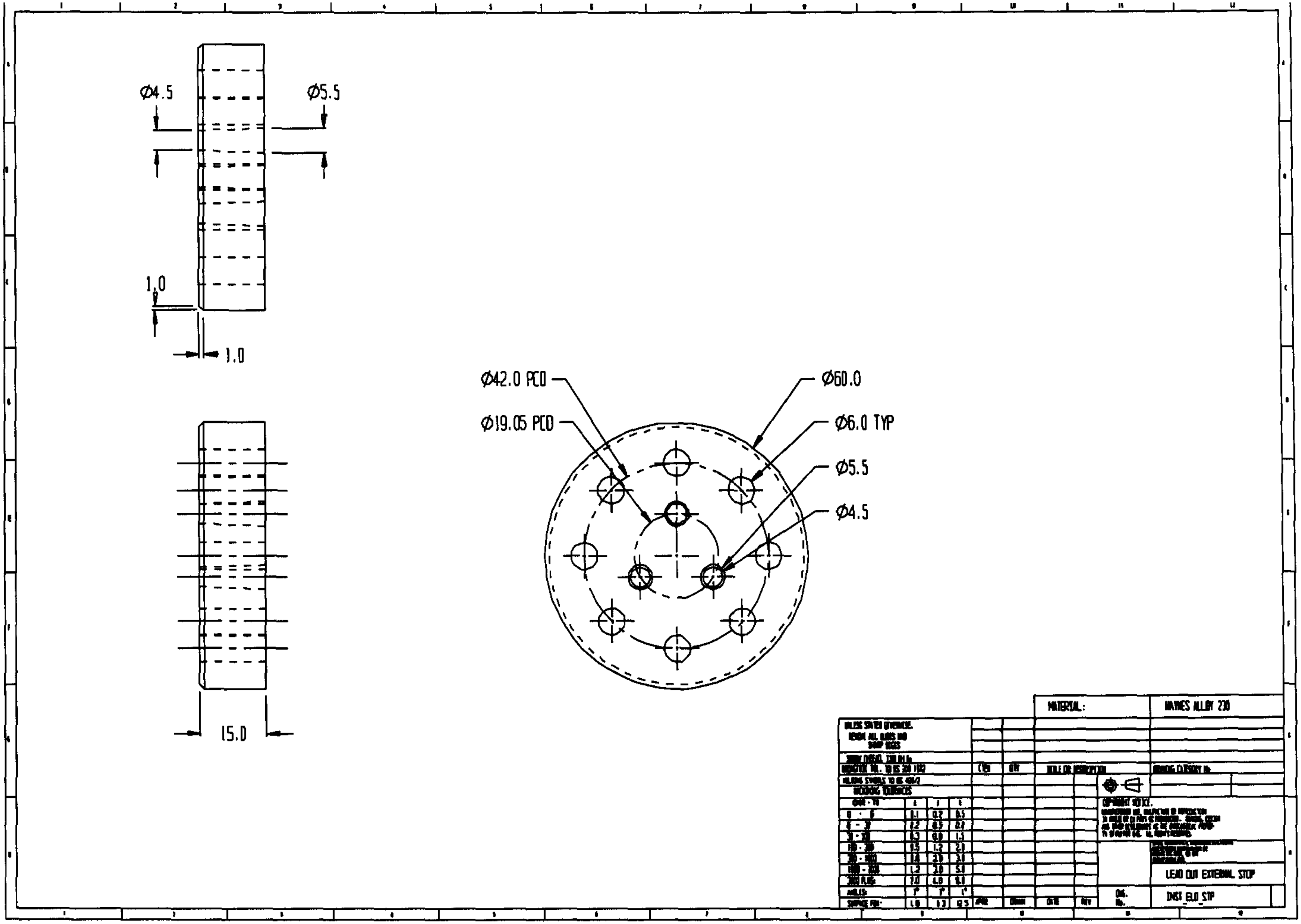
Ø4.5
Ø5.5
1.0
1.0
15.0
Ø42.0 PCD
Ø19.05 PCD
Ø60.0
Ø6.0 TYP
Ø5.5
Ø4.5
MATERIAL:
HAYNES ALLOY 230
LEAD OUT EXTERNAL STOP
INST ELO STP

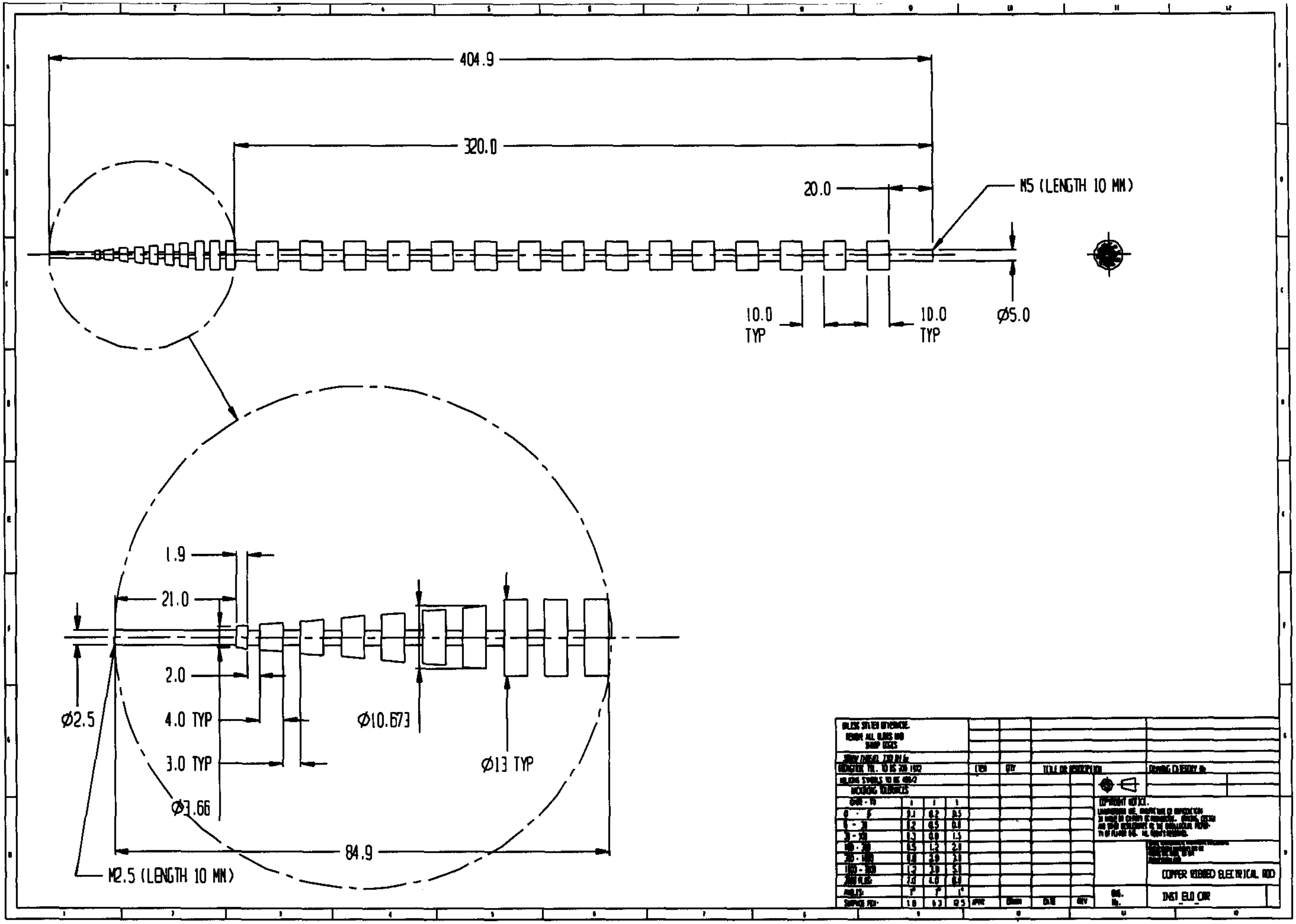
404.9
320.0
20.0
M5 (LENGTH 10 MM)
10.0 TYP
10.0 TYP
Ø5.0
1.9
21.0
2.0
4.0 TYP
3.0 TYP
Ø3.66
Ø2.5
Ø10.673
Ø13 TYP
84.9
M2.5 (LENGTH 10 MM)
ITEM
QTY
TITLE OR DESCRIPTION
COPYRIGHT NOTICE.
COPPER RIBBED ELECTRICAL ROD
INST_ELO_CIR

A7.4: Insulation drawings

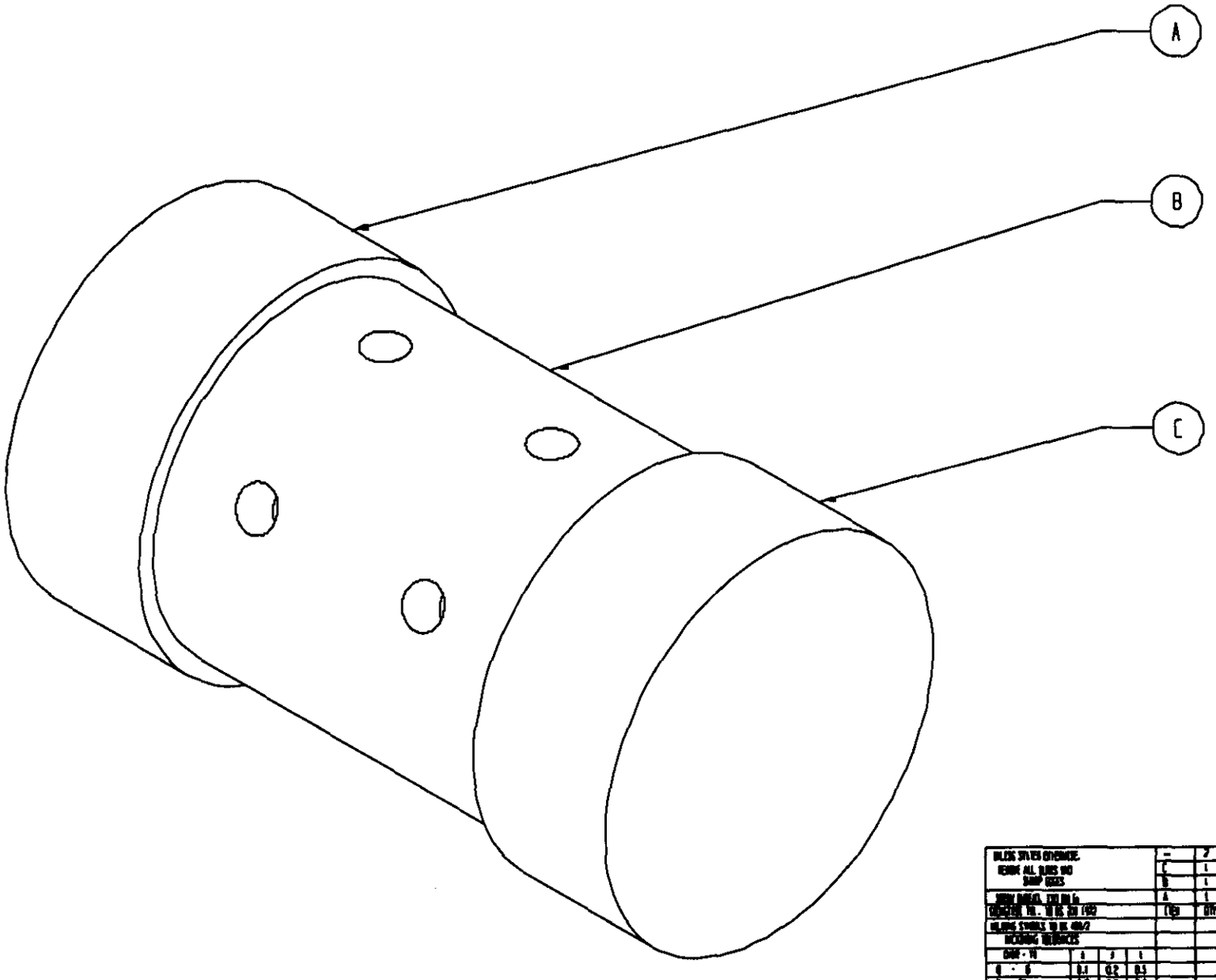

PRESSURE VESSEL INSULATION

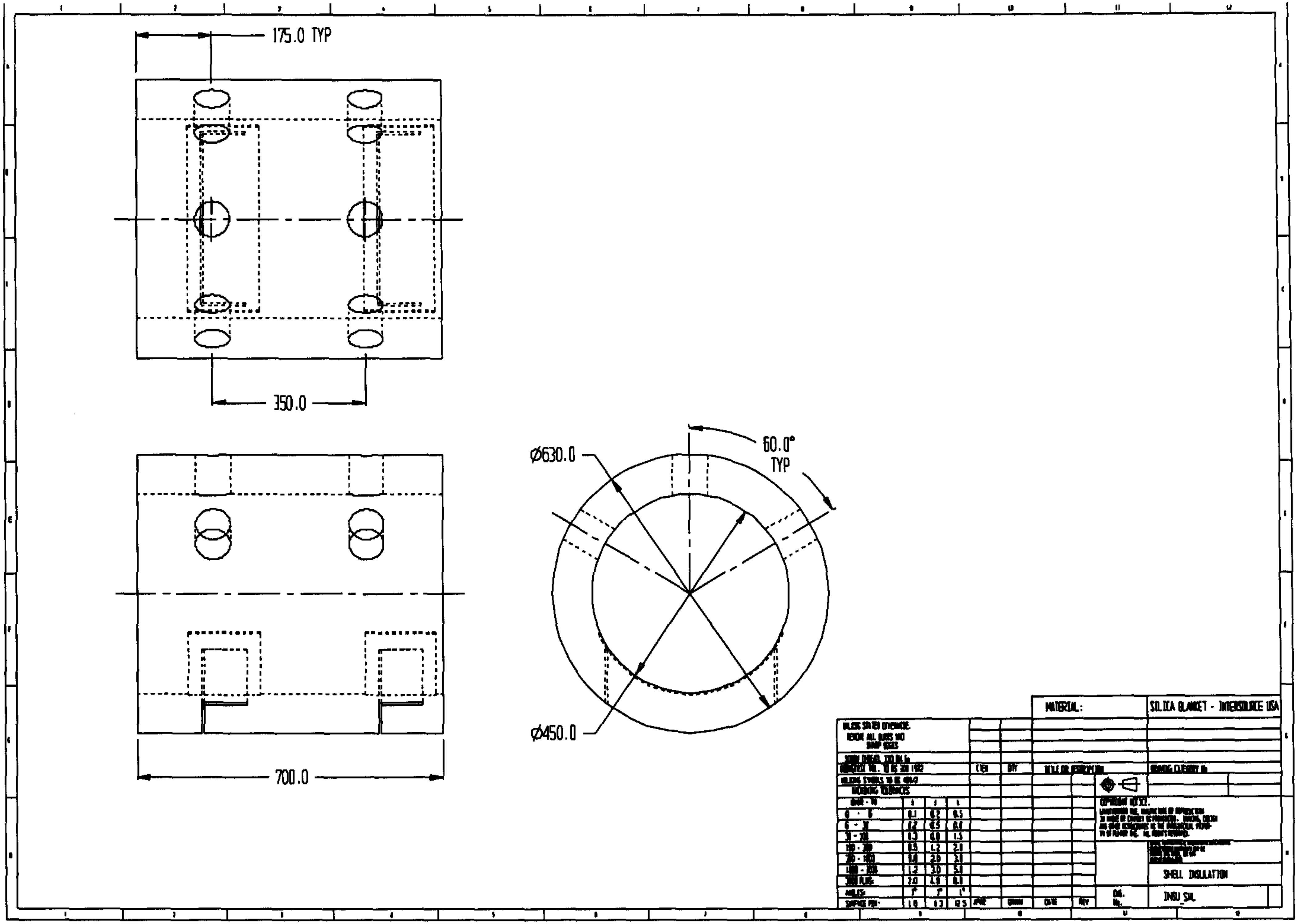

175.0 TYP
350.0
700.0
Ø630.0
Ø450.0
60.0° TYP
MATERIAL:
SILICA BLANKET - INTERSOURCE USA
SHELL INSULATION
INSU_SIL

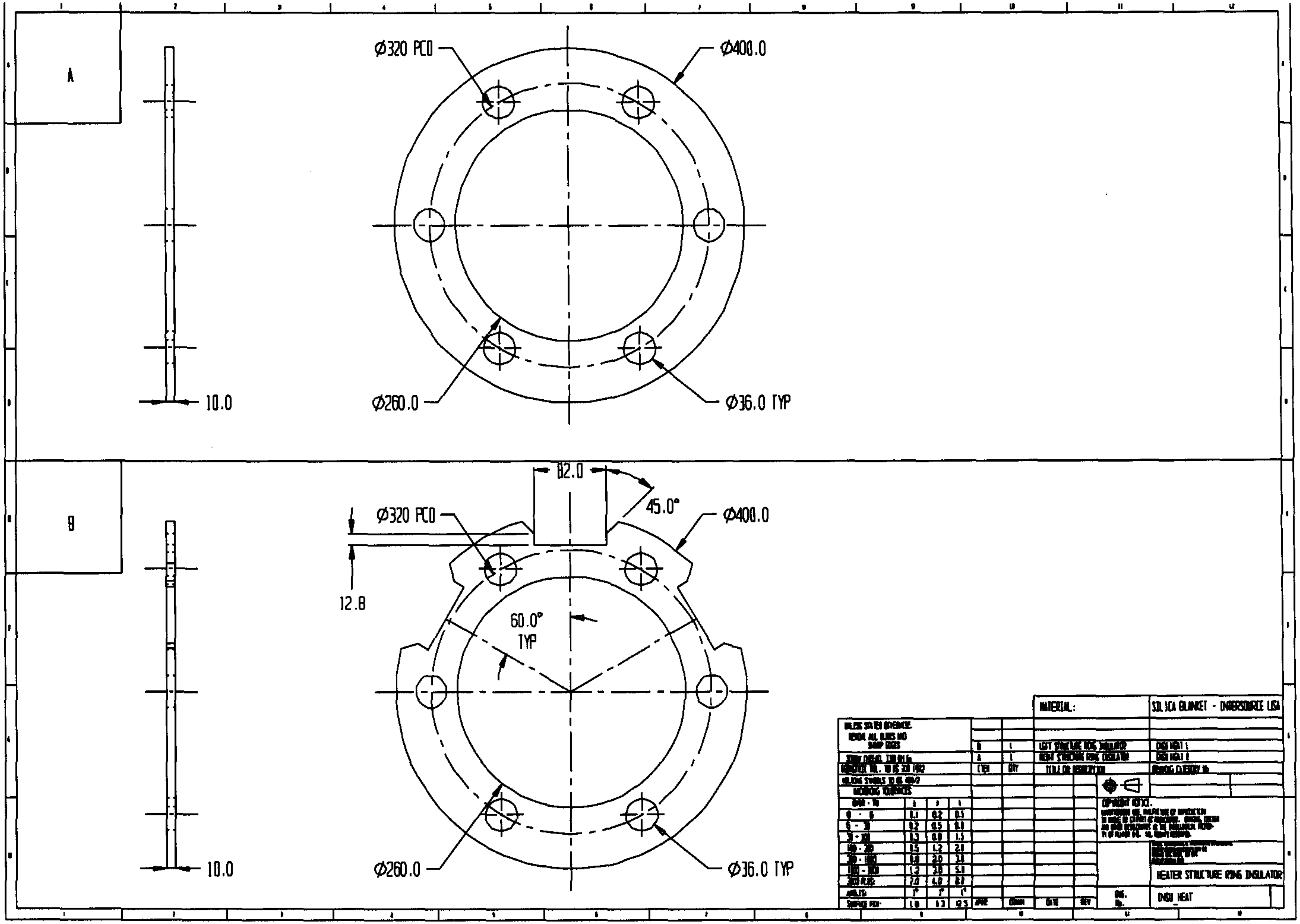
A
Ø320 PCD
Ø400.0
Ø260.0
Ø36.0 TYP
10.0
B
82.0
45.0°
Ø320 PCD
Ø400.0
12.8
60.0° TYP
Ø260.0
Ø36.0 TYP
10.0
MATERIAL:
SILICA BLANKET - INTERSOURCE USA
UNLESS STATED OTHERWISE.
B 1 LEFT STRUCTURE RING INSULATOR
A 1 RIGHT STRUCTURE RING INSULATOR
ITEM QTY TITLE OR DESCRIPTION
0 - 6 0.1 0.2 0.5
6 - 30 0.2 0.5 1.0
30 - 120 0.3 0.8 1.5
120 - 315 0.5 1.2 2.0
315 - 1000 0.8 2.0 3.0
1000 - 2000 1.2 3.0 5.0
2000 PLUS 2.0 4.0 8.0
ANGLES
SURFACE FIN 1.6 3.2 12.5
APPR CHKD DATE REV
COPYRIGHT NOTICE.
HEATER STRUCTURE RING INSULATOR
DWG. No.
INSU_HEAT

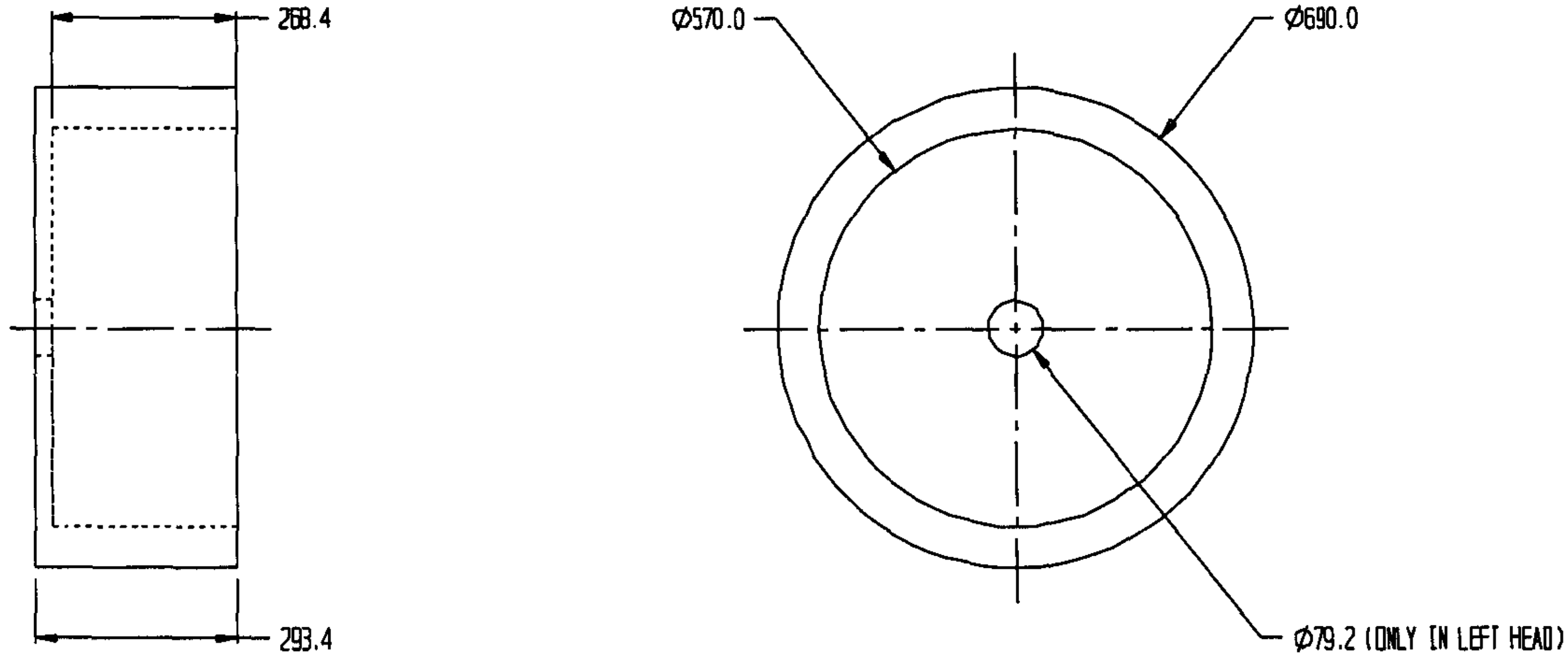

MATERIAL: SILICA BLANKET - INTERSOURCE USA

VESSEL HEAD INSULATION

DWG. No. INSU_HEAD

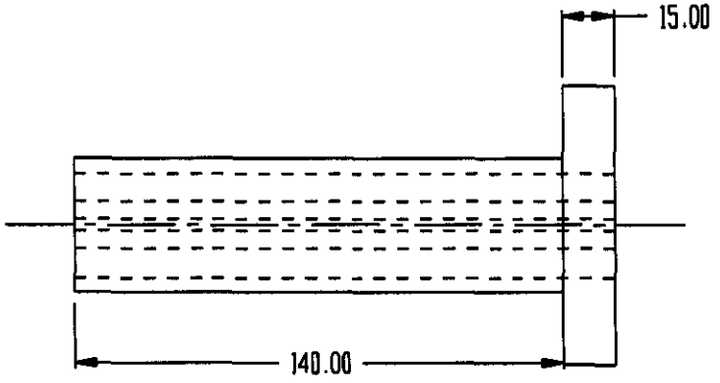

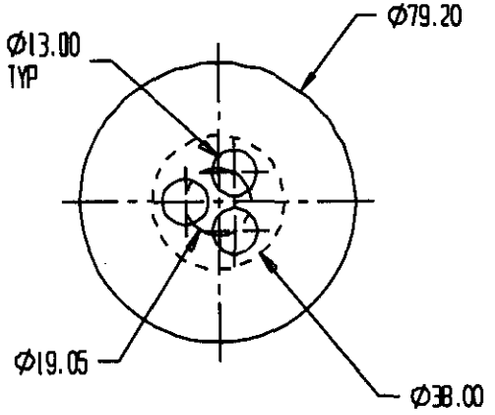

MATERIAL:	ZIRCAR ALUMINA TYPE ZAL-15
	ALUMINA RTV INSULATION
DWG. No.	INSU RTV